DSPACE

https://dspace.org/

The use of geostatistics in the extraction and mine planning of brick making clay

Von Wielligh, Madelein Heila Magdalena

2016-07-14
http://hdl.handle.net/10539/20585

Downloaded from a DSpace repository. https://dspace.org/

THE USE OF GEOSTATISTICS IN THE EXTRACTION AND MINE PLANNING OF BRICK MAKING CLAY

MADELEIN HEILA MAGDALENA VON WIELLIGH

A Research Report submitted to the Faculty of Engineering and the Built Environment, University of the Witwatersrand, in fulfilment of the requirements for the degree of Master of Science in Engineering.

October 2015

Declaration:

I declare that this report is my own, unaided work. I have read the University Policy on Plagiarism and hereby confirm that no Plagiarism exists in this report. I also confirm that there is no copying, neither is there any copyright infringement. I willingly submit to any investigation in this regard by the School of Mining Engineering and I undertake to abide by the decision of any such investigation.

_____

Signature

_____

Date

DEDICATED TO MY PARENTS MICHIEL AND COREEN NAUDE, MY HUSBAND HEINRICH AND MY CHILDREN MARISKA AND RECHARDT VON WIELLIGH

ACKNOWLEDGEMENTS

I wish to express my gratitude to the following persons:

Professor Richard Minnitt of the University of the Witwatersrand for his mentorship.

Doctor Michael Watson for his guidance, dedication, suggestions, and his willingness to assist me with his knowledge of geology.

Professor Christina Dohm for sharing her expert knowledge and for her guidance during the courses presented at the University of the Witwatersrand.

Corobrik for allowing me to use their exploration data for the purpose of this study.

Mr Farhad Fafai for his time and patience while training me in advanced Surpac software skills.

Gemcom and the Council for Geoscience for allowing me to use the Surpac software for the purpose of this study.

Jacques Perold for his initial training in open pit mining operations and in the Surpac software.

Mr L Wentzel for his assistance and for sharing his knowledge of clay pit mining.

Ms Adri van Heerden for her considerable effort in proofreading and editing the dissertation.

My husband and children for their patience and understanding during this long period of concentrated study.

The Lord Jesus Christ who gifted me with the talent and mental power to complete the dissertation and with a reverence for his creation of the sediments of the Earth.

ABSTRACT

Corobrik supplies a variety of uniquely coloured face bricks to the market. These bricks are manufactured by blending several clay varieties, which, when combined, provide a unique range of products. Colour variation in bricks is a major challenge with regard to product consistency, being influenced by the raw material composition and consistency. Homogeneity of the raw materials that are mined from year to year is crucial for continuously providing bricks of consistent colour. 'Top-face' clay mined at the Lawley Factory is an important raw material in the Nebraska product range being the major component affecting the colour of the product. Geological exploration borehole data were utilised for geostatistical analysis, variography and ordinary kriging by which means the variables SiO_2, Al_2O_3, Fe_2O_3 and K_2O, and loss on ignition (L.o.I) in the top-face clay was modelled, evaluated and interpreted. Geostatistics, a modified form of classical regression techniques, provides the tools to understanding spatial continuity of critical variables in naturally occurring clay deposits allowing one to study, explain, and describe them. Geostatistics has been applied to the modelling of the 'top-face' clay providing valuable information for improving mine planning. The kriging estimates indicated that the upper top-face layer is richer in K_2O and Fe_2O_3 than the bottom layer. This finding could contribute to improving mine planning, which, in turn, could assist in raw material consistency during the stockpile construction phase. The variability of K_2O in the deposit, together with the presence of Fe_2O_3, is the major contributor to the colour variability of the product and requires tight control. Estimating the clay domains 'sandy kaolin', 'chocolate', 'red kaolin', 'stained top-face' and 'smectite' that also occur in the deposit is recommended. Geostatistical methods and techniques applied in this study could be extended to all the ISO accredited factories of the Corobrik Group to assist in improving the colour consistency of the clay face-brick products.

TABLE OF CONTENTS

Acknowledgements iv

Abstract v

List of Table xiv

List of Figures xvi

List of Abbreviations xxv

TABLE OF CONTENTS VI

LIST OF TABLES XII

LIST OF FIGURES XIV

LIST OF ABBREVIATIONS XIX

CHAPTER 1 1

INTRODUCTION AND BACKGROUND 1

1. INTRODUCTION 1

1.1. Background 1

1.2. Mining history at Lawley 5

1.3. Aim and Objective of the study 16

1.4. Limitations of the study 17

1.5. Extent of the study 18

CHAPTER 2 19

CLAY AND CERAMIC FEATURES 19

2. BACKGROUND LITERATURE 19

2.1 Introduction 19

2.2 Clay 19

2.2.1 Background and origin 19

2.2.2 Chemical formation of clay 22

2.2.3 The alkali ions sodium and potassium 23

2.2.4 Iron and aluminium 23

2.2.5 Aluminium and silicon 25

2.3 Clay minerals 25

2.4 Clay occurrences in South Africa 28

2.5 Raw materials for brick making 29

2.6 Important minerals for brick making 31

2.6.1 The effect of minerals on the firing behaviour and properties of the ceramic ware.31

2.7 The chemical composition of brick making clays 34

2.8 Variables chosen for the study 34

2.9 Summary 36

CHAPTER 3 38

STOCKPILE CLAY SAMPLES AND THEIR CERAMIC PROPERTIES 38

3. CLAY CHARACTERISTICS AND CERAMIC PROPERTIES 38

3.1 Variability of oxides in clays 38

3.1.1 Variability of SiO_2, Al_2O_3, Fe_2O_3, K_2O and Loss on Ignition 38

3.1.2 The descriptive statistical summary of the SiO_2, Al_2O_3, Fe_2O_3, K_2O and Loss on ignition variables 40

3.1.3 Summary of stockpile clay sample variables 41

3.2 The correlation between oxides, minerals and full physical properties 42

3.2.1 Correlation between chemical composition and mineral composition 45

3.2.2 Correlation between mineral composition and ceramic properties 46

3.2.3 Correlation between chemical composition and ceramic properties 47

3.2.4 Summary of the correlation indices drawn between chemical, mineral and ceramic properties of the top-face clay stockpile variables. 49

CHAPTER 4 51

APPLIED GEOSTATISTICS 51

4. GEOSTATISTICAL BACKGROUND 51

4.1 Introduction 51

4.2 Geological domains and models 52

4.3 Statistical data analysis 53

4.3.1 Compositing and declustering 53

4.3.2 Descriptive data statistics 54

4.3.3 Multivariate data analysis 54

4.4 Continuity analysis 56

4.4.1 Traditional semi-variogram 60

4.4.2 Normal score semi-variogram 60

4.4.3 Log-normal semi-variogram 60

4.4.4 Covariance 60

4.4.5 Correlogram 60

4.4.6 Pairwise relative semi-variogram 60

4.4.7 Indicator semi-variogram 61

4.5 Semi-variogram modelling 61

4.6 Creation of a geological model 62

4.7 Estimation 63

4.8 Concluding remarks 75

CHAPTER 5 76

REGIONAL AND MINE-SCALE GEOLOGY 76

5. GEOLOGY OF SOUTH AFRICA 76

5.1. General description of South Africa's geological history 76

5.2. Brief description of Ecca Group formation, which forms part of the Karoo Supergroup 76

5.3. Geology of the clay sediments occurring at the Corobrik Lawley Factory near Lenasia, Soweto, in the Gauteng Province of South Africa 78

5.4. Regional geology of the clay sediments occurring at the Corobrik Lawley Factory79

5.5. Mine-scale geology of the clay sediments occurring at the Corobrik Lawley Factory 82

CHAPTER 6 86

GEOSTATISTICAL ANALYSIS OF DATA 86

6. STATISTICAL DATA EVALUATION 86

6.1. Data collection 86

6.2. Definition of geological domains 87

6.3. Data analysis 94

6.4. Data validation 94

6.5. Descriptive statistics for the upper and lower top-face clays 97

6.6. Contour maps 102

6.6.1. Top-face upper clay 102

SiO_2 contour map for top-face upper clay 102

Al_2O_3 contour map for top-face upper clay 102

Fe_2O_3 contour map for top-face upper clay 103

K_2O contour map for top-face upper clay 103

Loss on ignition contour map for top-face upper clay 104

6.6.2. Top-face lower clay 106

SiO_2 contour map for top-face lower clay 106

Al_2O_3 contour map for top-face lower clay 106

Fe_2O_3 contour map for top-face lower clay 106

K_2O contour map for top-face lower clay 107

Loss on ignition contour map for top-face lower clay 107

6.7. Summary 109

CHAPTER 7 110

GEOSTATISTICS 110

7. INTRODUCTION 110

7.1. Compositing and preparation of variogram modelling 110

7.2. Variography for the top-face upper clay 111

7.3. Variography for the top-face lower clay 119

7.3.1 Comparing variogram parameters between the top-face upper and lower clays 127

CHAPTER 8 129

ESTIMATION 129

8. ESTIMATION OF THE TOP-FACE UPPER AND LOWER CLAY VARIABLES 129

8.1. Introduction 129

8.2. Estimation methodology 130

8.3. Estimated grades 133

8.3.1. Top-face upper clay variable estimations 133

8.3.2. Top-face lower clay variable estimations 143

8.3.3. Comparison between the top-face upper and lower clay estimated variables. 153

8.3.4. Comparison between the mean of the combined top-face clays, as well as the mean and estimated grades of both the individual top-face upper and the lower clays 155

CHAPTER 9 158

CONCLUSION AND RECOMMENDATION 158

9. SUMMARY 158

9.1. CONCLUSION 158

9.2. RECOMMENDATION 162

REFERENCES 166

LIST OF TABLES

TABLE **PAGE**

Table 1-1. Burnt-clay masonry classification (SABS 227-1986). 4

Table 2-1. Typical colours observed for different iron oxide minerals (Velde, 2010). 24

Table 2-2. Typical colours observed for different iron oxide minerals (Velde, 2010). 30

Table 2-3. Chemical composition and descriptive statistics of top face clay from 350 individual samples taken from 70 stockpiles layers constructed. 35

Table 3-1. XRF summary statistics of the 350 stockpile samples. 39

Table 3-2. Correlation between chemical, mineral and ceramic variables from 8 stockpiles with each stockpile generally representing 10 layers of 5 samples each (approximately 50 samples). 44

Table 3-3. below provides a summary of the relationships of the chemical, mineral and ceramic property variables discussed in the previous sections. 49

Table 5-1: Classification of the Karoo sequence in the Lawley area (Jones, 1984). 83

Table 6-1. Classification of the different geological domains at Lawley, based on their mineralogical composition. 90

Table 6-2. Chemical composition of clay stockpiles mined with their minimum, maximum and average statistics. 91

Table 6-3. Typical example of data validation of drilled core. 96

Table 6-4. Example of chemical analysis data spot checks. 96

Table 6-5. Descriptive statistics of the top-face upper layer. 97

Table 6-6. Descriptive statistics of the top-face lower layer. 97

Table 7-1. Variogram parameters for the five top-face upper clay variables. 112

Table 7-2. Top-face upper clay variogram map parameters. 113

Table 7-5. Variogram parameters for the five top-face lower clay variables. 120

Table 7-6. Top-face lower clay variogram map parameters. 121

Table 8-1 Optimising block size for estimation. 132

Table 8-2. Block estimation of the top-face upper clay variables. 136

Table 8-3 Block estimation of the top-face lower clay variables. 145

Table 9-1. Fluctuation of variables in the top-face clay stockpiles compared with the top-face upper and lower clays. 159

LIST OF FIGURES

FIGURE **PAGE**

Figure 1-1. Lawley Factory product range (Corobrik, 2009). 1

Figure 1-2. Examples of buildings constructed with the Nebraska and Montana brick products (Corobrik, 2009). 2

Figure 1-3. Colour banding illustrated on building (Corobrik, 2009). 5

Figure 1-4. Open cast selective bench mining at Lawley. 6

Figure 1-5. Illustration of how clay loads are placed on the stockpile pad (Corobrik, 2010). 7

Figure 1-6. Profiling of stockpile after completion (Corobrik, 2010). 8

Figure 1-7. Colour variation year on year, illustrated with and without a flash mark on the brick. 9

Figure 1-8. Variation in brick background colour and flash mark, year on year. 10

Figure 1-9. Fired briquettes for season A stockpile, showing colour development over a temperature range of 1 050 °C to 1 150 °C. Variability in colour of the briquettes for each temperature at different positions is insignificant. 12

Figure 1-10. Fired briquettes for season B stockpile, showing colour development over a temperature range of 1 050 °C to 1 150 °C. Variability in colour of the briquettes for each temperature at different positions is insignificant. 13

Figure 1-11. Fired briquettes for season C stockpile, showing colour development over a temperature range of 1 050 °C to 1 150 °C. Variability in colour of the briquettes for each temperature at different positions is insignificant. 14

Figure 1-12. Fired briquettes for season D stockpile, showing colour development over a temperature range of 1 050 °C to 1 150 °C. Variability in colour of the briquettes for each temperature at different positions is insignificant. 15

Figure 1-13. Stockpile layering indicating composite sample positions of each layer for laboratory testing, where NE is North East, NW North West, C Centre, SW South West and SE South East. 16

Figure 2-1. Chemical processes and interaction levels responsible for clay minerals (Velde, 2010). 20

Figure 2-2. Illustration of time-temperature, showing the stability range of clays under weathering, sedimentation, burial digenesis and hydrothermal alteration conditions (Velde, 2010). 21

Figure 2-3. The clay cycle illustrated under geological conditions (Velde, 2010). 22

Figure 3-1. Variability of SIO_2, Al_2O_3, Fe_2O_3, K_2O and Loss on Ignition in 350 samples from 70 stockpile layers. 39

Figure 3-2. Histograms for SiO_2, Al_2O_3, Fe_2O_3, K2O and Loss on Ignition for the 350 stockpile samples. 41

Figure 3-3. Scatterplots between the mineral and chemical variables. 45

Figure 3-4. Scatterplots between the mineral and ceramic property variables. 47

Figure 3-5. Scatterplots between the chemical and ceramic property variables. 48

Figure 4-1. Typical example of a matrix scatterplot between different variables (Coombes, 2008). 55

Figure 4-2. The semi-variogram illustrating the different structures and distinguishing between geostatistics and statistics based on special correlation (Dohm, 2012). 58

Figure 4-3. Summary of different semi-variogram types (Coombes, 2008). 59

Figure 4-4. Variogram model nested (Coombes, 2008). 61

Figure 4-5. Pre-defined shapes associated with the semi-variogram of the kriging system (Coombes, 2008). 62

Figure 4-6. Series of equations used in ordinary kriging to calculate the weight values (Coombes, 2008). 69

Figure 4-7. Comparison between the distribution of block grades and true grades (Coombes, 2008). 73

Figure 4-8 Linear regression slope between true block grades and estimated block grades (Coombes, 2008). 73

Figure 5-1. The lithostratigraphic units in the Main Karoo Basin (modified after Johnson et al., 1997). 79

Figure 5-2. Schematic west–east section through the Ecca Group in the north-eastern part of the Main Karoo Basin (Van Vuuren, 1981) 80

Figure 5-3. Geological map of the geology underlying the Lawley quarry (Geological Map 2526, West Rand, 1:250 000-scale, Geologiese Opname). 81

Figure 5-4. One of the open clay faces in the Lawley quarry. The local names of the various clays occurring in the quarry are also indicated. 84

Figure 5-5. Light burning top-face and chocolate clays in the Lawley quarry. 84

Figure 5-6. The contact between the top-face clay at the top and the chocolate clay at the bottom is clearly outlined by the brown iron-stained marker. 85

Figure 6-1. Drill hole layout in the area adjacent to the current pit. 88

Figure 6-2. Drill hole layout and drill hole sections used for modelling. 89

Figure 6-3. Typical drill core indicating chocolate and top-face clays. 89

Figure 6-4. Top-face upper (blue) and lower (red) sections digitised from drill core to define each clay domain. 92

Figure 6-5. An illustration of a typical digitised section for domain creation, where top-face clay is demarcated blue. 93

Figure 6-6. Illustration of chemical analysis verification results from round robin testing. 95

Figure 6-7. Histograms for top-face upper clay and lower clay. 100

Figure 6-8. Probability plots for top-face upper clay and top-face lower clay. 101

Figure 6-9. Contour maps for top-face upper clay variables. 105

Figure 6-10. Contour maps for the top-face lower clay variables. 108

Figure 7-1, Lengths of top-face core samples logged. 111

Figure 7-2. Major, semi-major and minor variograms, including the major and semi-major variogram maps for SiO_2 in the top-face upper clay. 115

Figure 7-3. Major, semi-major and minor variograms, including the major and semi-major variogram maps for Al_2O_3 in the top-face upper clay 116

Figure 7-4. Major, semi-major and minor variograms, including the major and semi-major variogram maps for Fe_2O_3 in the top-face upper clay. 117

Figure 7-5. Major, semi-major and minor variograms, including the major and semi-major variogram maps for K_2O in the top-face upper clay. 118

Figure 7-6. Major, semi-major and minor variograms, including the major and semi-major variogram maps for L.o.I in the top-face upper clay.
119

Figure 7-7. Major, semi-major and minor variograms, including the major and semi-major variogram maps for SiO_2 in the top-face lower clay. 122

Figure 7-8. Major, semi-major and minor variograms, including the major and semi-major variogram maps for Al_2O_3 in the top-face lower clay. 123

Figure 7-9. Major, semi-major and minor variograms, including the major and semi-major variogram maps for Fe_2O_3 in the top-face lower clay. 124

Figure 7-10. Major, semi-major and minor variograms, including the major and semi-major variogram maps for K_2O in the top-face lower clay. 125

Figure 7-11. Major, semi-major and minor variograms, including the major and semi-major variogram maps for L.o.I in the top-face lower clay.
126

Figure 7-12. The nugget, sill and range parameters, comparison between the top-face upper and lower clays. 128

Figure 8-1. Solid created for the top-face upper clay domain. 130

Figure 8-2. Solid created for the top-face lower clay domain. 131

Figure 8-3. Solid created for the top-face upper and lower clay domains. 131

Figure 8-4. Kriging variance for the top-face upper clay variables. 137

Figure 8-5. Kriging efficiency for the top-face upper clay variables. 137

Figure 8-6 Conditional bias for the top-face upper clay variables. 137

Figure 8-7 Estimated SiO_2 top-face upper clay grades. 138

Figure 8-8 Estimated Al_2O_3 top-face upper layer grades. 139

Figure 8-9 Estimated Fe_2O_3 top-face upper layer grades. 140

Figure 8-10 Estimated K_2O top-face upper layer grades. 141

Figure 8-11. Estimated loss on ignition top-face upper clay grades. 142

Figure 8-12. Kriging variance for the top-face lower clay variables. 146

Figure 8-13 Kriging efficiency for the top-face lower clay variables. 146

Figure 8-14. Conditional bias for the top-face upper clay variables. 147

Figure 8-15 Estimated SiO_2 top-face lower clay grades. 148

Figure 8-16 Estimated Al_2O_3 top-face lower clay grades. 149

Figure 8-17 Estimated Fe_2O_3 top-face lower clay grades. 150

Figure 8-18 Estimated K_2O top-face lower clay grades. 151

Figu re 8-19 Estimated loss on ignition top-face lower clay grade. 152

Figure 8-20 Comparison between the top-face upper and lower clay kriging variance. 154

Figure 8-21 Comparison between the top-face upper and lower clay kriging efficiency. 155

Figure 8-22 Comparison between the top-face upper and lower clay conditional bias. 155

Figure 8-23 Comparison between the mean of the combined top-face clays and the top-face upper clay mean and estimated grades. 156

Figure 8-24 Comparison between the mean of the combined top-face clays and the top-face lower clay mean and estimated grades. 157

Figure 9-1 Comparison between the mean of the combined top-face clays and the top-face upper clay mean and estimated grades. 162

Figure 9-2 Comparison between the mean of the combined top-face clays and the top-face lower clay mean and estimated grades 162

LIST OF ABBREVIATIONS

$\tilde{C}_{AA}$	Average covariance between pairs of locations within A
CoV	Coefficient of Variation
^{0}C	Degrees Celsius
θ˚	Direction
FBS	Face bricks
FBX	Face bricks extra
FBA	Face brick aesthetic
h	Vector
$\tau_{\alpha}^{(OK)}(\boldsymbol{u})$	Ordinary kriging weights
$\tau_{\beta}^{(SK)}(\boldsymbol{u})$	Simple kriging weights
L.o.I	Loss on Ignition
M	Mean
NFP	Non-face brick plastered
NFX	Non-facing extra
OK	Ordinary kriging
pH	Power of hydrogen
SABS	South African Bureau of Standards
σ	Covariance
$\sigma_R^{\sim 2}$	Lagrange parameter

RF	Random Function
TF	Top-face
TFL	Top-face lower
TFU	Top-face upper
uk	K coordinate vector
u	Location
γ	Semi-variance
z	Sample
$Z_{OK}^{*}(u)$	Linear regression estimator (ordinary kriging)
z (u)	Non-sampled values/sample location

CHAPTER 1

INTRODUCTION AND BACKGROUND

1. INTRODUCTION

1.1. BACKGROUND

Corobrik is a leading clay face-brick manufacturer and has been in business for over 100 years. The company has been able to meet the changing needs and requirements of architects and consumers by offering a versatile range of brick products.

Corobrik provides a variety of uniquely coloured and textured bricks because of the large variety of clay materials that are mined and blended in various ratios during the manufacturing process. The company has 14 factories in South Africa, the majority of which are located in the Gauteng Province. The Lawley Factory is one of the factories situated in Gauteng that produce approximately 98 million bricks per annum. This factory produces three product ranges, namely Nevada, Nebraska, and Montana (Figs 1.1 and 1.2).



Figure 1-1. Lawley Factory product range (Corobrik, 2009).



Figure 1-2. Examples of buildings constructed with the Nebraska and Montana brick products (Corobrik, 2009).

The management of raw material is one of the key factors to ensure that the demands of costumers for consistency in the product range are met. Bricks are characterised by their diversity in terms of colour, shape and size and can be categorised, based on their physical properties, into two types, namely masonry units and engineering units. The South African Bureau of Standards (SABS) classifies masonry units into five classes according to SABS Specification 227-1986, as indicated in Table 1.1.

The Nebraska, Nevada and Montana products manufactured by the Lawley Factory are classified as FBS bricks as they are uniform in size and shape. However, the colour variation in the bricks poses a challenge. Various factors influence the colour of the brick, namely:

- the quality and consistency of the raw material
- the firing temperature
- the firing time
- the energy type used for firing.

Figure 1.3 shows a typical example of colour variation. The current practice for reducing this colour banding is to blend the bricks from different packs

on site. Variations in colour of the product also occur between different stockpiles. The challenge is to match the specification of the previous stockpile to the specification of the new stockpile in the attempt to ensure consistency in colour and physical properties.

Corobrik is the largest face brick supplier in South Africa. The company is committed to supplying products of consistent colour, size and strength. The role of the raw materials in this regard cannot be overemphasised. The homogeneity of the raw materials mined from year to year is crucial for a reliable supply of bricks with a consistent colour.

Table 1-1. Burnt-clay masonry classification (SABS 227-1986).

Class 1 Masonry units	Classification
FBS (Face bricks)	Units are selected or produced for their durability and uniformity of size and shape.
FBX (Face bricks extra)	Units are selected or produced for their durability and high degree of uniformity of size, shape and colour.
FBA (Face brick aesthetic)	Units are selected or produced for their durability and aesthetic effect derived from non-uniformity of size, shape and colour.
NFP (Non face brick plastered)	Units suitable for general building work that is to be plastered.
NFX (Non facing extra)	Units suitable for plastered or un-plastered general building work below damp-proof course, or under damp conditions or below, or below ground level where durability rather than aesthetics is the criterion for selection.
Class 2 Engineering units	Classification
Engineering units	Any class of masonry unit produced for structural or load-bearing purposes in face or non-face work, where the manufacturer supplies to an agreed compressive strength. An engineering unit is designated by the addition of the letter E, followed by the number equal to the nominal compressive strength in mega-Pascal.



Figure 1-3. Colour banding illustrated on building (Corobrik, 2009).

1.2. MINING HISTORY AT LAWLEY

Extensive mining of clay has taken place at Lawley for more than 50 years. The red clays are still in abundance, but the lighter coloured clay, such as top-face (tf), has become less available on the current properties mined by Corobrik.

Mining at Lawley is done by the open cast method and the overburden is removed and used for rehabilitation. The different clay types are mined selectively with an excavator. The individual clay layers are hauled with dumper trucks and stockpiled separately. The pit is mined with a maximum bench height of 3 m and a slope angle of 33°. The mining procedure is illustrated in Figure 1.4.

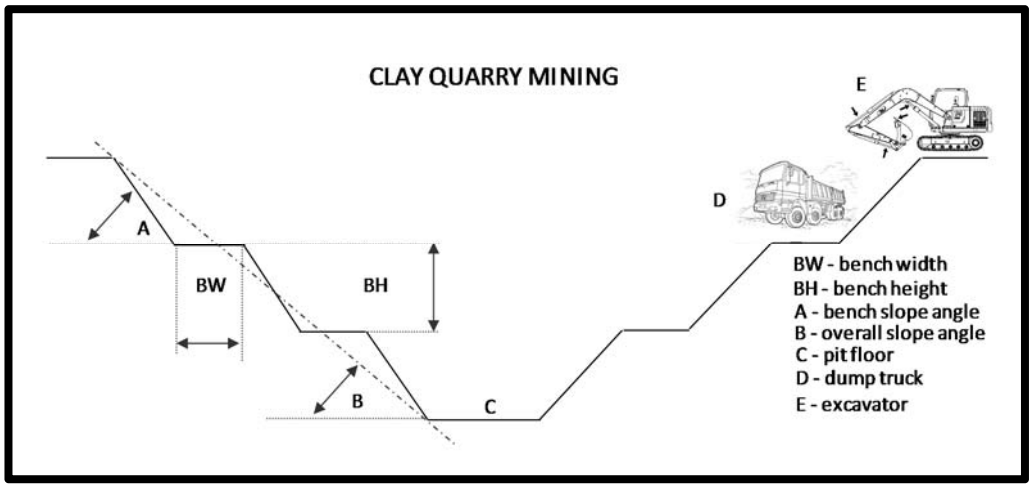


Figure 1-4. Open cast selective bench mining at Lawley.

Stockpiles for each of the clay types are constructed by building layers approximately 300 mm thick, whereby each one is sloped before the next layer is placed on the stockpile. The layers are sampled and analysed for their chemical composition. The construction of the layered stockpiles is illustrated in Figures 1.5 and 1.6 (Corobrik, 2010).

The Lawley Factory is expected to provide consistently coloured clay-brick products to the market year after year. Managing the changeable product colours is a logistical challenge with a rippling effect on the functions down the value chain, e.g. from managing the raw material during the mining phase to managing the variability of the products on the building site. Figures 1.7 and 1.8 illustrate the range of the colour variations in the Nebraska product year after year.

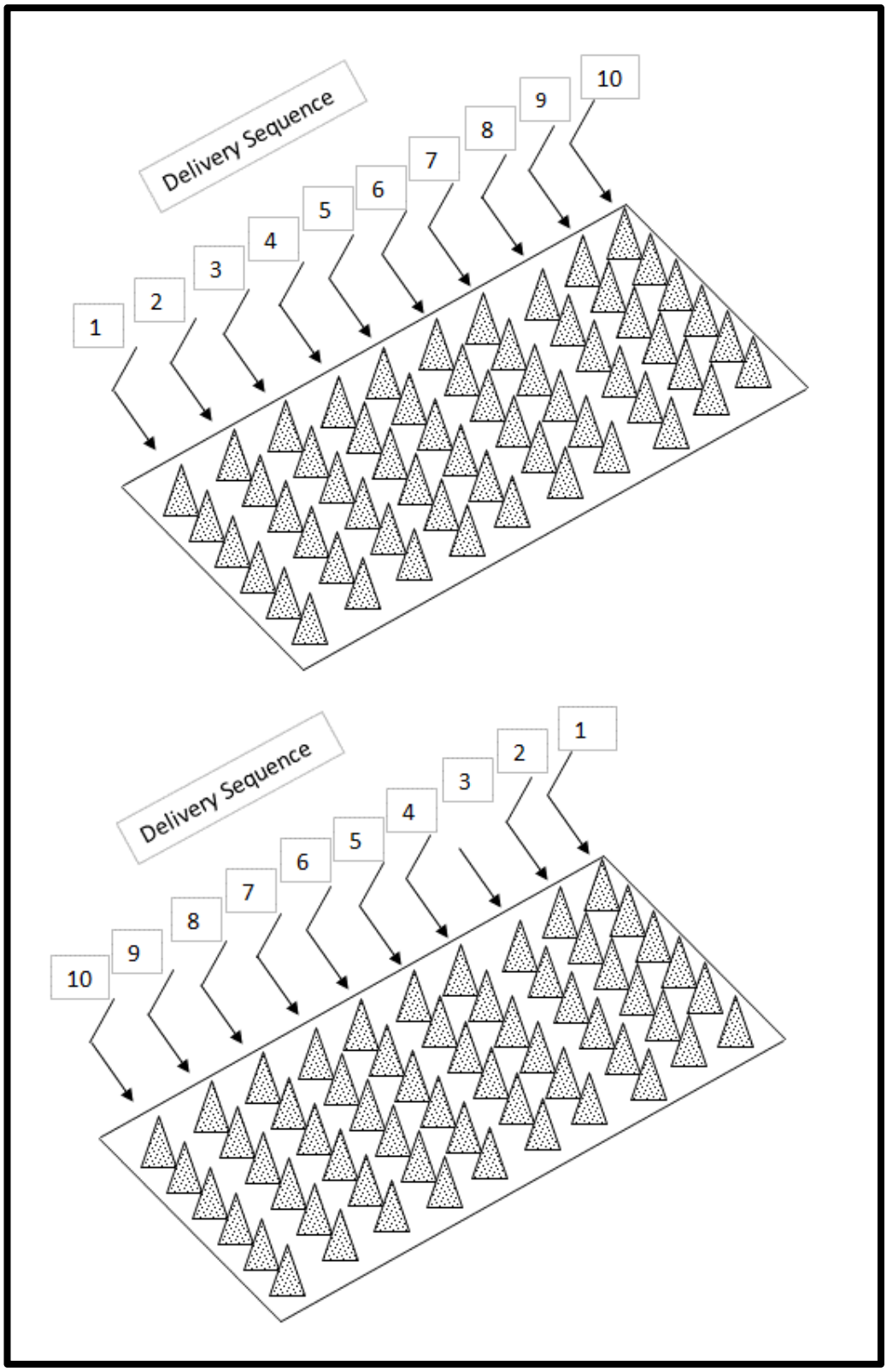


Figure 1-5. Illustration of how clay loads are placed on the stockpile pad (Corobrik, 2010).

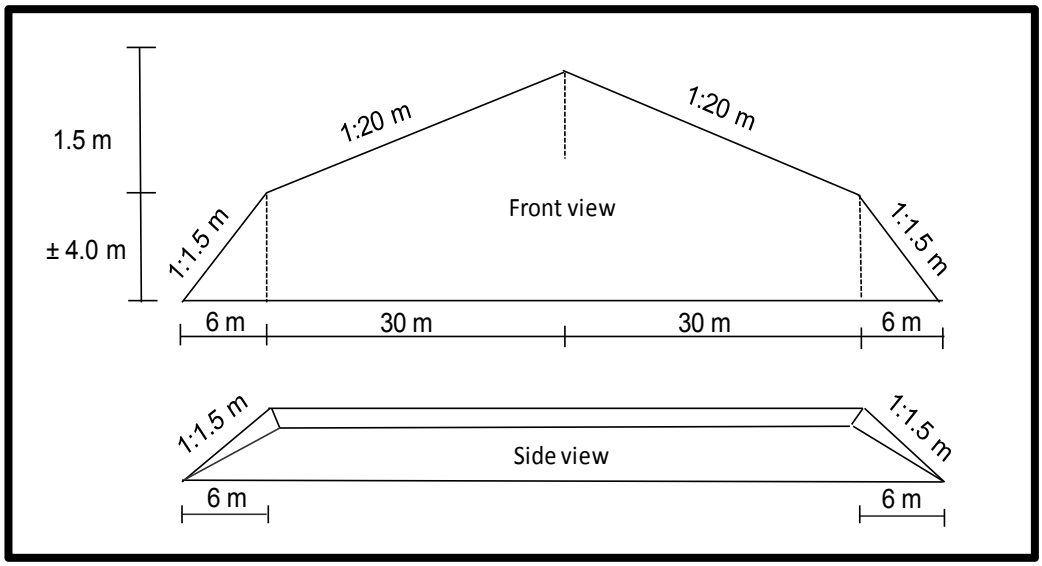


Figure 1-6. Profiling of stockpile after completion (Corobrik, 2010).

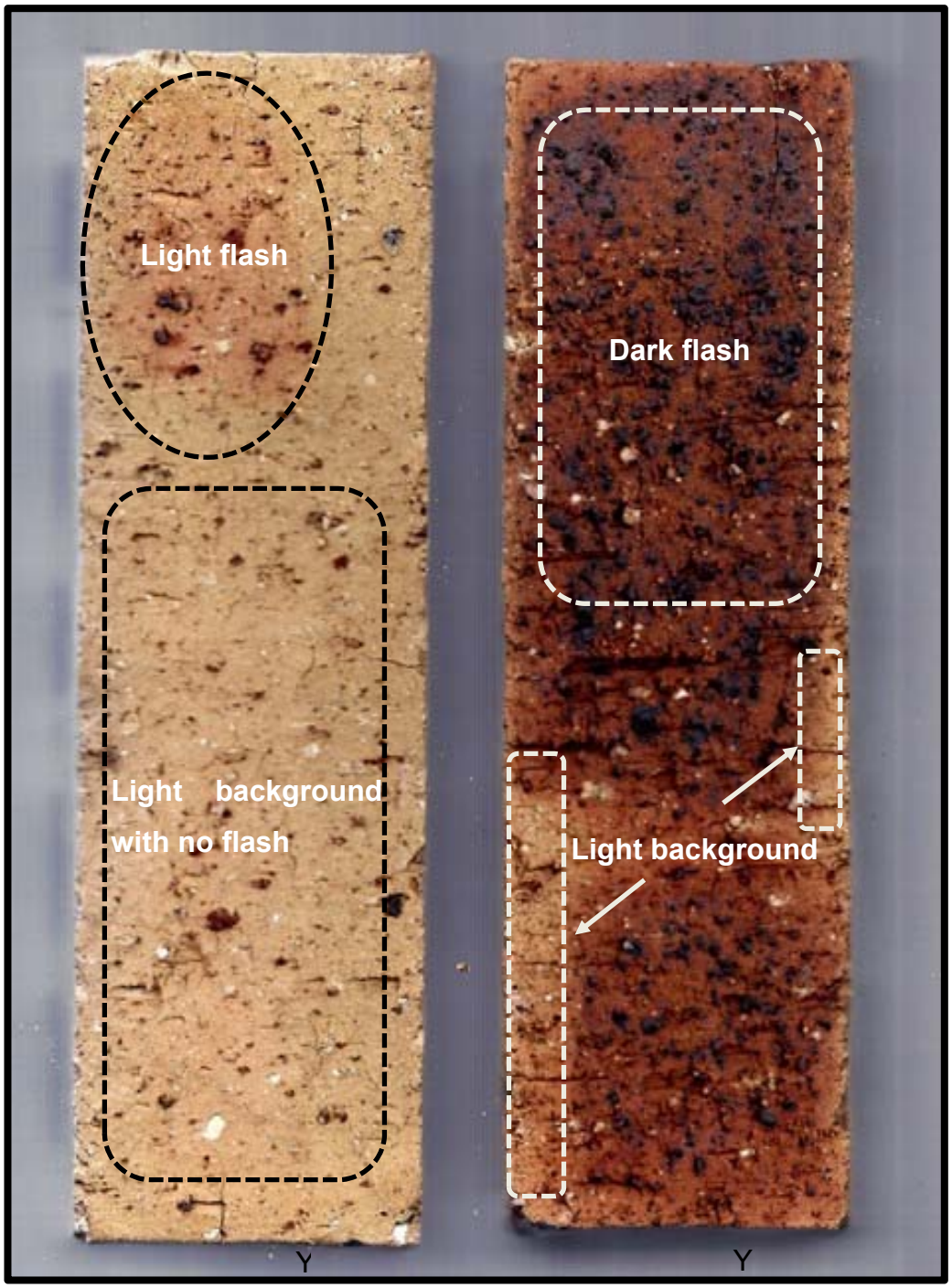


Figure 1-7. Colour variation year on year, illustrated with and without a flash mark on the brick.

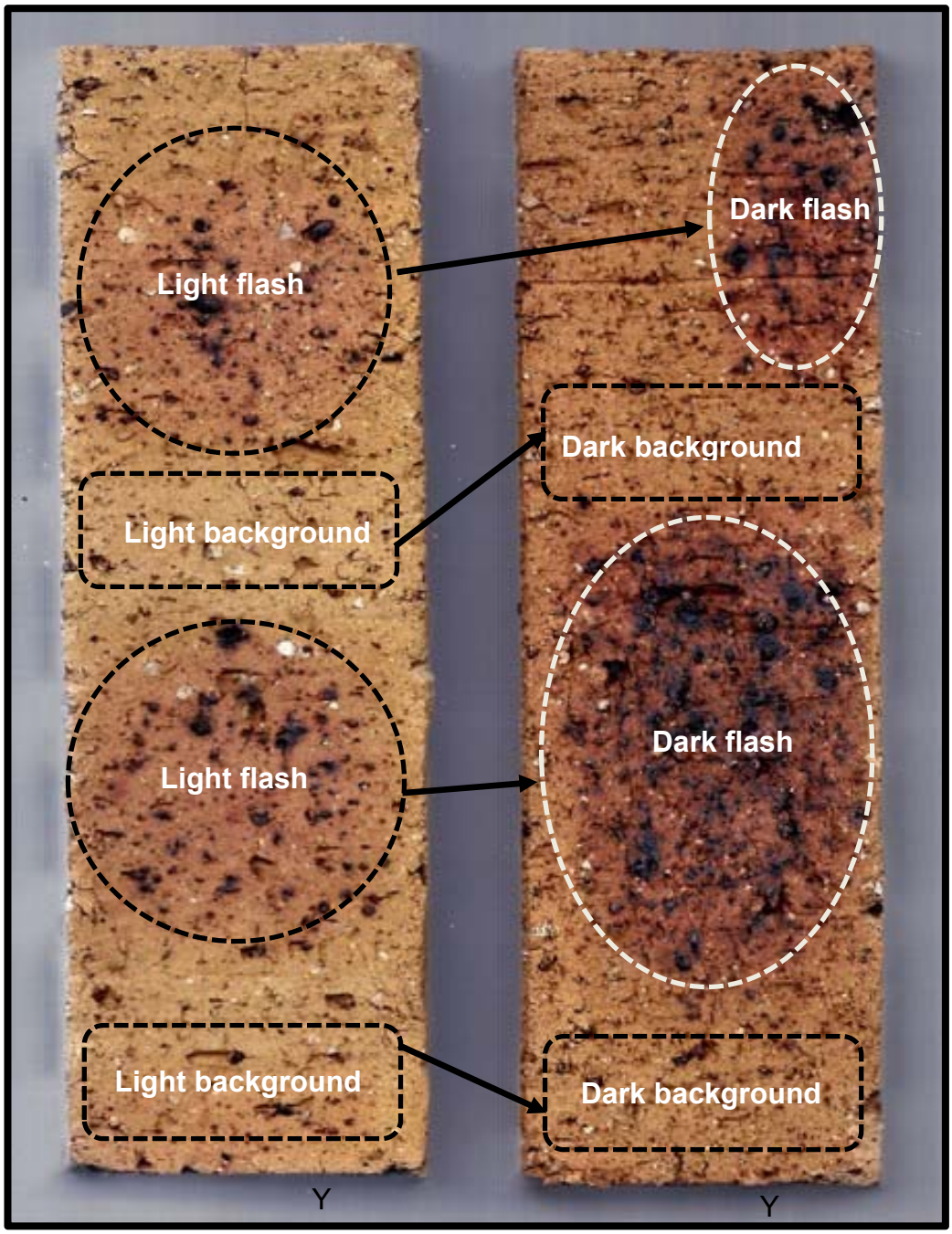


Figure 1-8. Variation in brick background colour and flash mark, year on year.

These product colour changes can partly be ascribed to the variability of the raw materials used. In the attempt to manage these variations, adjustments are needed in either the mix formulation or the process parameters to compensate for the colour deviations.

The variability of the raw material is dependent on:

- The geochemical distribution of elements in the raw material.

- The mining of similar/dissimilar clay layers in the pit.
- Stockpiling and homogenising the clay types, layer by layer, on the stockpile.
- Reclaiming of the stockpile fed to the plant.

The colour variation of the laboratory-fired briquettes for the top-face stockpiles that were mined over four seasons are shown in Figures 1.9 to 1.12. These fired briquettes were manufactured by bulking each individual clay layer at five different positions on the stockpile, as is illustrated by Figure 1.13. Comparing the colour of the briquettes for a particular mining season at different positions and at different temperatures illustrates the colour consistency. However, when the colour of the briquettes for different seasons is compared, distinct differences are noticed, especially at temperatures ranging between 1 050 °C and 1 150 °C.

To prevent extreme colour variation in products that are allocated to long-term projects, ‘micromanagement’ is needed, both in the stockyard and on site. This process involves extensive human capital intervention and time resources. However, if colour variations are not carefully controlled, colour banding of the wall face will result, which could lead to customer complaints and compensation claims.

Therefore, controlling and managing, at the start of the value chain, the clay raw-material factors responsible for the fired colour variation will likely minimise intervention and crisis management further down the value chain. Additionally, yields and colour consistency in the product can be expected year after year.



Figure 1-9. Fired briquettes for season A stockpile, showing colour development over a temperature range of 1 050 °C to 1 150 °C. Variability in colour of the briquettes for each temperature at different positions is insignificant.

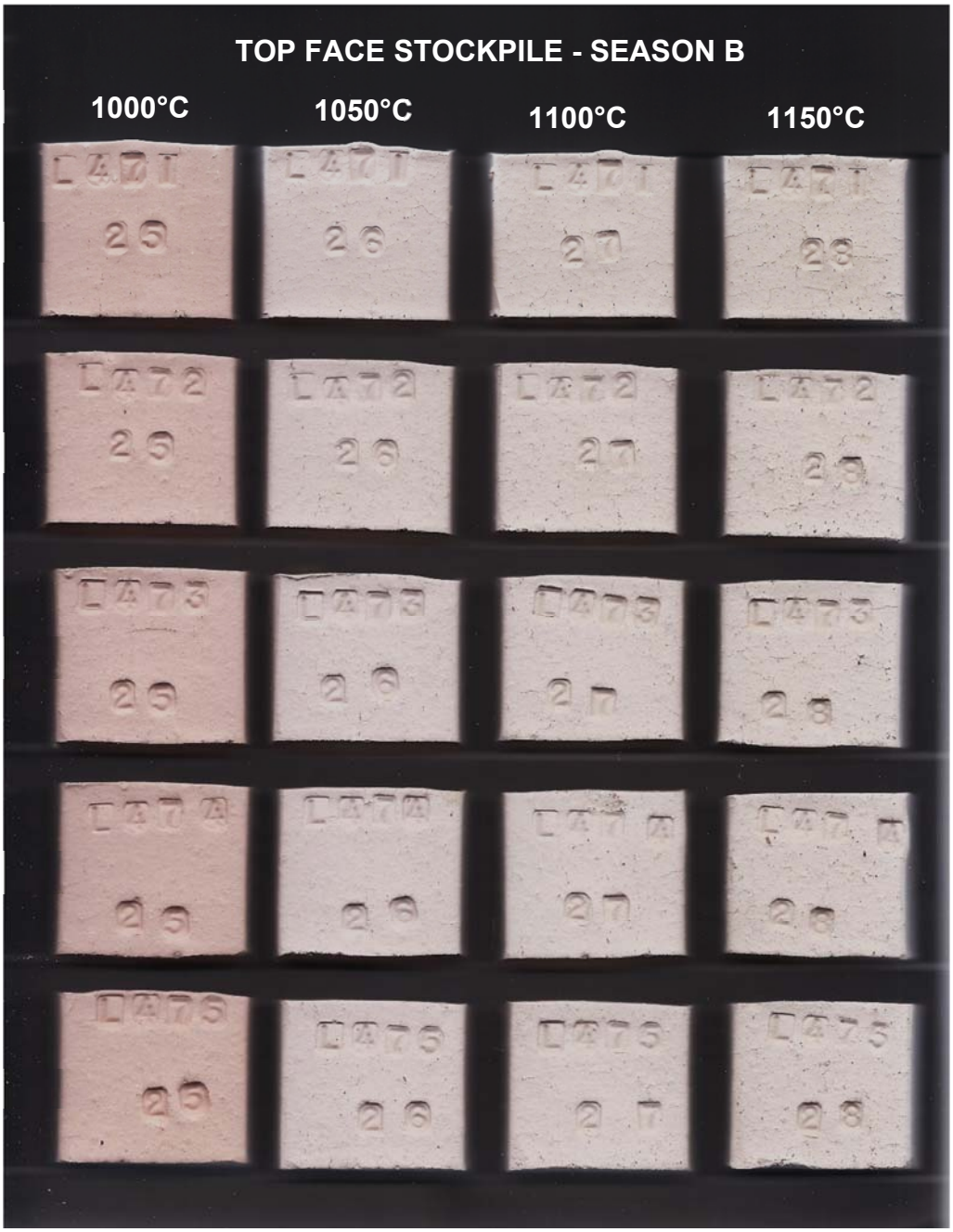


Figure 1-10. Fired briquettes for season B stockpile, showing colour development over a temperature range of 1 050 °C to 1 150 °C. Variability in colour of the briquettes for each temperature at different positions is insignificant.



Figure 1-11. Fired briquettes for season C stockpile, showing colour development over a temperature range of 1 050 °C to 1 150 °C. Variability in colour of the briquettes for each temperature at different positions is insignificant.



Figure 1-12. Fired briquettes for season D stockpile, showing colour development over a temperature range of 1 050 °C to 1 150 °C. Variability in colour of the briquettes for each temperature at different positions is insignificant.

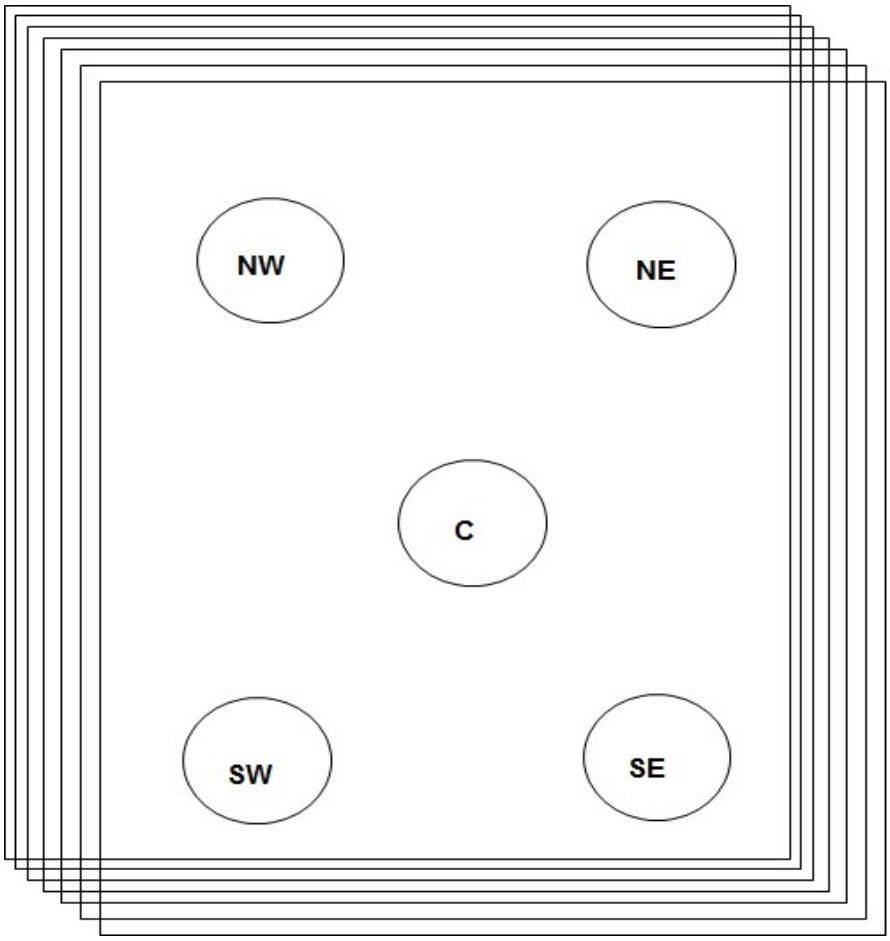


Figure 1-13. Stockpile layering indicating composite sample positions of each layer for laboratory testing, where NE is North East, NW North West, C Centre, SW South West and SE South East.

1.3. AIM AND OBJECTIVE OF THE STUDY

The batching mix of one of the light burning products at Lawley contains more than 50 percent of a light burning top-face clay. Therefore, the latter was chosen for the study. An exploration project undertaken on a neighbouring farm in 2009 and 2010 made geological data available for study. This is most important, as understanding the geochemical distribution of elements in the top-face clay layer could assist in improving colour consistency and, therefore, prompted further investigation.

Therefore, the main objective of the study is:

- To ascertain if stockpile consistency could be improved year on year by making use of geostatistical techniques to define the top-face clay layer.

- Using ordinary kriging as a geostatistical technique, to determine if the geochemical distribution of elements (variables) in the top-face clay layer could be defined and modelled.
- To ascertain whether the estimated kriged values could reveal how the different variables are distributed within the top-face clay layer.
- To establish if the estimated kriged values could guide future quarry development and planning.

The secondary objective of the study, using Surpac Software, is to:

- Construct a solid of the top-face clay layers based on the drill core data.
- Build a three-dimensional block model of the top-face clay layers.
- Use ordinary kriging to estimate the geochemical distribution of certain major elements (SiO_2, Al_2O_3, Fe_2O_3, K_2O and loss on ignition) within the top-face clay layers.
- Use the estimated kriged grades in the block model as guide for predicting and minimising the colour variation of the final product by:
  - Improved quarry development planning.
  - Management of raw material quality during the mining phase.
  - Advance warning to the manufacturing process of unavoidable raw material changes, to allow for the necessary process adjustments.
  - Allow better control of product colour variation in the downstream value chain, such as the despatch and marketing divisions.

1.4. LIMITATIONS OF THE STUDY

The exploration project indicated that several clay layers (domains) were present in the explored area. These domains include both red and light burning clay varieties. The light burning clays include both top-face and chocolate clays. This study focuses only on the light burning top-face clay, which is a constituent in the batching mixes of the Nebraska and Nevada light clay-brick products.

The study does not attempt to explain the geology of the deposit under investigation. Although various clay types occur in the study area, only the top-face clay was chosen for the study. The study is limited to the application of the geostatistical ordinary kriging estimation techniques applied to specific variables that are distributed within the clay layer. The data set is limited to sixty boreholes that were drilled in the study area.

1.5. EXTENT OF THE STUDY

The study were twofold. Firstly, factors such as the mineralogical and chemical composition of clays received theoretical attention in chapter 2. This was done to provide the reader with some understanding of their effect on the final properties of the manufactured brick product. This was followed in chapter 3 by statistical evaluation of stockpile variability over several mining seasons involving samples from stockpile layers. Correlations were drawn between the chemical composition, mineralogical composition and ceramic properties of the.

The second part of the study focussed on geostatistics. The procedure and the theoretical background for modelling and estimating the variables within a deposit were considered. Regional and mine scale geology received attention in chapter 4. Chapters 5 provided a theoretical background on applied geostatistics, whilst Chapter 6 was dedicated to geostatistical analysis of borehole drilled in the exploration area. Variography received attention in Chapter 7 and estimations in Chapter 8.

Chapter 9 concludes the study and the valuable contribution of geostatistics to the field of clay mining and improving ceramic product consistency. Special emphasis was placed on the distribution of the SiO_2, Al_2O_3, Fe_2O_3, K_2O and loss on ignition variables in the top-face clay layer and their effect on the final product. This research report focused on applying the geostatistical technique, ordinary kriging, to assist in modelling the top-face clay with regard to its oxide and loss on ignition distribution within the deposit. Additionally, by doing so, mine planning and, consequently, the quality and consistency of stockpiles year on year could be improved.

CHAPTER 2

CLAY AND CERAMIC FEATURES

2. BACKGROUND LITERATURE

2.1 INTRODUCTION

Since ancient times, clay has been used to model, throw and mould products. When clay is exposed to heat, it changes into a hard, solid, durable product. Clay is the most extensively used raw material in the production of ceramic goods (Grimshaw, 1971). According to Lurie (1984), 'clay', a term used in the context of mineralogy, is a mineral that has different arrangements of hydrated aluminium. Most of the clays in South Africa are used for the manufacture of tiles, pipes, bricks, whitewares, refractories and pottery.

Clay material is distinctly different in its geochemical composition, not only from one location to another, but also between the layers within the same deposit. These different geochemical compositions allow the manufacture of differently coloured face brick products. Understanding the geochemical fingerprint of clays can be useful in controlling the process parameters and the quality of the final clay-brick product.

The following section provides a brief background on the origin of clay, its chemical formation and the minerals present, which are the vital elements in the colour development and physical properties of a face brick product.

2.2 CLAY

2.2.1 Background and origin

Clays are unconsolidated materials with different compositions and they are primarily associated with minerals of detrital or weathered origin (Sacmi, 2002). The diversity of clay occurrences is related to the different formation processes, such as sedimentary deposition, weathering, hydrothermal activity, or the weathering of sedimentary deposits (residual), as well as the origin of the original rock types and the climatic conditions (Deer, Howie and Zussman, 1992).

Velde (2010) explains that clays form because of the interaction between aqueous solutions (water) and rock. Dissolution and recrystallisation occurs and this process causes the creation and alteration of the clay minerals. The type of clay minerals formed depends on the ratio of water and rock, since clay is not stable in an anhydrous environment. The ratio of water and rock determines the type of chemical reaction that will take place and, ultimately, the type of clay that will form. Dissolution is usually the first step in the water-rock interaction. The higher the water to rock ratio, the more elements will be dissolved into solution, while the others remain in the solid state as the framework of the altered rock. During this reaction, voids are produced during the clay forming process.

Figure 2.1 depicts the relationship between the amount of water and rock available for interaction, illustrating the geological phenomena that give rise to the different clay minerals. These geological processes are weathering, deposition of sedimentation, burial, diagenesis and hydrothermal alterations (Velde, 2010).

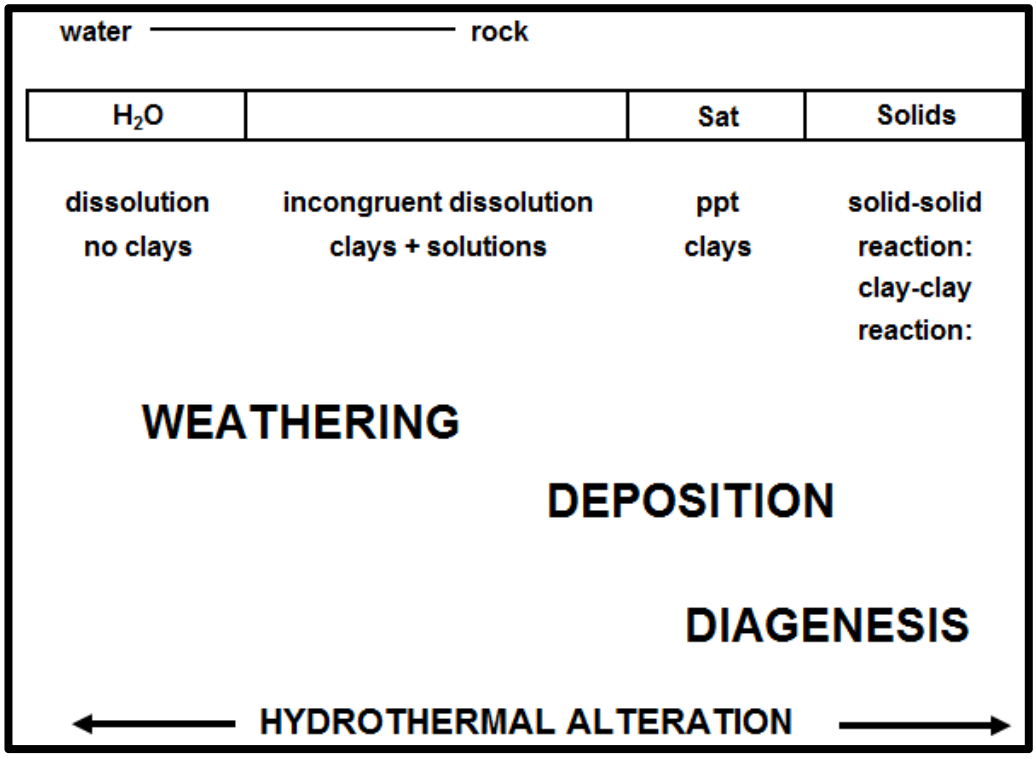


Figure 2-1. Chemical processes and interaction levels responsible for clay minerals (Velde, 2010).

The variety of clays occurs in different environmental settings close to the surface of the Earth. Temperature and time are limiting factors that play a role in the type of clay formed. Clays are stable near the Earth's surface, in temperatures between 50 °C and 80 °C, but change into other minerals beyond these temperatures. Typical changes are micas and feldspars. Figure 2.2 indicates the coordinates for the origin and evolution of clays and their stability over time and temperature.

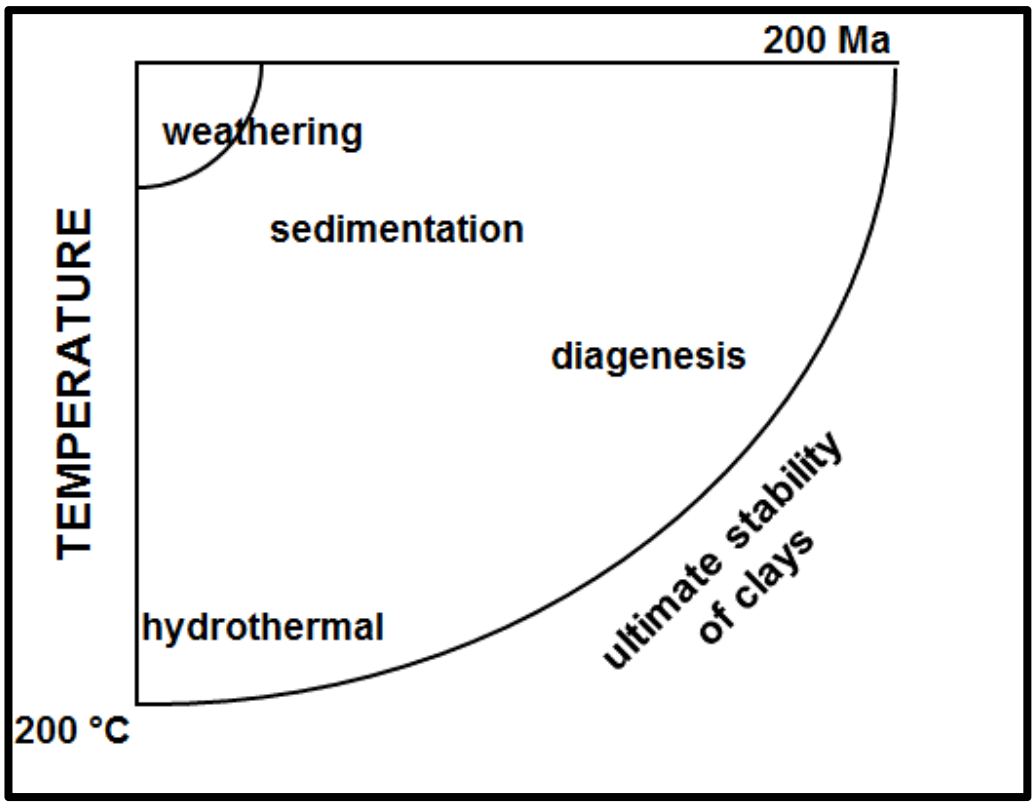


Figure 2-2. Illustration of time-temperature, showing the stability range of clays under weathering, sedimentation, burial digenesis and hydrothermal alteration conditions (Velde, 2010).

Velde (2010) explains that the transportation of clays and their origin begin at the surface of the Earth. The continued deposition eventually results in the burial of the clay and its slow transformation into rock. The rock, in turn, can rise again to the Earth's surface where it will be eroded and altered. Figure 2.3 illustrates the process of clay formation. A logarithmic scale was used on the vertical axis, which depicts depth, to emphasise the scale of the events.

The most common clays are derived from sedimentary deposits from rivers into the sea. As the clay is transported from a freshwater to a salt-water environment, the clay becomes partially flocculated because of the enactment of salt on the suspension. The turbulence of the water causes further segregation of the different clay minerals. Consequently, clays in a coastal area are predominantly kaolinitic-illitic formations, whereas in inland areas the clays are more likely illitic-montmorillonitic (Millot, 1970).

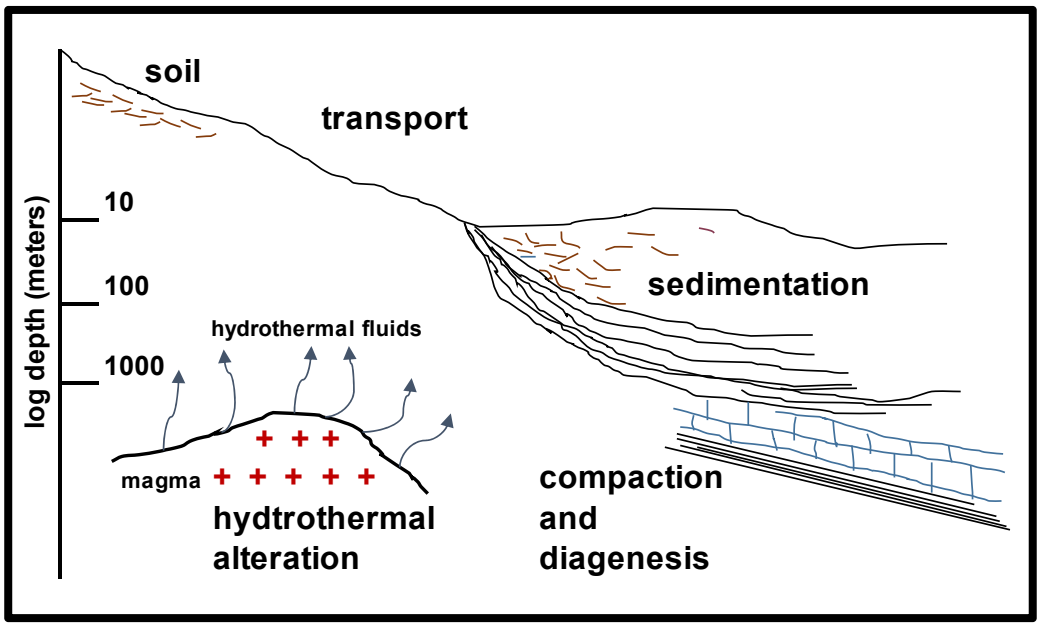


Figure 2-3. The clay cycle illustrated under geological conditions (Velde, 2010).

2.2.2 Chemical formation of clay

The interaction of water and rocks rich in silicate minerals results in the formation of clays. Clay minerals are therefore hydrous minerals, more so than other minerals. The most important reaction in describing the origin of clay is as follows (Velde, 2010):

$$\text{rock} + \text{water} \rightarrow \text{clay} \qquad (2.1)$$

According to Velde (2010), silicate minerals become hydrated by the exchange of the hydrogen in the water. Most clay minerals have (OH) molecules in their structure that impart specific characteristics to them.

According to Millot (1970), the major elements present in clays are Si, Al, Fe, Mg, Na and K.

2.2.3 The alkali ions sodium and potassium

The behaviour of the K^+ ions and the Na^+ ions in solution differs in the hydrosphere because the K^+ ions do not become hydrated and their volume is three times smaller than is that of the Na^+ ions. In solution, the adsorption of the K^+ ions by the fine-grained particles in sediments is preferred. Sodium, for instance, is less abundant in micas than is potassium. Because of the behaviour of the K^+ ions in crystals, the K^+ ions, and not the Na^+ ions, best fit the crystallochemical arrangements needed for the stability of mica. The irregular micas mostly contain the Na^+ ions (Millot, 1970).

2.2.4 Iron and aluminium

Millot (1970) explains that oxidation and reduction conditions play an important role in the weathering process, where the reaction of iron is most important. Iron occurs in both silicates and carbonates, in a reduced form of Fe^{2+}. When iron reaches the hydrosphere with oxygen, it takes on an oxidised form of Fe^{3+}. The equilibrium that existed in the crystalline lattice breaks down, which subsequently makes the crystal vulnerable to weathering. Iron can then be transported in a ferrous (Fe^{2+}) state (in water that is rich in organic matter. When an oxidised environment is reached, the organic matter is destroyed and iron precipitates in the ferric ($Fe3^+$) state.

During weathering, reducing water causes the mobilisation of iron in the ferrous state, either in ferric-humic complexes or in true solution. The iron is subsequently removed and the remaining fraction is released in situ, which subsequently gives rise to iron predominantly in the form of goethite. At the same time, soluble iron reaches the basins downstream in one of the following four forms (Millot, 1970):

- a pigment (in a free state),
- siderite (in a carbonate state),

- colL.o.Idal pyrites of sediments (in the sulphide state), or
- the silicate state.

During diagenesis, iron is inclined to re-enter the silicate structure and the silication of the iron oxide results in the formation of chamosite in iron ore and glauconite in marine deposits and will eventually develop to form chlorite (Millot, 1970).

Alumina, according to Millot (1970), which is similar to iron, enters silicate combinations earlier than iron, because it is hardly mobilised compared with the rapid mobilisation of iron. In regions of moderate weathering, sericites and illites are formed, and in regions of intense weathering, kaolinite is formed. Iron and alumina are both released in the form of a hydroxide in the hydrosphere, but the release is short-lived as they soon occupy the micaceous lattices of chlorite or mica. Iron readily enters into complexes with silica or organic anions, predominantly humic matter.

According to Velde (2010), iron oxide is not a clay mineral, although its particle size is the same as is that of clays. Iron oxides are very noticeable in soils, sediments and sedimentary rocks as they are strong colouring agents and they indicate under what chemical conditions the material containing these oxides had formed. The typical colours of the different iron oxide minerals are given in Table 2.1.

Table 2-1. Typical colours observed for different iron oxide minerals (Velde, 2010).

Colour	Mineral	Composition
Red	Haematite	Fe_2O_3
Yellow to brown	Goethite	α-FeOOH
Orange	Lepidocrocite	γ-FeOOH
Black	Maghemite	FeO

The iron-oxide mineral goethite forms at low pH levels, whereas haematite forms under neutral or high pH conditions in an oxidation environment.

Haematite also forms under arid conditions (a lack of water). Lepidocrocite, on the other hand, forms under reducing, low pH conditions, and maghemite under extreme reducing conditions at a very low pH level (Velde, 2010).

2.2.5 Aluminium and silicon

Millot (1970) explains that although aluminium is similar to iron it is also in certain ways similar to silicon. Silicon, during weathering in an open environment is more soluble than is aluminium. Silicon can be removed in one of two ways. The silicon can be immediately interrupted during its migration to the subterranean weathering horizons, where argillaceous and siliceous neoformations form in the weathering profiles. Or the migration lingers on where the silica collects in the sedimentary basins, and reorganises, which gives rise to the argillaceous and siliceous neoformations in the sediments.

If drainage is strong enough for the silica to be removed in solution, the remaining alumina can crystallise into gibbsite. Frequently, however, water solutions constantly provide silica to alumina, which is required for the formation of clay minerals. Aluminium and silicon elements recombine as soon as they are released and they tend to organise together into clay. If they do not recombine, alumina remains in situ with iron, and silica is removed with the minerals lime and magnesia.

2.3 CLAY MINERALS

Clays are classified under phyllosilicates because their particles are shaped in a sheet-like form and they are flatter rather than long and wide. The nature of the structure is such that the strongest forces are in a two-dimensional arrangement. The tighter the atoms are packed together, the stronger the bond is, and the weaker the bond, the more loosely the atoms are packed and the easier the bonds can be broken. The strongest bonds in a two-dimensional arrangement will cause crystals to grow faster in this direction, resulting in a sheet-like structure. The ratio of thickness to width and length in phyllosilicates is in the order of 1 to 20 (Velde, 2010).

According to Velde (2010), the ionic bonds in clay minerals are highly covalent, with about half the ions being oxygen, while the remaining major cations are silicon and aluminium.

Kingery *et al.* (1976) explains that the properties of clays depend mainly on their structures. Different clay minerals have different combinations of silicate layers, including other cations and hydroxyl ions. The mineral clay types are defined by the specific arrangement of SiO_4-tetrahedron layers, including the cation and hydroxyl ions. Typical phyllosilicates include kaolinite, montmorillonite, pyrophyllite, palygorskite and illite.

2.3.1 Kaolinite

Kaolinite is used in the production of bricks and ceramics and as a coating/filler for papers, plastics and paints (Deer, Howie, and Zussman, 1992). According to Millot (1970), the name kaolin comes from a hill in China called Kaolin, where kaolin has been extracted for centuries. Kaolinite is a layered silicate mineral with two sheets, octahedral and tetrahedral. Oxygen ions occupy the tetrahedral tips, with the centre occupied by silicon oxide that is shared by the four oxygen ions. The six tips of the octahedral sheet are occupied by oxygen ions or hydroxyl groups, with the centre occupied by aluminium oxide. A kaolin layer is formed by a linked silica tetrahedral sheet and alumina octahedral sheet (Fig. 2.4).

According to Deer, Howie and Zussman (1992), minor variation in the chemical composition of kaolin occurs with lesser amounts of different ions present. It is suggested that these ions (Fe, Cr, Ti, Mg and K) are present because of impurities, such as anatase or rutile, or in interlayered mica, and does not form part of the kaolinite structure. The cation exchange capacity of kaolinite is low compared with other clays such as illite and smectite, while its anion exchange capacity is higher compared with most clay.

2.3.2 Illite/Mica/Muscovite

The term illite, according to Millot (1970), is derived as a group name from the state of Illinois in America. The name was originally given to the entire group of clay minerals with structures similar to mica.

Millot (1970) explains that in the clay structure forming the four silicon ions, less than one of the ions is replaced by an aluminium ion, which causes a balanced decrease of alkali ions between the layers. Frequently, Mg, Fe^{2+} and Fe^{3+} ions partially replace Al octahedral ions.

According to Deer, Howie and Zussman (1992), illite is chemically different from muscovite in that it contains less potassium and more silica, with a clay particle size of < 2 μm, and it is similar to mica. Illite has an ion exchange capacity greater than that of kaolin, but noticeably less than that of smectite. Illite dehydrates at different stages. The water adsorbed on the surface of the particles and interlayered sheets is released rapidly below 110 °C, and the remainder between 110 °C and 350 °C. With the release of $(OH)^-$ ions, water is released between 350 °C and 600 °C, whereas mica loses little to no water (Deer, Howie and Zussman, 1992).

2.3.3 Smectite

Smectite is closely related to mica, except for the bonds between the layers that are weaker than are those of mica. The weaker bonds allow water to enter between the layers, causing an inconstant stacking periodicity (Millot, 1970).

Deer, Howie and Zussman (1992) explains that smectite shows expandable properties because of the water or organic molecule uptake between its structural layers, and it has a marked cation exchange capacity. The smectite type depends on the amount of interlayer water adsorbed, the nature of the interlayer cations and the physical condition. Smectite is useful in the manufacture of bricks, ceramics, paper, rubber, paints, drilling muds and moulding sands.

2.3.4 Feldspar

The feldspar minerals are the most abundant constituents of igneous rocks, with a wide range of compositions. Most feldspars are chemically classified as members of the ternary system $NaAlSi_3O_8$ (albite, Ab)–$KAlSi_3O_8$ (K-feldspar, Or)–$CaAl2Si_2O_8$ (anorthite, An). The alkali feldspars are those with compositions between $NaAlSi_3O_8$ and $KAlSi_3O_8$, while those between $NaAlSi_3O_8$ and $CaAl2Si_2O_8$ are the plagioclase feldspars (Deer, Howie and Zussman, 1992).

2.3.5 Quartz

According to Deer, Howie and Zussman (1992), quartz is one of the most abundant minerals, occurring in sedimentary, metamorphic and igneous rocks. There are three principle crystalline forms of SiO_2, namely quartz, tridymite and cristobalite, each with its own distinct crystal structure. Cristobalite and tridymite are high-temperature forms of SiO_2. Quartz, the low-temperature form of SiO_2, usually consists of almost 100 percent SiO_2, with other oxides present in minor proportions as small inclusions.

2.3.6 Haematite

The ideal composition for haematite is Fe_2O_3 and, in fine powder form, it is distinguished from magnetite and ilmenite by its bright red colour. It is a rare mineral in igneous rocks and occurs mainly in sediments. In sediments, it is the major cause of the red coloration of rocks (Deer, Howie and Zussman, 1992).

Goethite, according to Deer, Howie and Zussman (1992), is a weathering product of iron-bearing minerals such as magnetite, pyrite and siderite, and is formed under oxidation conditions. If dehydrated, goethite (α-FeO.OH) is transformed into haematite (α-Fe_2O_3).

2.4 CLAY OCCURRENCES IN SOUTH AFRICA

Lurie (1984) explains that the majority of clays in South Africa could be classified as either kaolinite or montmorillonite, as is presented in Table 2.2. Lurie (1984) further explains that clays are seldom found in their purest form but they are usually a mixture of several major clay minerals and

some minor minerals. The usability of clay can be determined by practical laboratory tests (physical analysis) to establish their suitability for use in the manufacturing of ceramic products.

2.5 RAW MATERIALS FOR BRICK MAKING

Stein (1982) explains that although different clays are used to manufacture bricks, the relationship between the properties of the clays and their industrial behaviour has not been sufficiently studied, mainly because of the enormous variety of clay types. The minerals present in the clay types influence the drying, forming, firing behaviour, colour and quality of the brick product. Quantifying the chemical and mineralogical composition of the clays assists in determining the suitability of the clay for brick making. The most important properties of clays are determined by their mineralogical composition. Clay minerals are silicates that form plate-like crystals. These minerals consist of SiO_4 tetrahedral silica sheets that are linked to one or two octahedral sheets of Al $(O\text{-}OH)_6$ (two-layer minerals), or Mg $(O\text{-}OH)_6$ (three-layer minerals). In both these sheets, individual elements can be replaced by other elements and the charge imbalance is countered by additional elements in the crystal lattice. Occasionally, a negative surplus charge remains, which is then balanced by the adsorption of cations between the individual layers. Water is often stored in the interstitial layers, giving the clay high-swelling properties.

Table 2-2. Typical colours observed for different iron oxide minerals (Velde, 2010).

Clay	Classification	Description	Occurrence
Kaolin	China clay	Soft white, impurity free	Cape Peninsula, West-Stellenbosch, Kommetjie–Fish Hoek, Saldana Bay, Vanrhynsdorp
	Ball clay	Plastic, burning white Represent kaolinised granite, transported with organic material	Stellenbosch
	Fire clay	Refractory and subdivided into types based on their physical properties. Flint clay (bulk density > 2.3) Plastic fire clay (bulk density < 1.90) Occurs in Ecca shales	Witwatersrand, North and East Pretoria, Hammanskraal, Middelburg, Belfast, Soutpansberg
Shale		Weathering of the Bokkeveld shales, some are classed as ball clays.	Aberdeen–Riversdale
Residual clays	Various types	Derived from Dwyka shale and tillite	Grahamstown
Bentonite	Montmorillonite	Variable-swelling clay, formed from weathered volcanic tuff at the base of the Ecca Group.	Koppies

2.6 IMPORTANT MINERALS FOR BRICK MAKING

According to Stein (1982), the most essential minerals for the manufacturing of high-grade clay-brick products are kaolinite, illite and quartz. Kaolinite provides good sintering behaviour, while illite provides plasticity and quartz provides stability.

Non-essential minerals, such as:

- Iron oxide is responsible for the red colouring of the brick.
- Chlorite and muscovite provide the early liquid or glass phase to the brick.
- Organic materials present in large quantities can cause black coring.

2.6.1 The effect of minerals on the firing behaviour and properties of the ceramic ware.

During the firing process, new mineral and liquid phases are formed, which, upon cooling, are transformed into glass. The type and range over which these changes occur depend on the mineralogical composition of the clays, grain size distribution, chemical composition of the raw materials used, heating rate, firing temperature, soaking time at high temperatures, the shape of the brick, the kiln atmosphere and the vapour pressure. The changes occurring during the firing process are illustrated in Figure 2.4 (Stein, 1982).

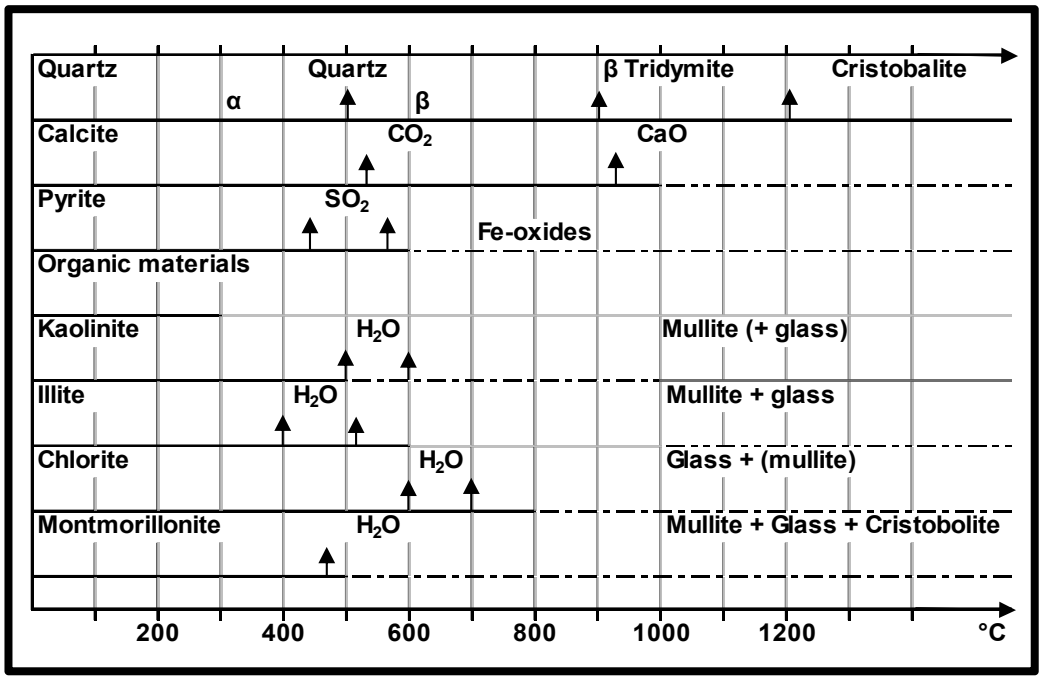


Figure 2.4. Mineral changes occurring during firing of raw materials (Stein, 1982). Continuous lines indicate that the lattice is largely unchanged, dashed lines indicate different changes in the crystal lattice.

Kaolinite

Stein (1982) explains that kaolinite is a high-temperature mineral and forms no glass phase. Sintering temperatures of up to 1 200 °C are needed to promote the formation of high-temperature minerals (mullite and cristobalite). Disordered kaolinite, however, forms mullite at lower temperatures. The mullite formation from kaolinite can also incorporate Fe-ions. In this form, the iron will not contribute to the red colouring of the ceramic body and the amount present in the lattice will depend on the temperature. Mullite changes colour from white to yellow with increasing temperature (Brownell, 1976). An iron content of < 1 percent in kaolinitic clays is required to ensure a pure white ceramic body. However, a reducing atmosphere, according to Brindley (1974), accelerates mullite formation, which incorporates high product strength at low temperatures. The presence of illite and other fluxes in the clay does not allow the necessary high temperatures to be reached, because of the excessive liquid phase formation.

Illite

Illite is high in K_2O and therefore has a low melting point (1 050 °C to 1 150 °C). Between 1 030 °C and 1 100 °C, firing shrinkage is extensive in this temperature range upwards and steady phases are formed here in the ceramic body. Iron is also contained in the illite lattice and is released at approximately 900 °C as red haematite. In the absence of CaO, the red colouring of the ceramic body will continue (Stein, 1982).

Montmorillonite

This mineral has a variable composition and will produce different high-temperature phases according to the type of composition. Iron is common in the lattice and, during firing, iron is released as haematite at approximately 800 °C. A red-coloured product will be produced if adequate amounts are present in the body (Stein, 1982).

Mica

Micas, according to Stein (1982), (present in muscovite and sericite) introduce K_2O to the ceramic body. K_2O is a good flux and promotes liquid phases at a temperature as low as 950 °C, with a short sintering range. Clays high in mica present difficulties during the firing stage because of the early liquid phase formation (Brownell, 1976). This can be improved by the addition of CaO, or pure kaolinitic clay.

Quartz

This mineral, present in lime-free clay, acts as a filler or stabiliser, with barely any reaction with the clay minerals. Quartz increases the permeability of the ceramic body, promoting the release of gas. Excessive quantities reduce the compressive strength of the body owing to cooling cracks. The latter result from the inversion of α to β quartz at 573 °C, which is associated with a high-volume change (Stein, 1982).

Iron oxides

According to Stein (1982), iron oxide present in the range 4–8 percent and in the absence of MgO and CaO, promotes an intense red colour to the ceramic body because of the formation of haematite (Fe_2O_3). It is an

advantage to have an even distribution of fine-grained iron oxides in the clay. The red colour of the ceramic product is enhanced during the firing process when haematite is formed because of the decomposition of other minerals. At low temperatures, an orange colour develops, which darkens as the temperature increases to an intense red colour. A reducing atmosphere. The colour of haematite is dependent on the temperature in the kiln and results in the formation of magnetite (Fe_3O_4) and wustite (FeO), both of which are black in colour compared with the red colour of the haematite. Changing the kiln atmosphere behind the firing zone from reducing to oxidising, causes the magnetite and wustite to re-oxidise and the bricks acquire irregular red patches (Figs 1.4 and 1.5).

Organic material

Carbon (coal) and hydrocarbons can generally be found in combination with grey, blue-grey and black clays and, to some extent, in light-grey and grey clays, but seldom in red and yellow clays. The organic material is often the cause of black coring and these materials should be burned out before the liquid formation commences (Stein, 1982).

2.7 THE CHEMICAL COMPOSITION OF BRICK MAKING CLAYS

The alkali content in clay is important as it affects the sintering behaviour of the clay. High-alkali content induces early vitrification, high-firing shrinkages and black coring. Al_2O_3, associated with clay minerals, also increases the firing shrinkage and, in association with alkalis, high-density bodies are produced.

2.8 VARIABLES CHOSEN FOR THE STUDY

The ceramic behaviour of raw materials is influenced by various factors, as can be seen from the preceding sections. This study only focusses on the chemical distribution of variables in the clay and not on the distribution of the minerals and ceramic properties. The relationship between the chemical composition, mineralogical composition and ceramic properties becomes important for predicting the behaviour of the clay material during the manufacturing process.

The type of minerals present significantly affects the ceramic behaviour of a material. For instance, the K_2O derived from mica will behave differently from K_2O derived from a feldspar during the firing process. To further complicate matters, K_2O will influence the colour of a ceramic product differently in the presence of Fe_2O_3 and even the fluctuation thereof, than on its own. Due to the specific thermal behaviour of the chemical variables in clays, it is important to understand the relationship between the chemical variables, the mineral composition and ceramic properties, if mine planning is to be improved.

The relationship between the chemical composition, mineralogical composition and ceramic properties requires some characterisation. Correlation is a valuable statistical tool for this purpose. The correlation will provide some insight into the relationship between the chemical composition, mineral composition and ceramic properties. The chemical variables modelled/estimated can then be used for predicting the mineral composition and ceramic behaviour of the clay in the deposit.

The chemical composition of the clay studied is given in Table 1.2 and was obtained from 350 samples taken from 70 stockpile layers.

Table 2-3. Chemical composition and descriptive statistics of top face clay from 350 individual samples taken from 70 stockpiles layers constructed.

	SiO_2	Al_2O_3	Fe_2O_3	TiO_2	CaO	MgO	Na_2O	K_2O	L.O.I.
Average	55.10	27.19	5.40	1.15	0.06	0.30	0.04	1.95	8.74
Mininum	46.36	15.63	0.76	0.78	0.00	0.12	0.00	0.24	3.85
Maximum	71.41	36.74	14.40	1.75	0.40	0.66	0.23	3.26	17.92
Range	**25.05**	**21.11**	**13.64**	0.97	0.40	0.54	0.23	**3.03**	**14.07**
Standard Deviation	**4.31**	**5.07**	**3.54**	0.25	0.04	0.08	0.04	**0.88**	**2.18**
Variance	**18.59**	**25.70**	**12.53**	0.06	0.00	0.01	0.00	**0.77**	**4.76**

The table shows SiO_2, Al_2O_3, Fe_2O_3, TiO_2, K_2O and L.o.I. to be the main variables present. The data indicate high variability in the SiO_2, Al_2O_3, Fe_2O_3, K_2O and L.o.I. Because these variables, in combination, affect the ceramic behaviour of the clay, it is crucial to understand their relationships.

Choosing only one chemical variable will be an injustice to understanding the ceramic behaviour of the material for future mine planning. Choosing only Fe_2O_3 without considering the presence of K_2O would ignore the major effect that the combination of the two exerts on the colour of the ceramic product. Likewise, choosing only SiO_2 and not considering Al_2O_3 would ignore the major effect on the shrinkage behaviour that the combination of the two brings about in the ceramic product. It is for this reason that the variables chosen, namely; SiO_2, Al_2O_3, Fe_2O_3, K_2O and L.o.I were studied in relation to one another to clearly define and characterise the deposit. The correlation between the chemical variables, the mineral composition and ceramic properties will further assist with improving mine planning and raw material quality control. The second section in Chapter 3 is devoted to correlation, which measures linear relationships and is most appropriate for normal (symmetrical) data.

2.9 SUMMARY

The geochemical composition of clays is different at different locations and between the layers of the same deposit. The variety of clay occurrences is associated with the different formation processes. The properties of clays are determined by their structures. Different clay minerals have different combinations of silicate layers, cations and hydroxyl ions. The majority of clays in South Africa can be classified as either kaolinite or montmorillonite and are seldom found in a pure form. The most important characteristics of clays are determined by their mineralogical composition. Different clay minerals affect the drying, forming, firing behaviour, colour and quality of the brick product in different ways. Laboratory tests (full physical analysis) can indicate the suitability of clays for the manufacture of ceramic products. The minerals most essential for the manufacturing of clay-brick products are kaolinite, illite and quartz.

During the firing process, new mineral and liquid phases are formed. Kaolinite forms mullite, which changes colour from white to yellow with increasing temperature. Illite has a low melting point and the iron in its lattice, also present in montmorillonite, promotes a red colour. Micas are

good fluxes and introduce short sintering ranges. Quartz is a stabiliser, which increases permeability and promotes gas release. Iron oxide promotes a red product colour, which is further enhanced when haematite is formed on the decomposition of the other minerals during the firing process. Organic material causes black coring, and alkalis in clays affect the sintering behaviour.

CHAPTER 3

STOCKPILE CLAY SAMPLES AND THEIR CERAMIC PROPERTIES

3. CLAY CHARACTERISTICS AND CERAMIC PROPERTIES

The origin of clay and the environment in which it formed define its ceramic characteristics during the manufacturing process. Applied analytical techniques, such as X-Ray Fluorescence (XRF) and X-Ray Diffraction (XRD) are well-established methods used to identify the chemical and mineral composition of these minerals. In addition to the identification of the clay characteristics, full physical analysis (i.e. determining ceramic properties) provides insight into the physical behaviour of the material during the forming and firing processes. A combination of these analytical techniques can be used to define the behaviour of the clay material during the manufacturing process and this is integral to the characterisation of the raw material.

3.1 VARIABILITY OF OXIDES IN CLAYS

The variability of SiO_2, Al_2O_3, Fe_2O_3, K_2O and loss on ignition variables for 350 samples obtained from 70 stockpile layers were highlighted in the preceding chapter and will be the focus of this study. The fluctuation of these stockpile layer variables is illustrated in Figure 3.1. The histograms are depicted in Figure 3.2, and Table 3.1 provides the summary statistics. The latter were obtained using the data analysis tool pack function in Microsoft Office Excel software with continuous data.

3.1.1 Variability of SiO_2, Al_2O_3, Fe_2O_3, K_2O and Loss on Ignition

Figure 3.1 and Table 3.1 illustrate that SiO_2 varies between 46.36 % - 71.41 %, Al_2O_3 between 15.63 % - 36.74 %, Fe_2O_3 between 0.76 % - 14.40 %, K_2O between 0.24 % - 3.26 % and loss on ignition (L.o.I) between 3.85 % - 17.92 %. The range, which is the difference between the maximum and minimum sample values, also illustrates the variability. These fluctuations are of note. Minimizing the variability can greatly improve the ceramic behaviour and colour consistency of the final brick product.

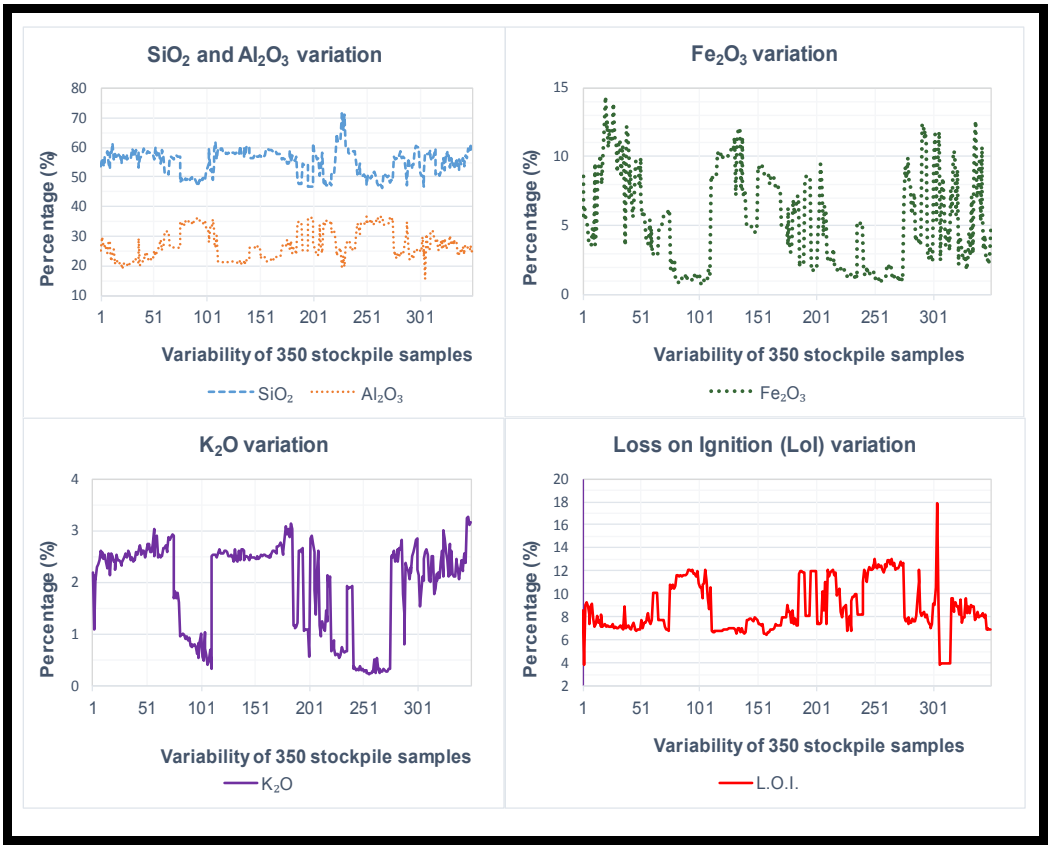


Figure 3-1. Variability of SiO_2, Al_2O_3, Fe_2O_3, K_2O and Loss on Ignition in 350 samples from 70 stockpile layers.

Table 3-1. XRF summary statistics of the 350 stockpile samples.

Descriptive statistical summary	SiO_2	Al_2O_3	Fe_2O_3	K_2O	L.O.I.
Measure of location	**Central tendency**				
Mean	55.13	27.12	5.44	1.96	8.72
Median	56.37	25.97	4.94	2.42	7.95
Mode	56.20	21.00	10.10	2.48	7.29
Measure of spread	**Dispersion or variability about the mean**				
Standard deviation	4.29	5.06	3.54	0.87	2.17
Variance	18.43	25.65	12.53	0.76	4.72
Range	25.05	21.11	13.64	3.03	14.07
Minimum	46.36	15.63	0.76	0.24	3.85
Maximum	71.41	36.74	14.40	3.26	17.92
Measure of shape	**Departure from symmetry**				
Kurtosis	3.27	1.94	1.89	2.15	3.14
Skewness	-0.08	0.44	0.38	-0.82	0.55

3.1.2 The descriptive statistical summary of the SiO_2, Al_2O_3, Fe_2O_3, K_2O and Loss on ignition variables

To describe the distribution of the variables, descriptive statistics were used. The mean and the standard deviation are two descriptive statistical measures that are utilised for describing the distribution. Whilst the mean describes the centre of the distribution, the variance provides a great amount of information about the normal distribution. The mean and variance for each variable is given in Table 3.1 and the histograms in Figure 3.2. The dispersion of values about the mean for all variables are greater than zero. This indicates that values are indeed dispersed about the mean. The higher the value the greater the dispersion. The dispersion about the mean, in descending order are Al_2O_3 (25.65), SiO_2 (18.43), Fe_2O_3 (12.53), L.o.I (4.72) and K_2O (0.76).

The mean, median and mode are measures of location or central tendency. The mean is the arithmetic average of the data values, the median the midpoint of the arranged values in increasing order and the mode simply the value that occurs most frequently. The mean, median and mode for SiO_2, Al_2O_3, K_2O and L.o.I are similar and it can be deduced that their distributions are symmetrical/normal. The mean and median for Fe_2O_3 are also similar, but the mode notably higher than both the mean and median, indicating skewness. From Figure 3.2 and statistics in Table 3.1 it is shown that Al_2O_3, Fe_2O_3 and loss on ignition are positively skewed (median < mean) with a longer tail of high values to the right. The median is higher than the mean for SiO_2 and K_2O indicating they are negatively skewed, with longer tails of small values to the left. From the histograms presented in Figure 3.2 it can be deduced that the variables under investigation are all symmetric/normal.

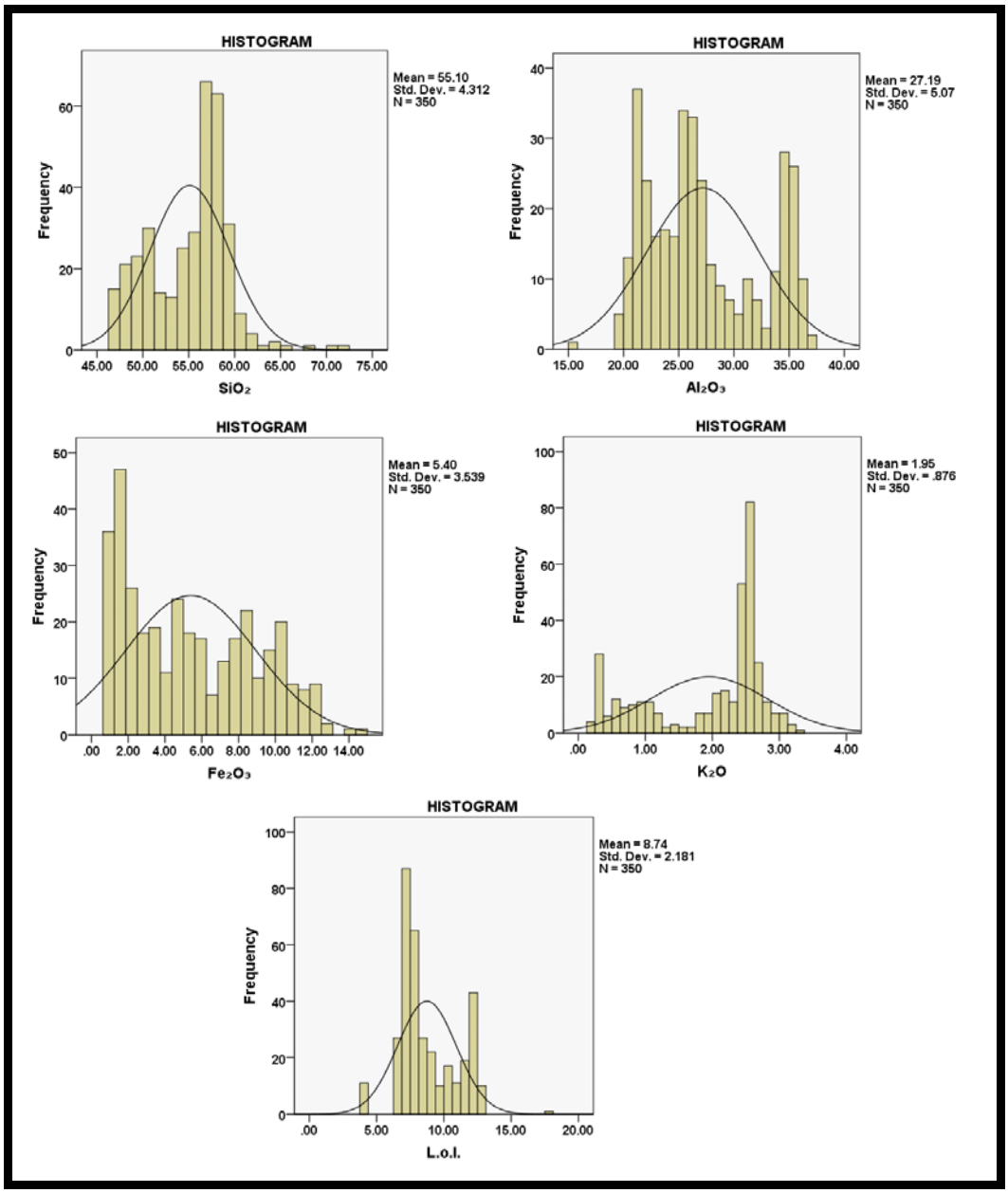


Figure 3-2. Histograms for SiO_2, Al_2O_3, Fe_2O_3, K_2O and Loss on Ignition for the 350 stockpile samples.

3.1.3 Summary of stockpile clay sample variables

The graphs and summary statistics confirm the symmetric nature of the SiO_2, Al_2O_3, K_2O, Fe_2O_3 and L.o.I variables. The histograms reveal bimodal data, which indicates mixed populations and would require domaining. Latter is a spatial volume with consistent geology, a single grade population and a single search orientation. The chemical variability

observed from the stockpile data would indicate that different geological domains are used for constructing the top-face stockpile.

K_2O is a fluxing agent and Fe_2O_3 a strong colourant. These variables are sensitive to the oxidation/reduction atmosphere in the kiln. The kiln atmosphere is mainly determined by the organic material and the carbon in the raw material, the fuel used and the oxygen supply to the kiln. Carbon is introduced as an additive to the brick recipe prior to manufacturing to induce a flash/reduction mark on the face of the brick (Fig. 1.4). The fluctuation in carbon content changes the kiln atmosphere. Increased carbon will induce a reduction atmosphere, which, in turn, will cause the flash to intensify if the Fe_2O_3 content is high. An increased K_2O content will promote early liquid phases and cause increased shrinkage, resulting in product size reduction and, in the presence of Fe_2O_3, an intensified darker colour. The fluctuation of these variables therefore necessitates strict control, especially if the colour and size of the product are to be consistent year after year.

3.2 THE CORRELATION BETWEEN OXIDES, MINERALS AND FULL PHYSICAL PROPERTIES

The preceding section indicates that the variables under investigation are symmetrical/normally distributed. In Chapter 2 attention was drawn to the effect of the chemical composition and mineral composition on the ceramic behaviour of clay materials during the manufacturing process. Because this study focusses only on the geochemical distribution of five chemical variables it is important to demonstrate the relationship between the chemical composition, mineral composition and ceramic properties of the clay investigated. The presence/absence of certain chemical constituents assists in determining the behaviour of the material during firing, but rarely provides information on the workability of the material, for instance the extrusion moisture and dry shrinkage. For this reason the mineral composition is of great importance and therefore the emphasis on the relationship between the mineral, chemical and ceramic properties is crucial.

The chemical, mineral and ceramic property data were obtained from eight stockpiles. Generally one stockpile is constructed per year, depending on demand. Each stockpile consist of at least ten layers with five samples per layer. A stockpile therefore generally represents approximately 50 samples. The relationships between the chemical composition, mineral composition and ceramic properties of these stockpiles were determined using the Pearson correlation coefficient due to the symmetrical nature of the data.

The Pearson correlation coefficient (ρ) calculates an index which measures the nature of the relationship between variables. The coefficient varies over a range of +1 to -1 and indicates the estimated linear relationship of the sampling data. It reveals both the direction and magnitude of the relationship and the degree to which the variables move together or in opposite directions (Cooper & Schindler, 2003).

Table 3.2 depicts the correlation index of the mineral, chemical and ceramic property variables, and their corresponding scatterplots are given in Figures 3.3 to 3.5 respectively.

Table 3-2. Correlation between chemical, mineral and ceramic variables from 8 stockpiles with each stockpile generally representing 10 layers of 5 samples each (approximately 50 samples).

Pearson Correlation, N=8	Haematite	Quartz	Kaolinite	Mica	Illite/Smectite Interstratification	SiO_2	Al_2O_3	Fe_2O_3	K_2O	L.o.I	Extrusion moisture	Dry shrinkage	Fired shrinkage	Water absorption	Compressive strength
Haematite	1.0														
Quartz	0.1	1.0													
Kaolinite	-0.4	-0.9	1.0												
Mica	0.6	0.7	-0.9	1.0											
Illite/Smectite interstratification	-0.4	0.0	0.1	-0.4	1.0										
SiO_2	-0.2	0.5	-0.4	0.3	-0.3	1.0									
Al_2O_3	0.1	-0.6	0.6	-0.5	0.1	-0.9	1.0								
Fe_2O_3	0.4	0.1	-0.5	0.6	0.1	-0.3	0.0	1.0							
K_2O	-0.1	0.5	-0.6	0.5	0.0	0.7	-0.9	0.3	1.0						
L.o.I	0.0	-0.6	0.6	-0.6	0.2	-0.9	0.9	-0.2	-0.9	1.0					
Extrusion moisture	-0.1	-0.9	0.8	-0.5	-0.2	-0.6	0.8	-0.1	-0.7	0.7	1.0				
Dry shrinkage	0.0	-0.8	0.7	-0.6	0.2	-0.8	0.9	0.1	-0.7	0.8	0.8	1.0			
Fired shrinkage	0.8	0.2	-0.5	0.7	-0.2	-0.3	0.1	0.7	0.1	-0.1	-0.1	0.1	1.0		
Water absorption	-0.7	-0.5	0.7	-0.7	-0.1	-0.1	0.3	-0.7	-0.5	0.5	0.6	0.4	-0.8	1.0	
Compressive strength	0.9	0.2	-0.5	0.6	-0.1	-0.3	0.1	0.7	0.1	-0.1	-0.2	0.1	0.9	-0.9	1.00

3.2.1 Correlation between chemical composition and mineral composition

Figure 3.3 depicts the scatterplots of the mineral and chemical variables present in the stockpile samples and Table 3.2 provides their correlation indices. The scatterplots indicate the strength of the linear relationship between the variables. Haematite has a strong positive relationship with Fe_2O_3 and mica. Quartz a strong positive relationship with SiO_2, K_2O and mica and a strong negative relationship with Al_2O_3, L.o.I and kaolinite. Kaolinite has a strong positive relationship with Al_2O_3 and the L.o.I, and a strong negative relationship with Fe_2O_3, K_2O and mica. Mica, on the other hand, has a strong positive relationship with Fe_2O_3 and K_2O and a strong negative relationship with Al_2O_3 and L.o.I. These relationships would indicate that Fe_2O_3 is likely to be accounted for by the presence of haematite and mica, SiO_2 and K_2O from quartz and mica and Al_2O_3 and L.o.I from kaolinite. These relationships indicate that the chemical variables can be used to predict the mineral present.

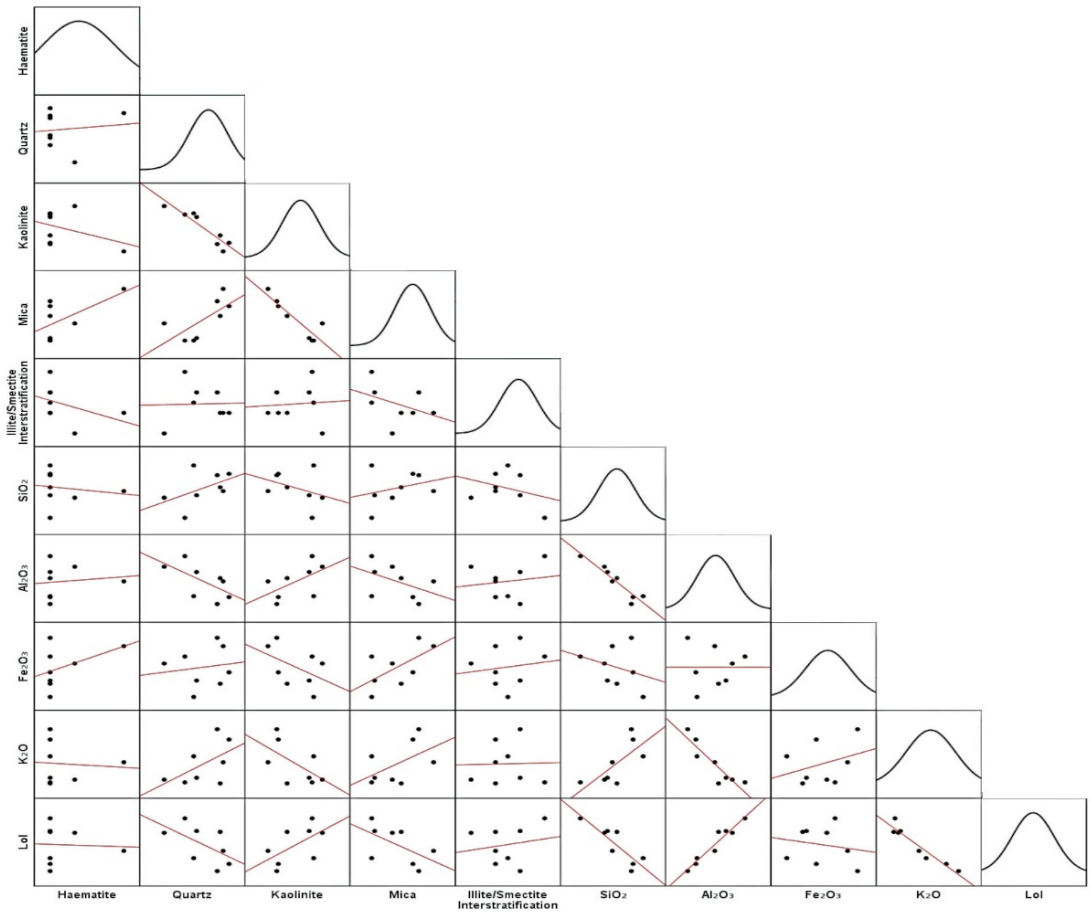


Figure 3-3. Scatterplots between the mineral and chemical variables.

3.2.2 Correlation between mineral composition and ceramic properties

The preceding section provided some insight into the relationship between the chemical and mineral composition within the clay. This section attempts to demonstrate the relationship between the mineral composition and the ceramic properties of the clay. The correlation indices are summarised in Table 3.2 and linear relationship shown by scatterplots in Figure 3.4.

Haematite has a very strong positive relationship with fired shrinkage and compressive strength and a very strong negative relationship with water absorption. Quartz has a strong negative relationship with extrusion moisture, dry shrinkage and water absorption, whereas kaolinite has a strong positive relationship with extrusion moisture, dry shrinkage and water absorption, and a strong negative relationship with fired shrinkage and compressive strength. Mica has a strong positive relationship with fired shrinkage and compressive strength and a strong negative relationship with extrusion moisture, dry shrinkage and water absorption.

Determining the relationship between the minerals present and the ceramic properties can assist with predicting ceramic behaviour of the material during the manufacturing process. In section 3.2.1 the relationship between the chemical composition and the mineral composition were determined. In this section the relationship between the mineral composition and ceramic properties was determined. The section to follow will illustrate the relationship between the chemical composition and ceramic properties.

The negative and positive correlations between the minerals and the ceramic properties of the material emphasise the importance of the role these minerals play in the behaviour of the material during the manufacturing process. It is shown that the clay mineral kaolinite play an important role in both the unfired and the fired briquettes. Extrusion moisture, dry/fired shrinkage and water absorption increase and compressive strength decrease with an increase in kaolinte. Mica, which introduces a liquid phase, plays an important role in enhancing the compressive strength of the material. An increase in haematite contribute to higher compressive strengths and lower water absorptions.

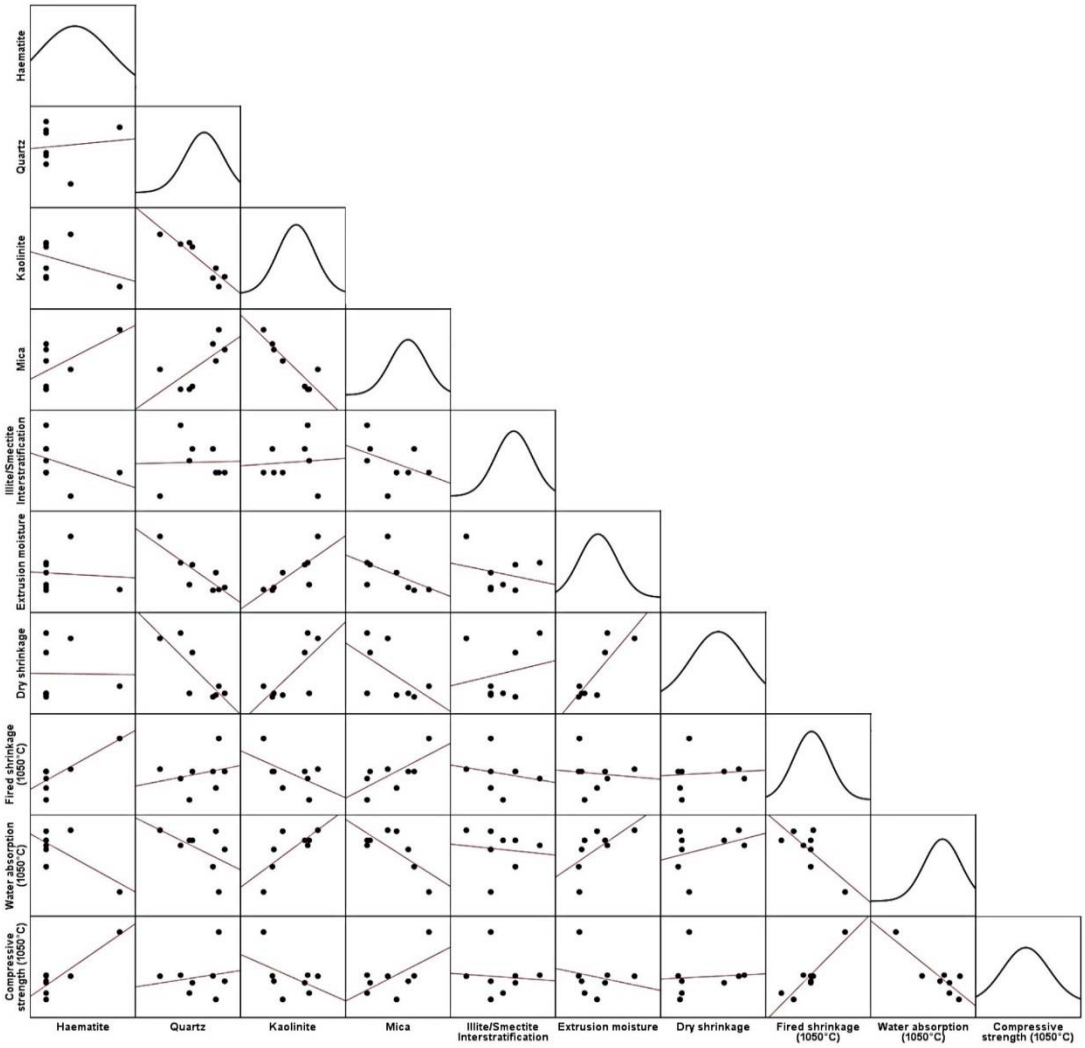


Figure 3-4. Scatterplots between the mineral and ceramic property variables.

3.2.3 Correlation between chemical composition and ceramic properties

Figure 3.5 illustrates the scatterplots between the chemical variables and the ceramic properties of the eight top-face clay stockpiles. SiO_2 has a weak negative relationship with fired shrinkage and compressive strength and a strong negative relationship with extrusion moisture, dry shrinkage and water absorption. Al_2O_3 and L.o.I have a strong positive relationship with extrusion moisture and dry shrinkage and a very weak relationship with fired strength and compressive strength. L.o.I also has a strong positive relationship with water absorption, as opposed to Al_2O_3 with a weaker relationship to water absorption. K_2O reveals a weak positive relationship with fired shrinkage and compressive strength, and a strong negative relationship with extrusion moisture, dry shrinkage and water

absorption. Fe_2O_3 has a very strong positive relationship with fired shrinkage and compressive strength, a weaker positive relationship with drying shrinkage, a very strong negative relationship with water absorption and a somewhat weaker negative relationship with extrusion moisture.

The correlation between the chemical composition and the ceramic properties indicates the significance of the relationships. Not only do the minerals correlate with the ceramic properties but also with the chemical composition.

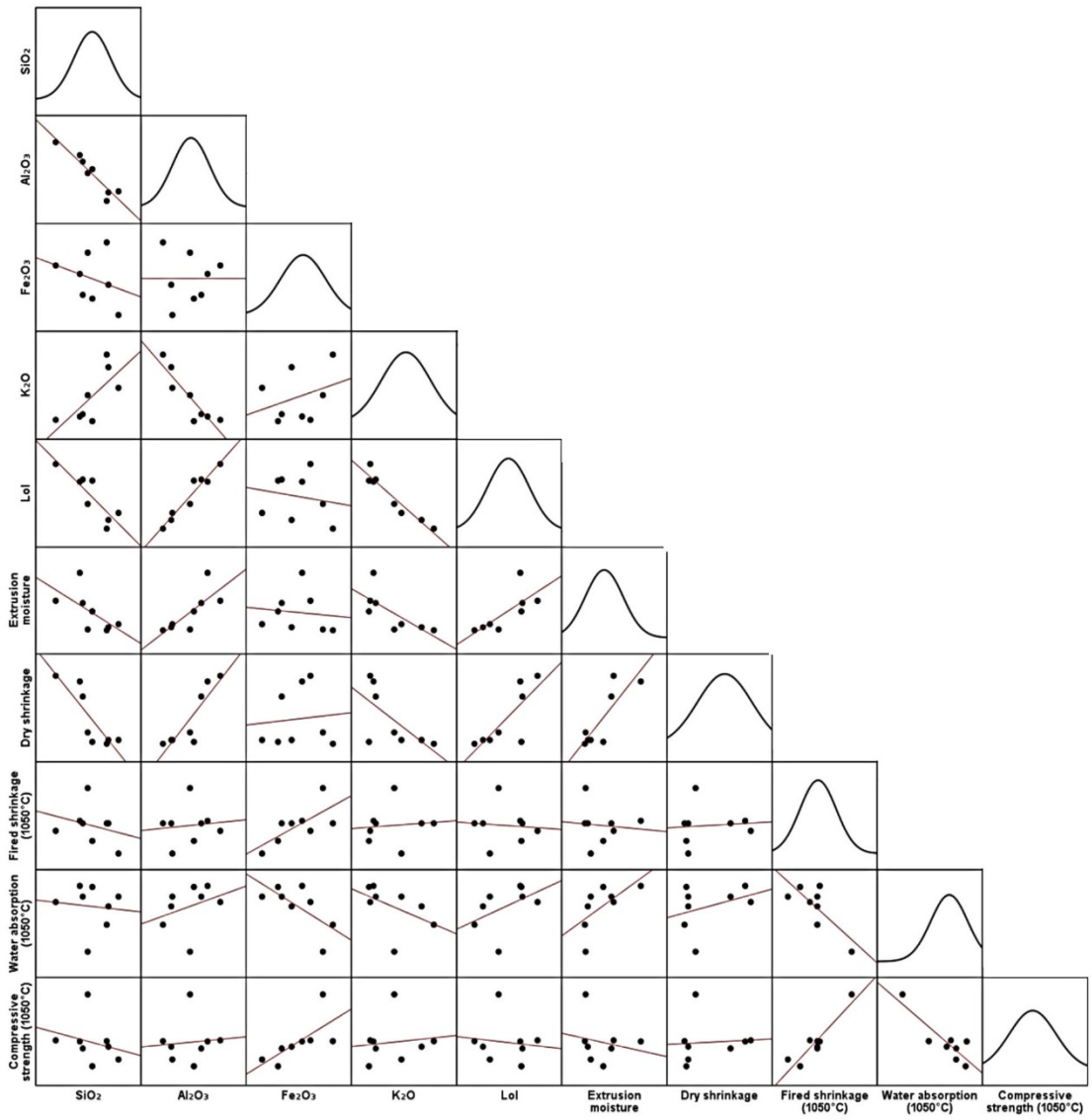


Figure 3-5. Scatterplots between the chemical and ceramic property variables.

3.2.4 Summary of the correlation indices drawn between chemical, mineral and ceramic properties of the top-face clay stockpile variables.

Table 3-3. below provides a summary of the relationships of the chemical, mineral and ceramic property variables discussed in the previous sections.

Variable	Negative variable relationship	Positive variable relationship
Haematite	Kaolinite, illite/smectite interstratification and water absorption	Fe_2O_3, mica, fired shrinkage and compressive strength
Quartz	Al_2O_3, L.o.I, kaolinite, extrusion moisture, dry shrinkage and water absorption	SiO_2, K_2O, mica
Kaolinite	Fe_2O_3, K_2O, SiO_2, mica, fired shrinkage, compressive strength	Al_2O_3, L.o.I, extrusion moisture, dry shrinkage and water absorption
Mica	Al_2O_3, L.o.I, illite/smectite interstratification, extrusion moisture and dry shrinkage	Fe_2O_3, K_2O, fired shrinkage and compressive strength
SiO_2	Al_2O_3, L.o.I, kaolinite, extrusion moisture and dry shrinkage	K_2O and quartz
Al_2O_3	K_2O, quartz, mica	L.o.I, kaolinite, extrusion moisture and dry shrinkage
Fe_2O_3	Kaolinite and water absorption	Mica, haematite, fired shrinkage and compressive strength
K_2O	L.o.I, kaolinite, extrusion moisture, dry shrinkage and water absorption	Quartz and mica
L.o.I	SiO_2, K_2O, quartz and mica	Kaolinite, extrusion moisture, dry shrinkage and water absorption
Extrusion moisture	SiO_2, K_2O, quartz and mica	Al_2O_3, L.o.I, kaolinite, dry shrinkage and water absorption
Dry shrinkage	SiO_2, K_2O, quartz, mica	Al_2O_3, L.o.I, kaolinite, extrusion moisture and water absorption
Fired shrinkage (1050°C)	Kaolinite and water absorption	Fe_2O_3, haematite, mica and compressive strength
Water absorption	Fe_2O_3, K_2O, haematite, quartz, mica and fired shrinkage	L.o.I, kaolinite, extrusion moisture and dry shrinkage
Compressive strength	Water absorption	Fe_2O_3, mica haematite and fired shrinkage

Contribution of chemical variables to the prediction of mineral and ceramic properties.

- SiO_2 can be used to predict the quartz, kaolinite, extrusion moisture and water absorption.
- Al_2O_3 can be used to predict kaolinite, quartz, mica, extrusion moisture, dry shrinkage and L.o.I.
- Fe_2O_3 can be used to predict haematie, mica, kaolinite, fired shrinkage, compressive strength and fired shrinkage.
- K_2O can be used to predict quartz, mica, kaolinite extrusion moisture, dry shrinkage and water absorption.
- L.o.I can be used to predict kaolinite, extrusion moisture, dry shrinkage, water absorption, quartz and mica.

The chemical composition serve as a good indication for the prediction of the ceramic properties of the clay. Since the chemical composition are derived from the mineral composition of the clay, they serve as the means of defining the clay deposit. Defining a clay deposit in terms of its chemical variable distribution can assist with mine planning and quality control. Planning the extraction of the clay to minimize chemical variability will enable value-added decision making, which, in turn, can assist with improved product quality and consistency.

CHAPTER 4

APPLIED GEOSTATISTICS

4. GEOSTATISTICAL BACKGROUND

4.1 Introduction

The stockpile variability, highlighted in Chapter 3, prompted a better understanding of the clay deposit to assist with improving the stockpile consistency. The borehole data obtained from the exploration project provided spatial data that could be studied. Understanding the spatial continuity of the data can assist in understanding and describing the nature of the clay deposit.

Dohm (2012), explains that geostatistics proved to be the preferred method for resources estimation and that it is a subdivision of applied statistics, which identifies elements such as:

- The geological setting of the data.
- The statistical values of the data (i.e. quality, thickness, etc.)
- The volumetric change between data samples against blocks (volume-variance effect).
- The geometry of the domain estimated (size and shape).
- The spatial continuity of the mineralisation (the variogram),
- The degree to which the data vary (difference at various block, support, composite, etc.).
- The spatial arrangement of the data (drilling grid against the estimation block size).

Coombes (2008), explains that geostatistics provides the means for exploring and understanding the sample data and it can be used for estimating the resource. It is the process of creating a three-dimensional model to replicate the in situ nature of the occurrence based on the scarce samples.

According to Isaaks and Srivastava (1989) it is a method modified from classical regression techniques and it offers the advantage of describing the natural continuity of the occurrence under investigation.

Geostatistics originated from work by Danie Krige together with Herbert Sichel on Witwatersrand gold mines in South Africa. George Matheron saw the implications of a paper published by Krige and developed “the theory of regionalised variables” (Dohm, 2012).

4.2 Geological domains and models

According to Coombes (2008), an accurate resource model depends on the geology. The geology contributes up to 90 % of the accuracy of the resource being estimated. Resource estimation requires the identification of the population of interest relevant to what is being estimated. This requires the understanding of the population boundaries and constraining it to only the relevant samples. This calls for domain creation, which involves (Coombes, 2008):

- The creation of limits for each mineralisation population, based on the understanding of the geological controls.
- The utilisation of statistical tools to validate the mineralisation populations.
- Building a three dimensional model of the population from a well understood and defined domain.

A domain, according to Coombes (2008), is a spatial volume that is constrained to a uniform geology (homogeneous), a single grade population in a single search orientation (isotropic). Homogeneity refers to uniformity throughout, whereas isotropy revers to uniformity of properties in all directions. The purpose of creating domains is to control the use of sample data during estimation, i.e. using only relevant data. Domains highlight changes in orientation of continuity, statistical population and geological consistency.

Isotropic according to Isaaks and Srivastava (1989), means having the same value when measured in different directions. In geostatistical terms,

isotropy is considered to exist when the change of data behaviour is the similar in all directions. A true isotropic condition in three dimensions is rare for most types of data. However, according to Isaaks and Srivastava (1989), an isotropic condition in two dimensions is more common.

4.3 Statistical data analysis

Coombes (2008), explains that statistical data analysis provides the means for understanding the data studied. Data analysis, as a minimum, should include summary statistics, histograms, probability plots and comments on domain differences and data characteristics. Summary statistics (descriptive statistics) assists with understanding the typical grade and variability of the occurrence being studied. Essential assumptions underlying geostatistical methods in mineral resource estimation are (Dohm, 2012):

- The sample values measured are reproducible and precisely measured.
- Sample values are accurately measured and represent the true value at that location.
- The samples are collected from a physically continuous, homogeneous population of all possible samples. The specific phenomenon measured at the sample location also exist at all un-sampled locations within the area studied and no sudden changes are evident.
- Un-sampled location values are related to sampled location values.

4.3.1 Compositing and declustering

According to Coombes (2008), representative statistics requires uniform reporting of sampling and drilling. Over sampling of high grades (infill drilling), in an area with known higher grades, will result in high grading the statistics. Clustering has an effect on the statistics used for describing the data and impacts on the selection of the estimation parameters. Declustering the data limits the impact on the statistics. Declustering techniques include (Coombes, 2008):

- Removing specific boreholes.
- Keeping a single sample for each space in a grid.
- Weighting of the samples by the number of samples within each grid space.

Coombes (2008), explains that compositing is a downhole declustering technique, used to ensure samples have an equal influence on the statistic. A bias is introduced when samples are collected over variable lengths. Compositing allows the weighting of sample grades according to the equivalent interval length. The interval length should be as close to the original sampling interval possible. A histogram of the sample lengths can be valuable when deciding on the composite interval.

4.3.2 Descriptive data statistics

Descriptive statistics is a preliminary step used for understanding the distribution of the data collected. The location, spread and shape characteristics are very useful for describing the distribution of the sample data (Cooper and Schindler, 2003).

According to Coombes (2008), data characteristics can be described by measures of what is typical (central tendency) and measures of how different the values are from the norm (dispersion of variables about the mean). Measures of what is typical include the mean, median and mode and measures of difference include the range, inter-quartile range, variance and the standard deviation. Other statistical measures useful for data analysis in resource estimation are the coefficient of variation, Sichel's mean and percentiles.

4.3.3 Multivariate data analysis

According to Cooper and Schindler (2003) multivariate data techniques can be classified as dependency and interdependency techniques. Examples of this technique include multiple regression, multivariate analysis of variance (MANOVA) and discriminant analysis. Coombes

(2008), explains that the first step in multivariate data analysis should be comparing each element against every other element by means of scatterplots. A straight line, according to Cooper and Schindler (2003), is fundamentally the best option available for modelling the relationship between two continuous variables. The scatterplot allows visual inspection of the relationship and the suitability of the statistic chosen. Figure 4.1 is a typical example of a matrix scatterplot, illustrating the relationship between different variables. A scatterplot represents the direction, magnitude and shape of a relationship. Three patterns can be observed from a scatterplot, namely (Isaaks and Srivastava, 1989):

- Positive correlation – if the larger value of the one variable tends to be associated with the larger value of the other variable, likewise for the smaller variable.
- Negative correlation – if the larger value of the one variable tends to be associated with the smaller value of the other variable, likewise if the smaller variable of the one variable is associated with the larger value of the other variable.
- Uncorrelated data – the increase in one variable has no apparent effect on the value of the other variable.

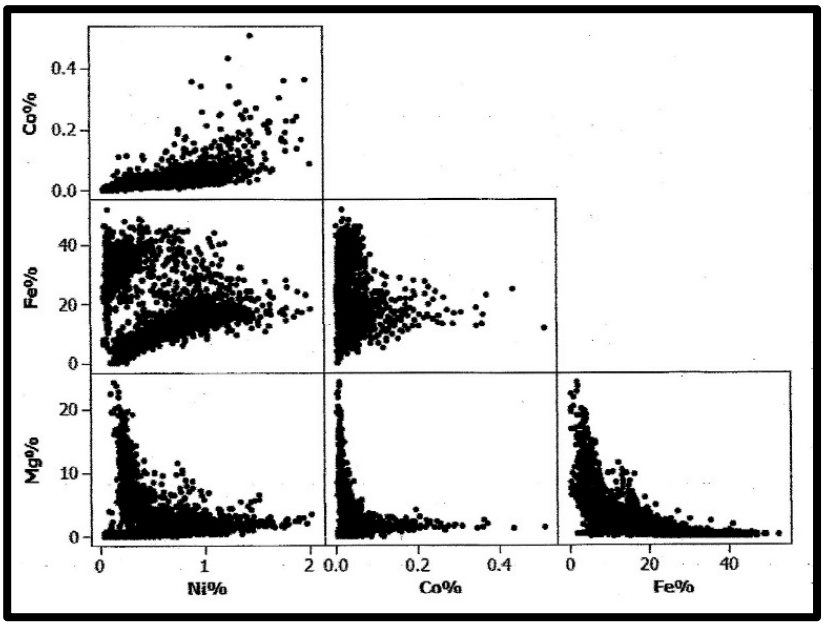


Figure 4-1. Typical example of a matrix scatterplot between different variables (Coombes, 2008).

A straight line represents a linear relationship whereas a parabolic line represents a nonlinear relationship. The assumption of linearity and bivariate normal distributions are checked by means of plots and analytical tests (Cooper and Schindler, 2003).

Coombes (2008), explains that it sometimes becomes necessary to differentiate relationships according to the domains. The correlation coefficient is a statistical measure that provides the strength of the relationships. A correlation coefficient greater than 0.6, in the Mining Industry, signals a strong relationship. A high correlation indicates that the variability in one variable is closely related to the variability in another. The relationship can be modelled and one element can be predicted from another. Variables showing a linear pattern on a scatterplot have a strong correlation. This type of modelling is called regression. Regression is the process of fitting a line to the data to provide a straight line equation that fits the data best.

4.4 Continuity analysis

Grade continuity analysis (variography) focusses on comparing samples according to the distance and orientation between them. It involves the preparation of the data for variography, variogram calculation, variogram modelling and interpretation (Coombes, 2008).

Variography data preparation

The context of the data requires a good understanding. This involves proper data collection (data integrity), understanding of the geological context (mineralisation) and the statistical characteristics (variability) of the domain. Certain assumptions integral to the calculation of the variogram are (Coombes, 2008):

- Data obtained are from a single grade population.
- Grade differences between pairs are consistent throughout the domain.

Semi-variogram calculation concepts

Coombes (2008), explains that the collection of all pairs of data, separated by a given distance can be plotted. The h-scatterplot is a plot that can be used to plot the grades of samples against the distance separating them. The h in the h-scatterplot refers to the distance of separation. An increase in the distance between data pairs will cause the grades of the pairs to become more different. On a scatterplot the cloud of points become wider with increasing distance and less correlated. The correlation coefficient can be used as a measure of the wideness of the cloud. Expressing the correlation coefficient as a function of the separation distance is called the correlogram. Expressing the variation as a function of separation distance is the covariance function.

The semi-variogram is a graph that represents the typical differences of grades plotted against the distance separating the samples. The semi-variogram can also be orientated. In an orientated semi-variogram, the differences between samples are based on the samples with a specific orientation. The formula for a semi-variogram is (Coombes, 2008):

$$\gamma(h) = \frac{\sum \{z(x) - z(x+h)\}^2}{2N_h} \tag{4.1}$$

where:

$\gamma(h)$ is the semi-variogram

z(x) is the sample value

z(x+h) is the sample value at a specific distance, and

N_h is the number of pairs being compared

h is the distance

Semi-variogram terms

According to Coombes (2008), the nugget effect, the sill and the range are structures used for describing the semi-variogram. Dohm (2012) illustrates the difference between geostatistics and statistics using the semi-

variogram depicted in Figure 4.2. The structures illustrated in Figure 4.2 can be described as follows:

Nugget effect **(C_o)** – the difference that exists between samples that were taken almost adjacent to one another (Coombes, 2008). According to Dohm (2012), the nugget incorporates the inherent variability of the mineralisation. The nugget represents the random component of samples, it indicates how variable a sample is from the sample directly next to it, it shows how dissimilar two parts of a sample are and it is supposed to take care of all errors encountered (measurements, human errors, intrinsic errors and random errors). The nugget is not able to manage the systematic bias encountered with consistent over or under statement of analyses.

Sill **(C)** – the increase in separation distance between samples also increases the difference between them. The sill is the point reached where the variance between sample grades is no longer influenced by their separation distance, but is the similar to the population variance. This point is characterised by the plateau reached on the semi-variogram.

Range **(a)** – the distance beyond which the samples are no longer spatially correlated. This is the distance where the sill is reached.

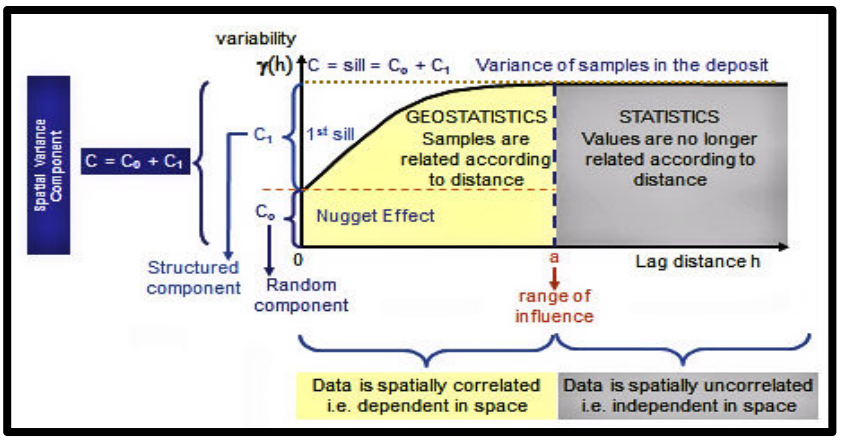


Figure 4-2. The semi-variogram illustrating the different structures and distinguishing between geostatistics and statistics based on special correlation (Dohm, 2012).

Semi-variogram types

The characteristics of the data, according to (Coombes, 2008), determine the type of variogram used. All the different variogram types are based on the formula presented in equation 4.1 above. The semi-variogram type depends on the data transformation before the calculation, or on the standardisation of the semi-variogram after differences between sample values are calculated. The different semi-variogram types are presented in Figure 4.3.

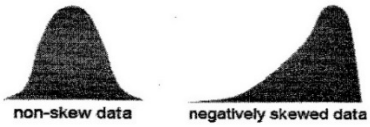
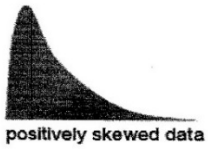
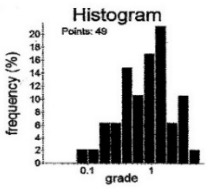
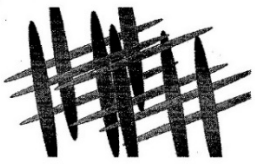
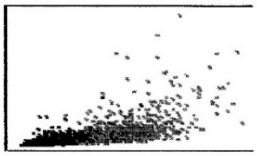
Situation	Variogram type
Non-skew or negative skew 	Traditional variogram Normal Score variogram Indicator variogram Covariance Correlogram
Positive skew 	Log-normal variogram Normal Score variogram Indicator variogram
Low number of samples 	Pairwise relative variogram
Variograms designed to pacify mathematicians ΓΔΏΘλδβμστυ	Semi-rodogram Semi-madogram
Describe variability in cross-cutting, rotating or multi-phase/mixed mineralisation 	Indicator variograms
Describe relationship between elements 	Cross-variograms

Figure 4-3. Summary of different semi-variogram types (Coombes, 2008).

4.4.1 Traditional semi-variogram

The traditional semi-variogram provides the foundation for describing the spatial relationship between samples used in the kriging algorithm. Paramount to the calculation is the assumption that grades compared are from the same population and that differences between them only depend on the distance between them.

4.4.2 Normal score semi-variogram

This semi-variogram is used for controlling the influence of extreme grades. This is accomplished by converting the grade distribution to a standard normal distribution before the variogram is calculated. (Coombes, 2008).

4.4.3 Log-normal semi-variogram

A useful way of revealing structures within positively skewed data is the log-normal semi-variogram. The semi-variogram is calculated from the logarithmic transformation of the grades. The parameters of the log-normal semi-variogram require re-scaling in order to reflect the variability of the data.

4.4.4 Covariance

Dohm (2012), explains that covariance measures the degree to which two variables move linearly together. According to Coombes (2008) it can be calculated form averaging the product of the samples grades from two samples separated by a given distance and then subtracting the product.

4.4.5 Correlogram

The correlogram is the covariance standardised by the standard deviations of all the first sample grades multiplied by the standard deviations of all the second sample grades (Coombes, 2008).

4.4.6 Pairwise relative semi-variogram

The pairwise semi-variogram is useful for revealing ranges that are likely not to be seen in other variogram types. It is useful when sample numbers are limited and the underlying data distribution is positively skewed. The

variogram is generated by standardising the square differences between pairs by the average square of the grade pairs (Coombes, 2008).

4.4.7 Indicator semi-variogram

According to Coombes (2008) the indicator semi-variogram is a traditional variogram calculated on indicator codes rather than grades.

4.5 Semi-variogram modelling

Modelling the semi-variogram requires that a line/curve be fitted through a series of points. Each point on the semi-variogram is the average of collected differences. Spares data can result in shapes not presented in text books, but as the data increase the variogram becomes smoother and better defined (Coombes, 2008). Pre-defined shapes in the kriging system are illustrated in Figures 4.4 and 4.5 below (Coombes, 2008).

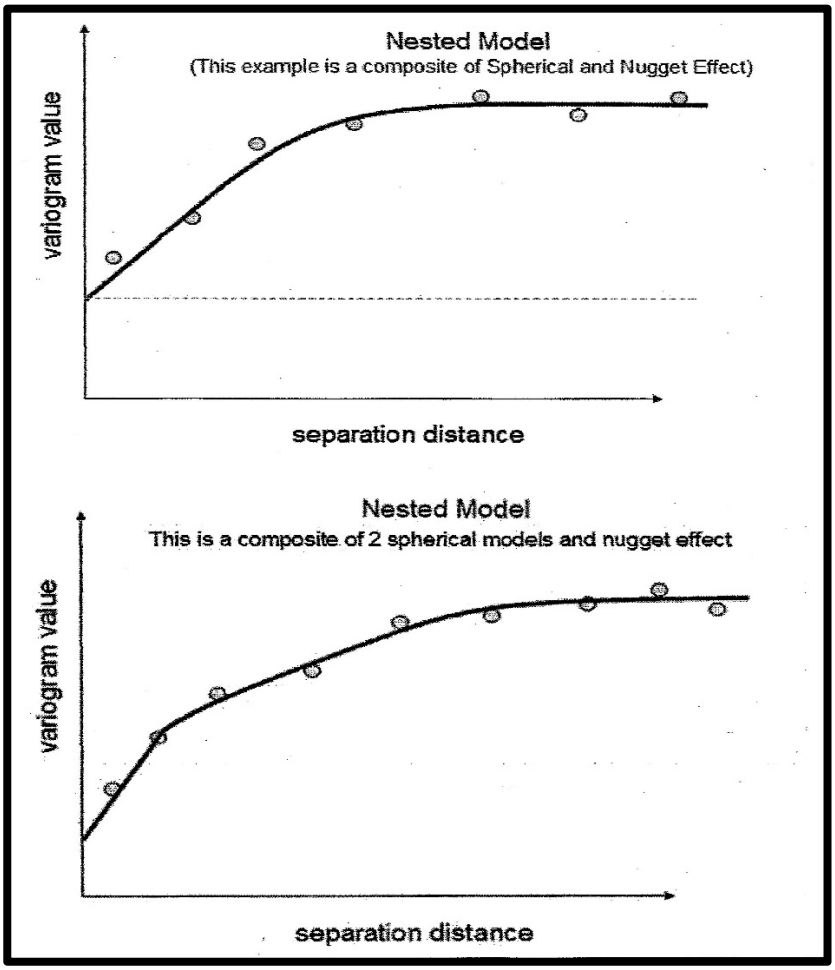


Figure 4-4. Variogram model nested (after Coombes, 2008).

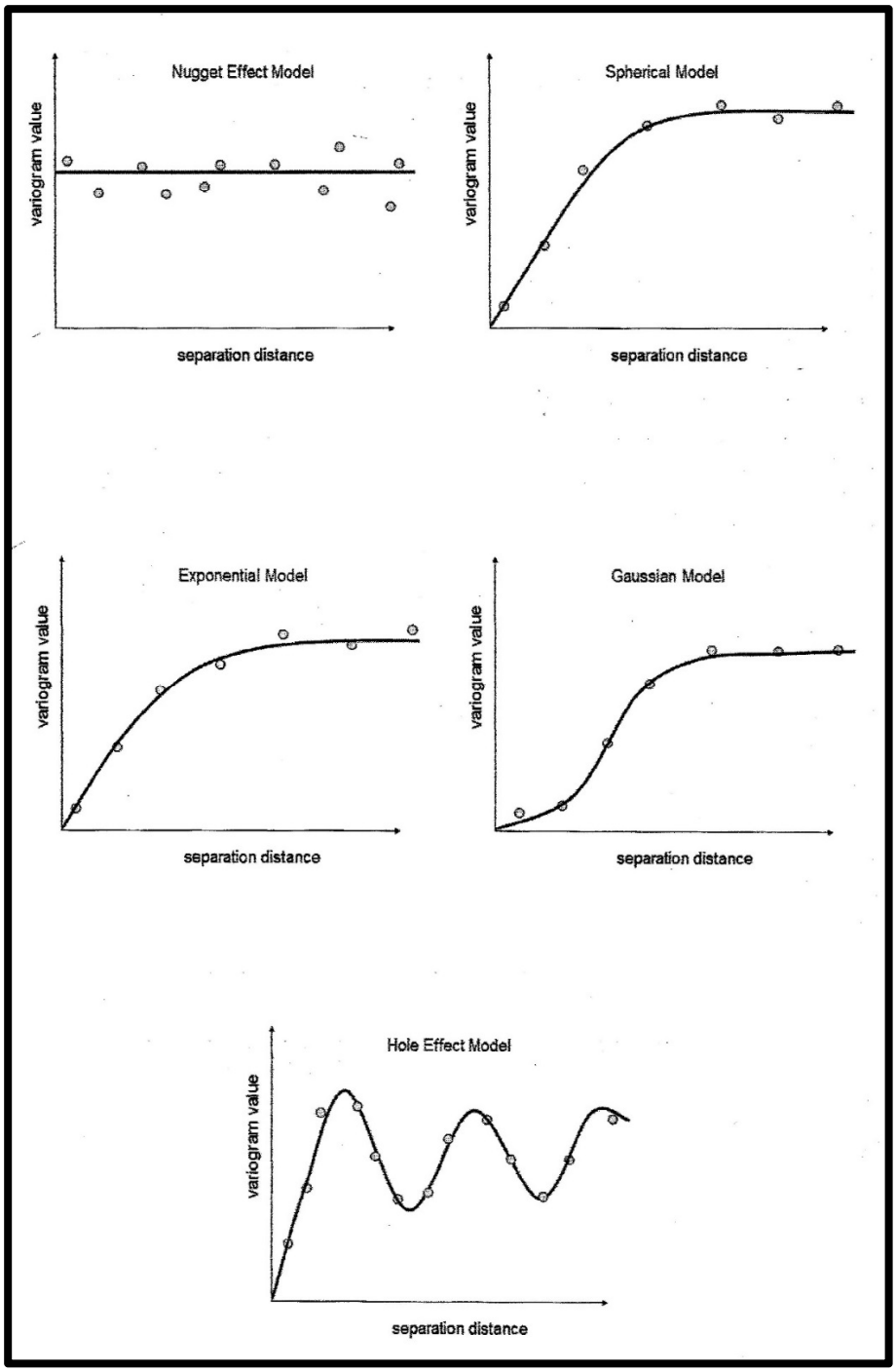


Figure 4-5. Pre-defined shapes associated with the semi-variogram of the kriging system (after Coombes, 2008).

4.6 Creation of a geological model

The preceding sections involved the analysis of data and the understanding of data patterns in the geological setting. This section will focus on creating a three dimensional model from the data analysed to

accurately represent the grades within the domain. According to Coombes (2008) the steps involve:

- The use of wireframes to create a three-dimensional model of the domain.
- Deciding on the most appropriate estimation method to use.
- Using estimation parameters most appropriate for the data set.
- Proceeding with estimation.

Coombes (2008), explains that a three dimensional solid of a geological domain is a wireframe. The wireframe is achieved by defining the section boundaries and then linking the sections by means of polygons. The volume of the blocks within the wireframe should closely represent the volume of the wireframe.

4.7 Estimation

Coombes (2008) explains that the estimation method, estimation parameters and estimation process are central to the creation of a three-dimensional model. Typical estimation techniques include inverse distance and kriging.

Inverse distance

Inverse distance is the simplest estimation technique according to Coombes (2008). Only a few parameters are needed for calculation. The technique considers samples closer to the estimation point to be more similar than samples further away. The closer samples will receive a greater weight by inverting the distance. To ensure an unbiased estimate grade, the inverse of the separation distances are adjusted to sum to one. These distances can be raised to a power (arbitrarily), which allows the closer samples to receive significantly greater weights than those further away. Selection of the power depends on how closely reproducible samples are. Where uncertainty exists in data reproducibility, i.e alluvial gold, a low power will suffice. A power raised to zero (when uncertainty in data reproducibility exists) will give a value of one and all samples will receive the same weight. In this case the estimate is the average of all the

samples chosen. The nugget effect is a useful guide for choosing the power. A high nugget effect signals low reproducibility and a low nugget effect good reproducibility. A high power can be used when the nugget effect is low and a low power, when the nugget effect is high (Coombes, 2008).

Kriging

According to Dohm (2012), the estimation procedure based on the variogram is referred to as kriging, after Professor Danie Krige. Kriging according to Bohling (2005), is an ideal interpolation process based on regression against known z values of nearby data points, weighted in relation to spatial covariance values. Interpolation algorithms estimate values for a specific location by drawing on the weighted sum of data values at neighbouring locations. Most interpolation algorithms assign weights to the function. The weights assigned increase with decreasing separation distances and decrease with increasing separation distances (Bohling, 2005).

According to Deutsch and Journel (1992), kriging determines weights by minimizing the variance of the errors. Dohm (2012) explains that kriging is the Best Linear Unbiased Estimator (BLUE), since it provides the smallest standard error, the narrowest confidence intervals and the greatest confidence in the estimates. It is a local estimation technique that provides the optimum set of weights with the minimum estimation variance. The technique is based on the variogram γ(h) to determine the value of the weights and the estimation variance. Dohm (2012) explains that kriging considers spatial character, size and shape of a section and the location of the samples and the change of support (volume-variance effect) is taken into account. The key assumption is that the structural model is valid.

Kriging estimators, according to Goovaerts (1997), are alternatives of the basic linear regression estimator Z*($\boldsymbol{\mu}$) and are defined as:

$$[Z_{SK}^{*}(\boldsymbol{\mu}) - m(\boldsymbol{\mu})] = \sum_{\alpha=1}^{n} \lambda_{\alpha}(\boldsymbol{\mu})[Z(\boldsymbol{\mu}_{\alpha}) - m(\boldsymbol{\mu}_{\alpha})] \quad (4.2)$$

where:

$Z(\boldsymbol{\mu})$: is the Random Variable (RV) at location $\boldsymbol{\mu}$

$\boldsymbol{u}_{\alpha}$: is *n* data locations

$m(\mu) = E\{Z(\boldsymbol{\mu})\}$: is the location-dependent expected value of RV $Z(\boldsymbol{\mu})$

$Z^{*}_{SK}(\boldsymbol{\mu})$: is the linear regression estimator, also known as the simple kriging (SK) estimator.

Z(μ)represents the random variable with a trend factor, m(μ), and a residual factor (R(u) = Z(μ)- m(μ)). The residual estimated at u by the kriging function is the weighted sum of residuals at neighbouring data points. Kriging weights (λ_{α}) from the semi-variogram characterise the residual component. The distinction between residual and trend is subjective and varies with scale (Bohling, 2005).

Dohm (2012), explains that the random function (RV) is a set of random variables Zi (i=1,2,…,k) with some spatial locations (xi) whose dependence on each other is defined by some probabilistic mechanism (joint distribution). Random variables have several possible outcomes and so do random functions, called realisations. All pairs of random variables separated by a certain distance (h), regardless of their locations, have the same joint probability distribution.

Stationarity

Stationarity according to Dohm (2012), is the independence of the univariate and bivariate probability laws from the location (x). Stated differently, it is a spatial process which has a correlation or variability structure independent from location, but depended on relative distance and direction. A stationary random function allows the use of the expected value and the variance to summarise the univariate behaviour of a set of random variables.

Deutsch and Journel (1992) explain that a correct decision of stationarity is critical for the reliability of the geostatistical interpretation. Combining

data across geological domains may mask important geological differences. On the other hand, splitting data into too many subcategories may lead to unreliable statistics based on too few data per grouping and general confusion.

The first aspect of stationarity is to make a decision on how to group the data for geostatistical analysis (Deutsch and Journel, 1992):

- Depositional zones of different quality/spatial behaviour.
- Rock types within the zones.
- Spatially coherent.
- Compromise geological precision and stable statistics.
- Manage available resources

Deutsch and Journel (1992) explain that the second aspect of stationarity is making a decision on how the statistical parameters vary in space:

- Reasonably constant – stationary.
- Locally varying – sometimes called non-stationary.

Ordinary kriging

Coombes (2008), explains that historical work done by Danie Krige and Georges Matheron, on estimation of gold grades from the Witwatersrand gold mines in South Africa, led to the discovery of the volume-variance effect. The volume-variance effect formed the basis for understanding reconciliations and resource estimation in the mining industry. Krige refers to his observations between actual and estimated grades as the "Regression Effect".

The volume-variance effect

The selection of larger mining volumes and the increase in grade dilution can be described by the volume-variance effect. In essence, the diluting effect of decreased selectivity causes a larger volume to have lower variability. In mining it relates to the fact that, if the volume-variance effect is not accounted for, sample grades will continuously be over or under

estimated. Estimates need to be adjusted to reflect the volume when applying selectivity criteria to a resource model and the degree of selectivity should be reported (Coombes, 2008).

Dohm (2012), explains that the information effect and the support effect are two of the main causes for incorrect resource predictions. The way in which data are combined in the neighbourhood of a block estimate is important. The information effect and the support effect give rise to the regression effect. According to Krige (1996), the information effect, which is the limited extent of the data available, can be reduced by more intensive and better-placed sample data.

Kriging technique

According to Coombes (2008), a linear estimation technique was developed by Krige and Matheron. The kriging technique provided the least overall difference between the predicted and actual mined grades without a bias. The linear estimation allows the direct application of weights to the sample grade for estimation. Two conditions are paramount, the overall difference between predicted and actual values should be very small and it should be without a bias. According to (Deutsch and Journel, 1992), ordinary kriging requires no knowledge of the stationary mean (m) and therefore remains unbiased. The algorithm for ordinary kriging estimation is as follows (Deutsch and Journel, 1992):

$$Z^*_{OK}(\boldsymbol{u}) = \sum_{\alpha=1}^{n} \lambda_\alpha^{(OK)}(\boldsymbol{u}) Z(\boldsymbol{u}_\alpha) \tag{4.3}$$

and the stationary OK system:

$$\begin{cases} \sum_{\beta=1}^{n} \lambda_\beta^{OK}(\boldsymbol{u}) C\left(\boldsymbol{u}_\beta - \boldsymbol{u}_\alpha\right) + \mu(\boldsymbol{u}) = C(\boldsymbol{u} - \boldsymbol{u}_\alpha), \alpha = 1, \ldots, n \\ \sum_{\beta=1}^{n} \lambda_\beta^{OK}(\boldsymbol{u}) = 1 \end{cases} \tag{4.4}$$

where:

$\lambda_\beta^{(OK)}(\boldsymbol{u})$: is the OK weights

μ (u): is the Lagrange parameter associated with:

$\sum_{\beta=1}^{n} \lambda_{\beta}^{(OK)}(\boldsymbol{u}) = 1$: is the constraint

Coombes (2008), explains that LaGrange Multiplier (λ) measures the degree of bias present. It is necessary to ensure the weights sum to one. The LaGrange Multiplier (λ) will increase when the surrounding samples are spares, clustered or requires extreme extrapolation. Isaaks and Srivastava (1989), explains that the LaGrange parameter is a technique used for converting a constrained minimisation problem (without affecting it) into an unconstrained one, as is indicated below (Isaaks and Srivastava, 1989):

$$\tilde{\sigma}_R^2 = \tilde{\sigma}^2 + \sum_{i=1}^{n}\sum_{j=1}^{n} w_i w_j \tilde{C}_{ij} - 2\sum_{i=1}^{n} wi \cdot \tilde{C}_{i0} + 2\mu(\sum_{i=1}^{n} w_i - 1) \qquad (4.5)$$

where: $2\mu(\sum_{i=1}^{n} w_i - 1) = 0$ produces the unbiased condition:

$$\sum_{i=1}^{n} w_i = 1 \qquad (4.6)$$

According to Isaaks and Srivastava (1989), this explanation offers a value for μ that is useful for calculating the resulting minimised error variance.

The actual grades are obtained from the variogram that is calculated by comparing pairs of actual sample values. The series of equations used for obtaining the smallest difference between predicted and actual values without a bias can be summarised in matrix form as follows (Coombes, 2008):

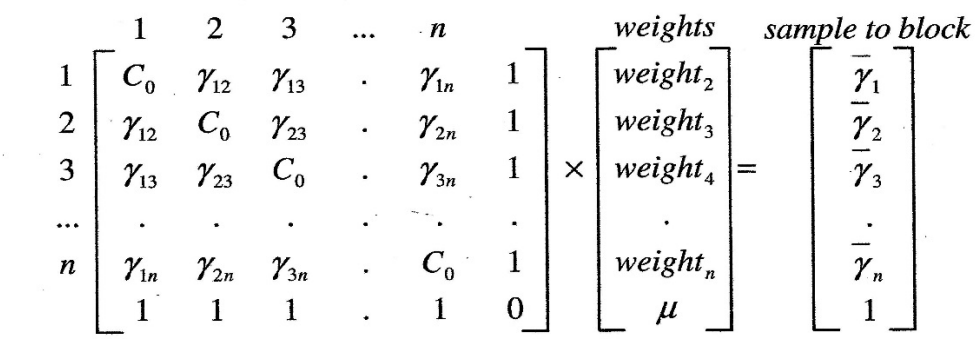


Figure 4-6. Series of equations used in ordinary kriging to calculate the weight values (Coombes, 2008).

According to Coombes (2008), to Coombes (2008), the variogram (γ) calculations are summarised in the first matrix representing the values between each sample near the block to be estimated. The numbers next to the symbol represents the number of the sample being compared (i.e γ_{13} is the separation distance between the 1st sample and the 3rd sample). C_o represents the nugget effect in the matrix. The average variogram between sample 3 and the discretisation points in the block is represented by $\overline{\gamma_3}$.

Coombes (2008), explains that the discretisation points are the points in a block that provide an understanding of change in volume between the samples and a block. The volume-variance correction is applied when the kriging system draws on the average variability between a sample and all the discretisation points within a block. Smaller blocks will have closer discretisation points than larger blocks. This relates to a more similar stretch of separation distances between sample and discretisation points, resulting in more similar variogram values. Contrary to smaller blocks, larger blocks are further apart. A larger range of variogram values is needed for calculating the average variability between the sample point and the block.

The kriging system reduces the calculation to weights (μ). The ordinary kriged estimate is obtained by applying the weights to the individual sample grades and ensures an unbiased linear estimate with the least

overall variability between predicted and actual estimates when compared to all other possible linear estimates (Coombes, 2008).

According to Coombes (2008), the weights are basically a function of the variogram model. The unique character of each domain can therefore be used to control the weights. The variogram model should therefore accurately reflect the variability of the data observed. A variogram plot shows how reasonably well the model reflects the calculated variability.

Kriging variance

Coombes (2008), explains that the kriging variance can also be calculated from the kriging system and provides in essence, a measure of confidence in the estimate. It is based on the sample arrangement surrounding a block and the variogram. This confidence measure can be calculated by weighting the sum of variograms between the sample and block, adding the LaGrange multiplier and subtracting the variability contained within the block. Coombes (2008), further explains that:

- *The point to block variability* is the average of the variogram values for each sample to the discretisation points.
- *The sum of the point to block variability weighted by the kriging weights* is obtained by adding the sample to block variability and then weighting them according to the influence each sample had on the estimate.
- *The variability within a block* is the average of the variograms values obtained from the distances between all the discretised points inside the block. The average will be large for large blocks, because it is subtracted in the formula, it lends itself to a reduced kriging variance.
- *The LaGrange multiplier* will increase with clustered data, spares data and extrapolated estimates surrounding the block. Poor data arrangement will cause the LaGrange multiplier to increase, which will result in a higher kriging variance.

Coombes (2008), explains that there are no sample values incorporated in the kriging variance and that the true variance of the estimate will depend on the sample values used to calculate the estimate. The kriging variance provides a relative measure of data coverage surrounding blocks.

Estimation parameters

Coombes (2008), explains the following in terms selecting estimation parameters:

- The quality of the model is greatly influenced by the way the data *is domained*. The geological boundary conditions (gradual or sharp changes in grade) determines how the data will be used for estimation.
- Selectivity and the degree of the volume-variance adjustment is greatly influenced by the *block size*. Small blocks causes a false sense of selectivity built into the model. Grades from adjacent blocks tend to be very similar causing a smoothed model. Confidence in the block size can be obtained by using Kriging neighbourhood analysis (kriging efficiency and slope statistics).
- Normally, more than four *discretisation* points in any direction will suffice.
- The interpretation and understanding of the geological setting is very important when choosing the search ellipsoid. Attention should be given to the continuity expected from the geology. The search ellipsoid and anisotropy can be based on the variography.
- The degree of smoothness in the model is influenced by the *minimum and maximum number* of closest samples. High selective zones may require that the maximum number of samples be limited. It is important to consider what the selectivity in the model should reflect.
- The *samples per drill hole* constraint is useful for controlling smearing in alternating bands of grades.

Choosing parameters for estimation should be guided by the data geometry relative to the grade continuity (Coombes, 2008).

Negative weights

The declustering process in kriging, according to Coombes (2008), causes negative weights. Samples screened by samples closer to a specific block causes the samples to add no value to the estimation process. The forced unbiasedness (weights summing to one) and screening can result in negative weights. Generally the negative weights are very small, but when applied to relatively high grades it can cause a negative estimate.

There are non-theoretical ways to deal with negative weights, namely (Coombes, 2008):

- Setting the negative weights to zero.
- Re-run the estimation and reduce the number of samples for the affected blocks (blocks with negative weights).
- Ignore negative weights.
- As a final resort, manually adjust the block grades to represent the volume.

Conditional bias

Coombes (2008), explains that goodness of fit statistics were proposed for assessing the suitability of the parameters used for estimation, which raised the concern of conditional bias. The blocks estimated are conditionally biased when high grades are under estimated and low grades are over estimated.

This, according to Coombes (2008), can occur when estimated blocks are way too small to accurately represent the grades at the location of the small blocks. Figure 5.7 illustrates a comparison between the distribution of block grades and true grades. The tails of the estimated histogram shows the estimates are to smooth. On a block-by-block basis there is a good relationship between the actual high - and low-grade blocks compared to the estimates.

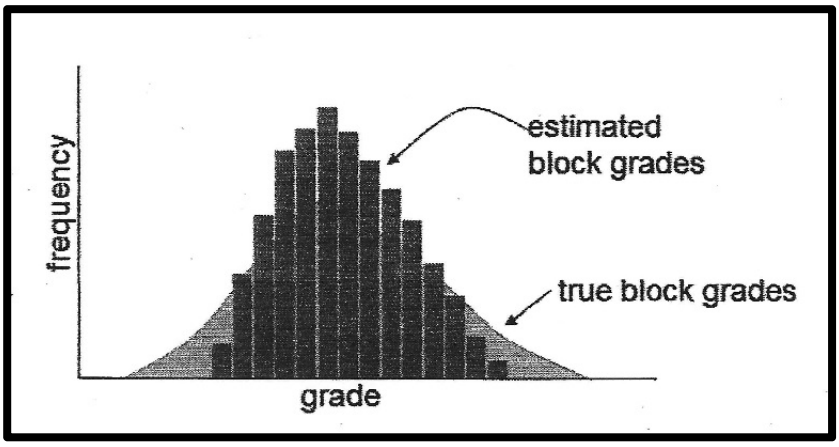


Figure 4-7. Comparison between the distribution of block grades and true grades (Coombes, 2008).

A consistent bias is present, i.e. the estimated high grades tend to be lower than the actual high grades and the estimated low grades tend to be higher than the actual low grades. Figure 4.8 serves to illustrate the over and under estimation. It is expected that a 1:1 relationship would give a regression slope of one between the estimated and actual data. Figure 4.8 shows that the regression slope between the actual and estimated values is less than one. The lower the slope the smoother the tails of the distribution of the estimated blocks (Coombes, 2008).

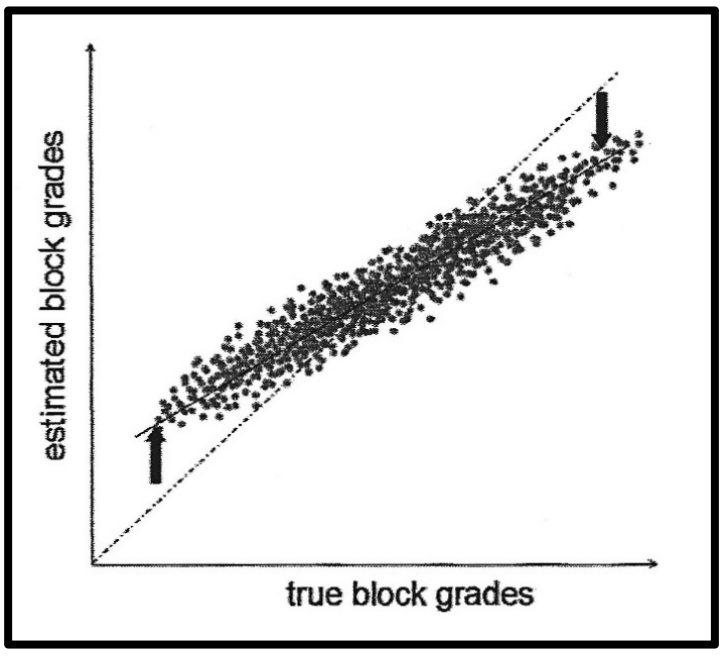


Figure 4-8 Linear regression slope between true block grades and estimated block grades (Coombes, 2008).

The goodness of fit statistics used for describing the above phenomena, according to Coombes (2008), are the kriging efficiency and the slope of regression.

Kriging efficiency

The kriging efficiency, according to Coombes (2008), estimates the percentage overlap expected between the histograms of the estimated block grades and true block grades. A perfect match between the estimated and true grade distributions is obtained when the kriging efficiency is 100 %. The kriging efficiency drops when blocks are more extrapolated than interpolated and when the data is more sparse or clustered. A negative kriging efficiency signals an extremely poor estimation. The kriging efficiency is calculated as follows (Coombes, 2008).

Slope of regression

Coombes (2008) explains that the slope of regression is used to estimate the slope of the linear regression equation between the estimated and true block grades. A regression slope of one indicates that the estimated high and low grades correspond accurately to the true high and low grades.

Block size optimisation

Both the slope and kriging efficiency statistics, according to Coombes (2008), are useful for estimating the block accuracy and conditional bias prior estimation. More accurate estimates can be expected from a block size where the kriging efficiency and slope statistic has been maximised. A range of parameters can be tested and the parameter providing the optimum kriging efficiency and slope statistic can then be chosen. The following process for optimising the block size is proposed by Coombes (2008):

- Choose a block size reasonable for the model after a variogram model has been constructed and sample data are available.

- Estimation parameters should be set to extremely high values:
  - Discretisation at 8x8x8
  - Search range at least three times the variogram range
  - Maximum number of samples, example 150.

- Create a test block model by starting with a specific volume continuing with additional block models for different block sizes to be tested.
- The kriging efficiency and slope should be calculated for all the blocks in each of the test block models.
- The range of the kriging efficiency and slope values should be plotted against the block size.
- The block size that maximises the kriging efficiency and slope should be chosen.
- A similar method can be followed for choosing the search ellipsoid, maximum number of samples per block and discretisation.

Coombes (2008), explains that the various forms of kriging efficiency and slope testing processes used in the mining industry only provide guidance until the real impact of each parameter is understood.

4.8 Concluding remarks

A brief literature background on geostatistics was provided to illustrate the importance of geostatistics in spatial studies. It is clear from the above that geostatistics is closely related to interpolation methods, which rely on statistical models and random function theory. These techniques are applied to model uncertainty related to spatial estimation and to simulations of a single spatial model that assume stationarity (the same statistical properties are valid over the entire domain). The literature background provided in this chapter forms the basis of the geostatistical analysis in the following chapters.

CHAPTER 5

REGIONAL AND MINE-SCALE GEOLOGY

5. GEOLOGY OF SOUTH AFRICA

5.1. General description of South Africa's geological history

Lurie (1984) explains that the Karoo Sequence covers about one-half of the South African surfaces. The main Karoo Supergroup sediments were created behind the Cape mountain ranges in an inland Karoo Sea (McCarthy and Rubidge, 2005).

The Karoo is a semi-arid region of South Africa and reveals its geology through horizontal layers, frequently seen in rocky outcrops. The Karoo is divided into two parts, namely the Little Karoo and the Great Karoo. The Great Karoo is underlain by the widespread Karoo Supergroup rocks, which were formed during very different climatic conditions than those prevailing today (McCarthy, 2009).

5.2. Brief description of Ecca Group formation, which forms part of the Karoo Supergroup

According to McCarthy (2009), the Ecca Group rocks were formed when South Africa was still a part of Gondwana, which, at that time, was located near the South Pole.

McCarthy (2010) explains that the eroded sediments in mountainous areas accumulated in a depression/basin. The depression/basin was caused by the surrounding mountains forcing the Earth's crust down and allowing sediments to accumulate in the basin. South Africa at that time, still a part of Gondwana, was located close to the South Pole and was covered in ice. There were no sediments to fill the basin and, instead, it was filled with water, creating an enormous inland lake. However, as Gondwana moved northwards, the climate warmed and the melting down of the glaciers begun. The melting glaciers moved down the mountains towards the lake, carving their way through the rock and producing valleys because of their

abrasive nature. Eventually, as the lake was reached, they melted and dumped all the rock, debris and fragments collected on their path into the lake. The grinding action of the glaciers smoothed the rock surface and formed fines (extremely small particles called flour), which washed down to the inland lake and settled through particle-size sorting.

These rocks remained unbroken in a fine matrix, known as ‘till’ and as ‘tillite’ when compacted. Excessive amounts of sediments accumulated in the depression over a period of time, which preserved the glacier marks. Eventually, the glacier meltdown resulted in the development of the Dwyka Formation we know today (McCarthy, 2009).

According to McCarthy and Rubidge (2005), the northward movement of Gondwana caused an enormous inland sea to appear, apparently connected to the open sea, which at the time had very little tidal activity. The Cargonian Highlands formed the high ground and the rivers from these mountains deposited their sediments along the northern coastline, forming large deltas, known today as the Ecca Group.

The rocks of the Ecca Group in the north are different from those in the south. The Karoo Sea was deep in the south with narrow coastal plains, with various deltas crossing the coastal plain and depositing sediments from the Cape mountain ranges into the basin. The deltas stretched out northwards, with fine-particle sediments collecting in front of the deltas. These particles spilled down into the deep trough from time to time, creating large, fan-shaped assemblage of turbidites (McCarthy and Rubidge, 2005).

McCarthy and Rubidge (2005) explain that the Cape Mountains continued to rise because of subduction in the south and provided an enormous amount of sediment to the Karoo Sea. The highlands to the north were increasingly eroded, with less sediment being supplied to the Karoo Sea. The highlands eventually became submerged under the Karoo Sea, which was slowly silting up. A narrow piece of land was formed where once there was only sea. The deltas lengthened northwards, as the inland sea, in the

south, filled with the sediments. In the process, new habitats were provided for life. Over time, the sea contracted to the size of a lake, which, today, marks the boundary between the Ecca Group and the Beaufort Group.

5.3. Geology of the clay sediments occurring at the Corobrik Lawley Factory near Lenasia, Soweto, in the Gauteng Province of South Africa

Jones (1984) explains that in the Lawley area, as the glaciers withdrew, rock fragments were left behind (tillite/diamictite) on clean-scoured depressions and in deep dolomite valleys (Chuniespoort Group, Transvaal Supergroup) that had been carved out by the glaciers. Today, these rock fragments are known as diamictites and they represent the lowest member of the Karoo Supergroup.

Jones (1984) explains that in this area the remnants of the Karoo Supergroup form part of a belt of clay outlier sediments. They were formed by the infilling of the depression, valleys and sinkholes of the pre-Karoo surface. These outliers also appear to be separate from the main basins of the Karoo Supergroup. Figure 5.1 illustrates the lithostratigraphic units in the Main Karoo Basin.

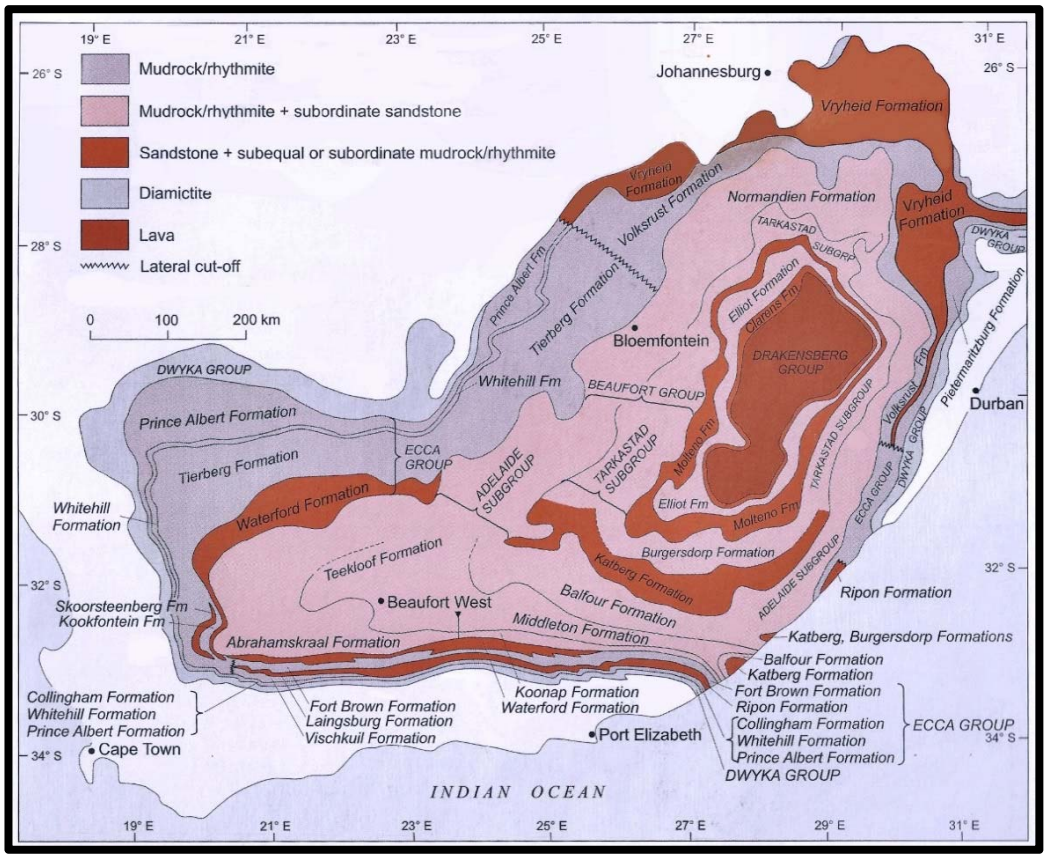


Figure 5-1. The lithostratigraphic units in the Main Karoo Basin (modified after Johnson et al., 1997).

5.4. Regional geology of the clay sediments occurring at the Corobrik Lawley Factory

The clay-rich sediments in the outliers of the Karoo rocks are believed to belong to the Ecca Group. The Ecca Group consists of different formations, which replicate the lateral facies changes that characterise this succession (Fig. 5.2). The exploitable clay deposits are believed to be the stratigraphic equivalent of the coal-bearing formation of the Main Karoo Basin.

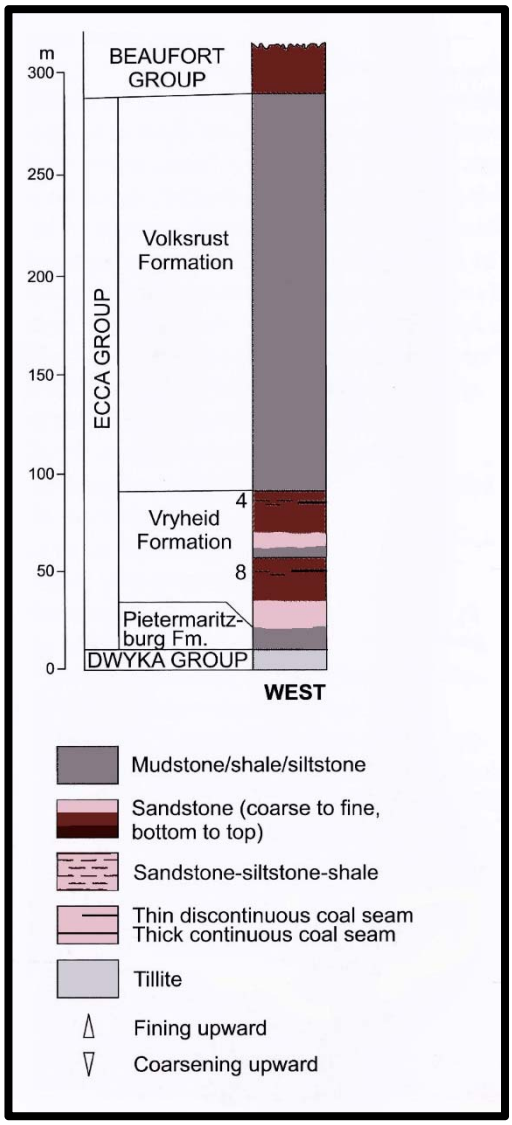


Figure 5-2. Schematic west–east section through the Ecca Group in the north-eastern part of the Main Karoo Basin (after Van Vuuren, 1981).

The Vryheid Formation is divided into a lower fluvial-dominated deltaic period, a middle fluvial period and an upper fluvial-dominated deltaic period (Fig. 5.1). This formation is of Permian age and is a sedimentary succession, consisting of grits, sandstone shales, coal seams and alternating lenses of clay, siltstone and conglomerate. These clays overlie pre-Karoo rocks (Fig. 5.3) and, in some areas, coal and carbonaceous shale of the Vryheid Formation and tillites/diamictite of the Dwyka Group (Horn and Strydom, 1998).

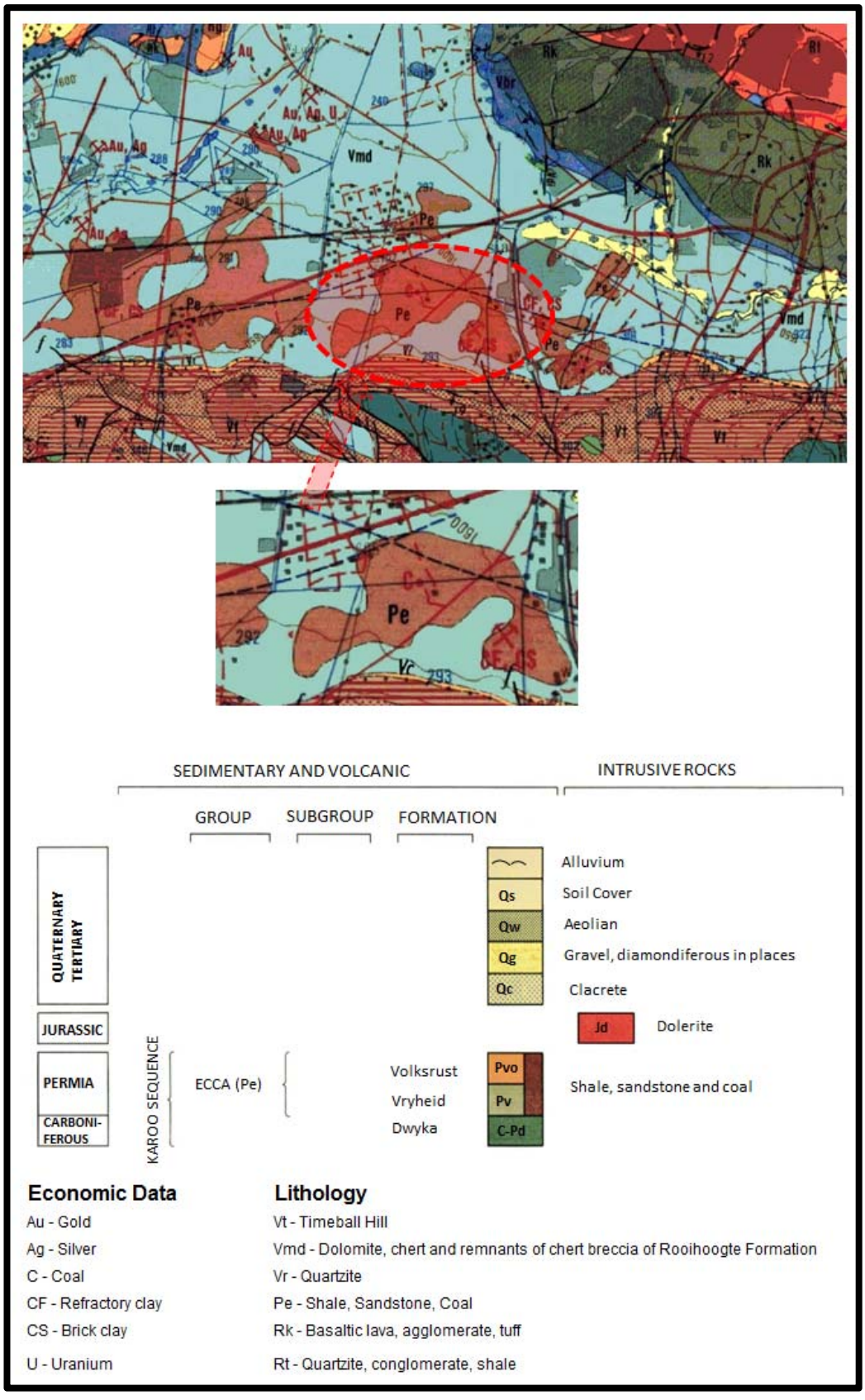


Figure 5-3. Geological map of the geology underlying the Lawley quarry (Geological Map 2526, West Rand, 1:250 000-scale, Geologiese Opname).

The Volksrust Formation is mainly an argillaceous unit, which inter-fingers with the overlying Beaufort Group and the underlying Vryheid Formation (Johnson, Anhaeusser, Thomas, 2006). In the West Rand area, brick makers have made extensive use of the Karoo clay occurrences. These clays consist of plastic to semi-plastic flint clay, which is used for face brick manufacturing (Horn and Strydom, 1998).

According to Horn and Strydom (1998), the Karoo outliers in the West Rand area can be summarised, from top to bottom, as follows:

- Overburden, varying between 2.5 and 12.5 m thick consisting of brown lateritic soil.
- Chert and quartzite pebble layers in a clay and soil matrix, 0.2 to 1.1 m thick.
- Clay zone with varying thickness of between 15.4 and 40.6 m, consisting of light-coloured plastic kaolinitic clay with red or yellow staining along palaeo-joints. Towards the middle of the succession, subordinate inter-beds of sandstone, conglomerate or shale are developed.
- Sandstone bed, approximately 0.2 m thick.
- Black carbonaceous clay, up to 5.7 m thick, at the base of the succession.

5.5. Mine-scale geology of the clay sediments occurring at the Corobrik Lawley Factory

Jones (1984) explains that the outliers of the Karoo Supergroup are unevenly shaped and cramped into slots eroded out of the Malmani Subgroup rock. The outliers are elongated, generally in a north–north-westerly direction, except for the northernmost outlier. The latter has a cruciform shape, with one limb being north–north-westerly aligned and the other west–south-westerly aligned.

Jones (1984) indicated that in the northernmost limb of the cruciform-shaped outlier, the Karoo Succession consists of 15 m of red mudstone overlying 8 m of pale cream and off-white shale and some 2 m of

carbonaceous clay. In the southernmost outlier, the red mudstone reaches a thickness of 35 m. Jones (1984) argues that it was doubtful that this could have resulted in facies changes. His opinion is that the uppermost members of the Karoo Sequence were probably preserved in the southernmost outlier, because this outlier had suffered more re-adjustment settlement or slumping than that to the north.

Jones (1984) described the Karoo sequence in the Lawley area from top to bottom as follows:

Table 5-1: Classification of the Karoo sequence in the Lawley area (Jones, 1984).

Description	Local name	Thickness (m)
Highly weathered, red mudstones with periodic and alternating chert pebble bands.	Red kaolin	> 25.0
Light-cream and off-white coloured kaolinitic shales.	Top-face	8.0
Dark-grey, brown and black carbonaceous mudstone.	Plastic clay	9.5
Dark-grey carbonaceous shales.	Carbonaceous shale	0.0 - 2.0
Grey and off-white coloured grits, siltstones and tillite.	Dwyka	> 3.0

The contact between the clay layers in the Lawley pit is illustrated in Figure 5.4, with a clear contact between the top-face and the plastic clay (chocolate) depicted in Figures 5.5 and 5.6.

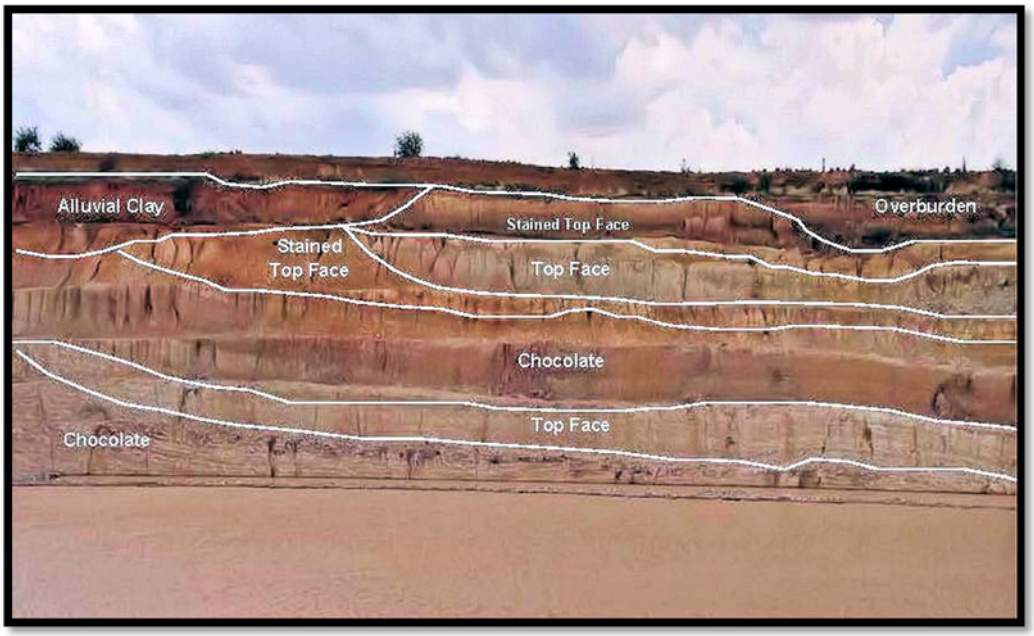


Figure 5-4. One of the open clay faces in the Lawley quarry. The local names of the various clays occurring in the quarry are also indicated.

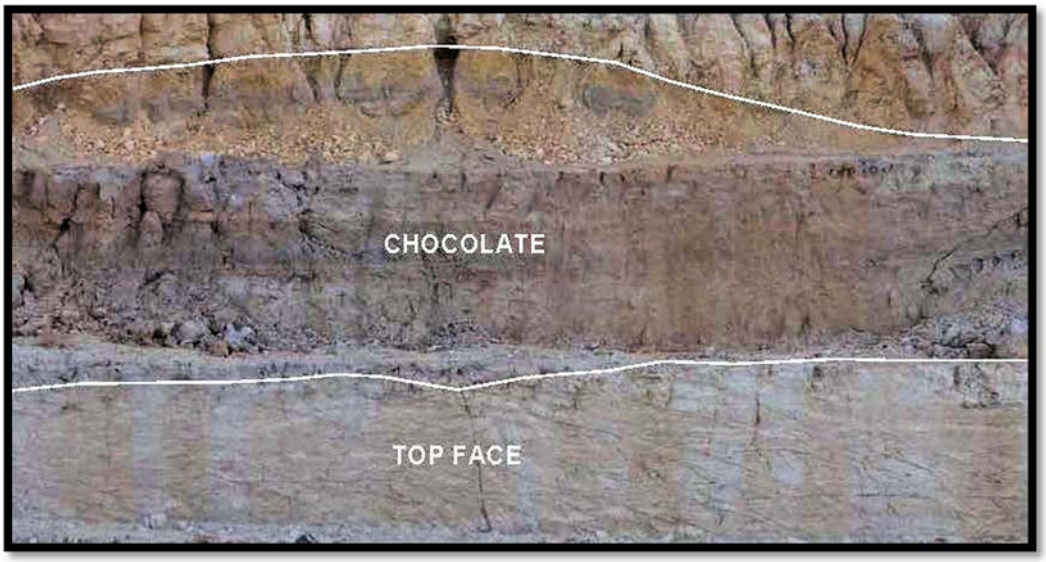


Figure 5-5. Light burning top-face and chocolate clays in the Lawley quarry.



Figure 5-6. The contact between the top-face clay at the top and the chocolate clay at the bottom is clearly outlined by the brown iron-stained marker.

The complexity of the individual clay layers in the Lawley pit is clearly visible from Figure 5.4. The quality of the raw materials mined from this pit depends mainly on the accuracy of the chemical data and the reliability of the geological model. The geology of this pit clearly illustrates the versatility of the different clays and the challenges they pose for the consistent quality of the raw material mined.

CHAPTER 6

GEOSTATISTICAL ANALYSIS OF DATA

6. STATISTICAL DATA EVALUATION

This chapter and the chapters to follow are devoted to geostatistical analysis and estimation of the top-face upper and lower domains. The aim is to understand and characterise the top-face variable fluctuations in order to assist with minimising stockpile variability during mine planning and stockpile construction phases.

The area investigated is depicted in Figure 6.1. Boreholes were drilled 1997, 1998, 2009 and 2010. The 1997 drill holes are indicated in black, the 1998 drill holes in blue, the 2009 drill holes in red and the 2010 drill holes in green. The 1997/1998 drill holes served as a guide for positioning the 2009/2010 boreholes. The 2010 boreholes were infill drill holes, based on information from the 2009 drill holes, with similar lithological domains depicted in the clay pit being mined (see Figs 5.4 to 5.6)

The data obtained from the 2009/2010 drill holes were used for domaining, geological modelling, geostatistical data analysis, variography (Chapter 7) and estimation (Chapter 8). The following sections explain the process of data collection, how the geological domains were created and the descriptive statistics of the data.

6.1. Data collection

Drill core was obtained through diamond drilling. The core was classified according to lithological units and chemical composition. Drill hole (2009/2010) positions are from a 50 x 40 m grid and is depicted by the red and green crosses in Figure 6.1. Figure 6.2 illustrates the drill hole layout and sections digitised for domain classification. Typical core samples taken are illustrated in Figure 6.3.

6.2. Definition of geological domains

The exploration project involving chemical data included 61 drill holes with depths varying from 6.75m to 35.75m. Only 34 of the 61 drill holes contained the top-face clay. The core length of the top-face upper clay varied from 0.34m to 4.50m with a maximum length of 4.16m. The core length of the top-face lower clay varied from 0.44m to 2.45m with a maximum length of 2.01m. Top-face upper and lower clays were both present in 6 of the 34 drill holes, with the top face-upper clay overlaying the top-face lower clay (Figure 6.4). Eighteen boreholes contained only the top face-upper domain and 4 boreholes only the top-face lower domain. In total, 24 drill holes contained the top-face upper clay and 10 drill holes the top-face lower clay. The chemical data obtained from these samples were used for geological modelling and estimation.

The top-face upper and lower clays were defined by creating sections from the 2009/2010 drill holes, as is illustrated by Figure 6.4. Figure 6.5 shows typical sections digitised for each clay domain. The top-face upper and lower clay domains are depicted in blue and the other clay types in different colours. The three dimensional model created from these sections receives attention in the following chapter.

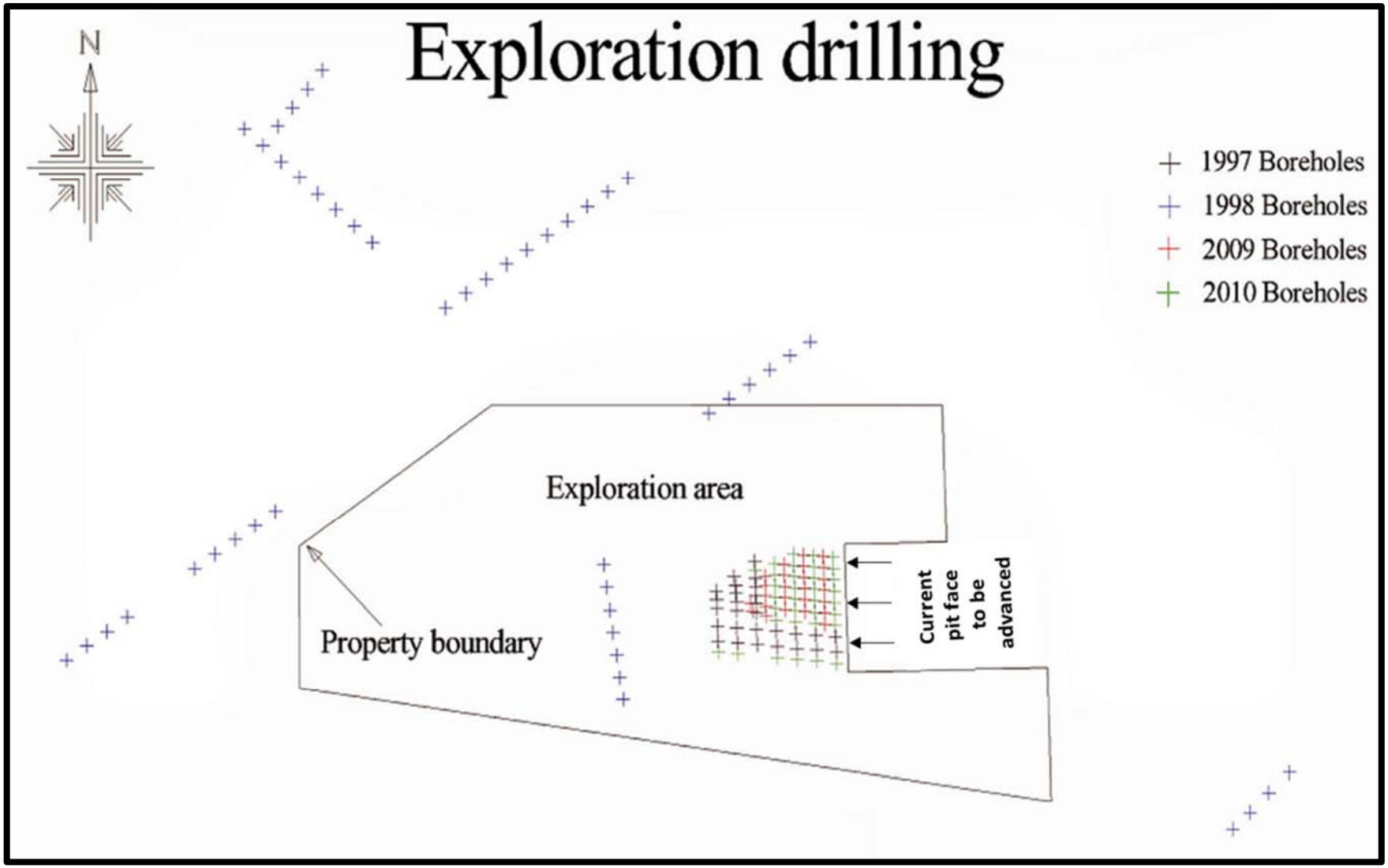


Figure 6-1. Drill hole layout in the area adjacent to the current pit.

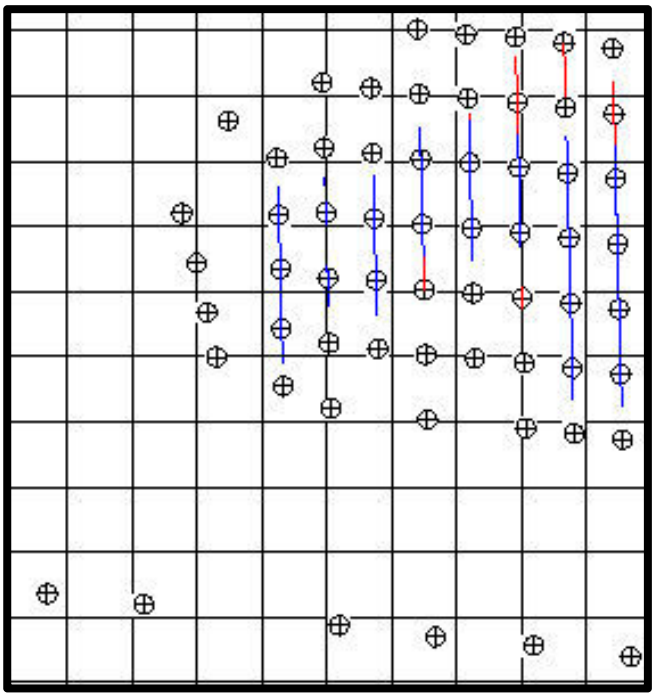


Figure 6-2. Drill hole layout and drill hole sections used for modelling.

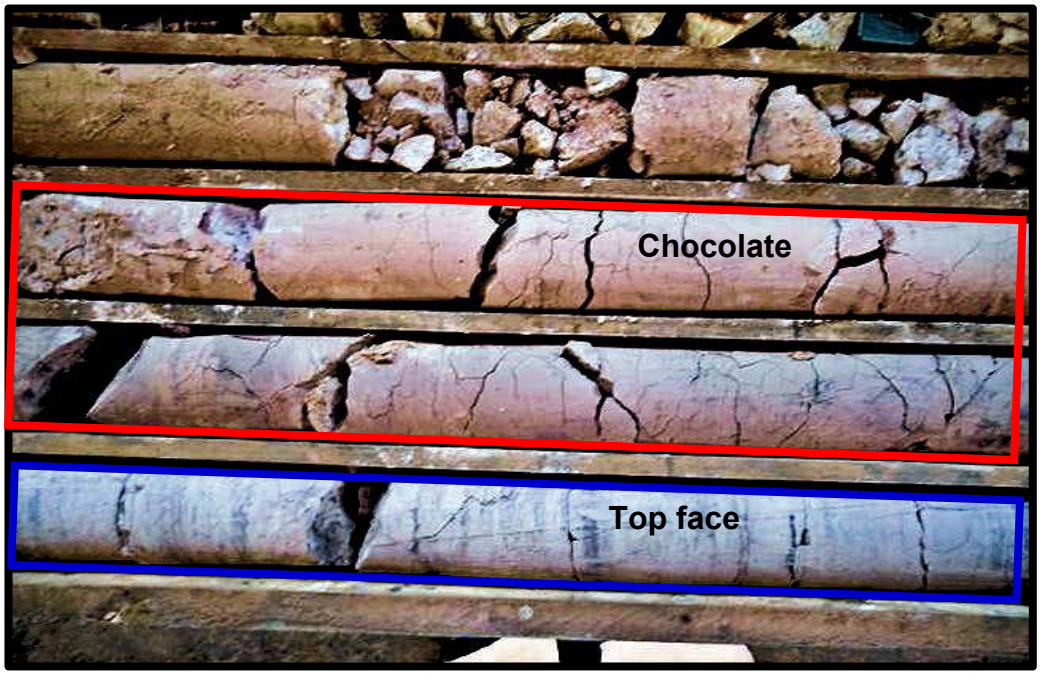


Figure 6-3. Typical drill core indicating chocolate and top-face clays.

Table 6-1. Classification of the different geological domains at Lawley, based on their mineralogical composition.

	MINERAL COMPOSITION PERCENTAGE						
DOMAIN	Kaolinite	Quartz	Mica	Smectite	Haematite/ Goethite	K-Feldspar	Plagioclase
Top face (TF)	55	36	5	2	1	1	
Stained top face (STF)	51	35	8	-	4	1	1
Red kaolin (RK)	65	13	9	3	9	1	
Chocolate (CHOC)	89	5	3	2	-	1	
Red shale (RS)	50	20	27	-	1	2	
Sandy kaolin (SK)	60	31	3	5	-	1	
Smectite (SMEC)	30	38	13	14	1	4	
Overburden (OVB)	47	36	8	-	8	-	

Table 6-2. Chemical composition of clay stockpiles mined with their minimum, maximum and average statistics.

	Chocolate									
	SiO_2	Al_2O_3	Fe_2O_3	TiO_2	CaO	MgO	Na_2O	K_2O	L.O.I	Total
Minimum	45.75	27.28	3.25	0.98	0.05	0.20	0.00	0.68	9.23	87.40
Maximum	54.80	34.63	6.60	1.60	0.18	0.45	0.15	1.78	11.85	112.03
Average	49.20	31.70	5.03	1.40	0.13	0.30	0.08	1.10	10.90	99.83
	Red Kaolin									
	SiO_2	Al_2O_3	Fe_2O_3	TiO_2	CaO	MgO	Na_2O	K_2O	L.O.I	Total
Minimum	42.34	27.38	7.30	1.02	0.04	0.08	0.02	0.66	9.10	87.94
Maximum	51.42	31.30	13.63	1.26	0.12	0.36	0.18	1.56	10.64	110.47
Average	47.68	29.16	10.86	1.14	0.08	0.18	0.06	0.98	9.72	99.86
	Smectite									
	SiO	Al_2O_3	Fe_2O_3	TiO_2	CaO	MgO	Na_2O	K_2O	L.O.I	Total
Minimum	57.25	18.78	7.90	0.88	0.33	1.55	0.00	1.70	7.50	95.88
Maximum	59.60	20.30	9.70	0.90	0.50	2.23	0.10	2.30	8.78	104.40
Average	58.40	19.43	8.70	0.90	0.40	1.58	0.05	2.03	7.98	99.45
	Stained top face (STF)									
	SiO_2	Al_2O_3	Fe_2O_3	TiO_2	CaO	MgO	Na_2O	K_2O	L.O.I	Total
Minimum	44.94	22.36	3.96	0.88	0.02	0.10	0.00	0.68	7.40	80.34
Maximum	61.90	30.24	12.38	1.22	0.12	0.44	0.10	2.04	10.88	119.32
Average	52.66	26.80	8.70	1.08	0.06	0.22	0.04	1.28	9.06	99.90
	Top Face (TF)									
	SiO_2	Al_2O_3	Fe_2O_3	TiO_2	CaO	MgO	Na_2O	K_2O	L.O.I	Total
Minimum	49.26	23.28	*1.94*	0.94	0.00	0.20	0.00	1.12	7.72	84.46
Maximum	60.00	33.88	*7.90*	1.50	0.12	0.38	0.06	2.40	11.24	117.48
Average	54.54	28.32	*4.56*	1.20	0.04	0.28	0.04	1.74	9.28	100.00
	Sandy Kaolin									
	SiO_2	Al_2O_3	Fe_2O_3	TiO_2	CaO	MgO	Na_2O	K_2O	L.O.I	Total
Minimum	57.63	18.23	0.75	0.55	0.03	0.38	0.00	0.28	6.58	84.40
Maximum	72.43	28.53	2.25	1.30	0.20	1.15	0.05	0.58	10.45	16.93
Average	62.43	22.70	1.23	0.90	0.13	0.68	0.03	0.38	8.28	96.73

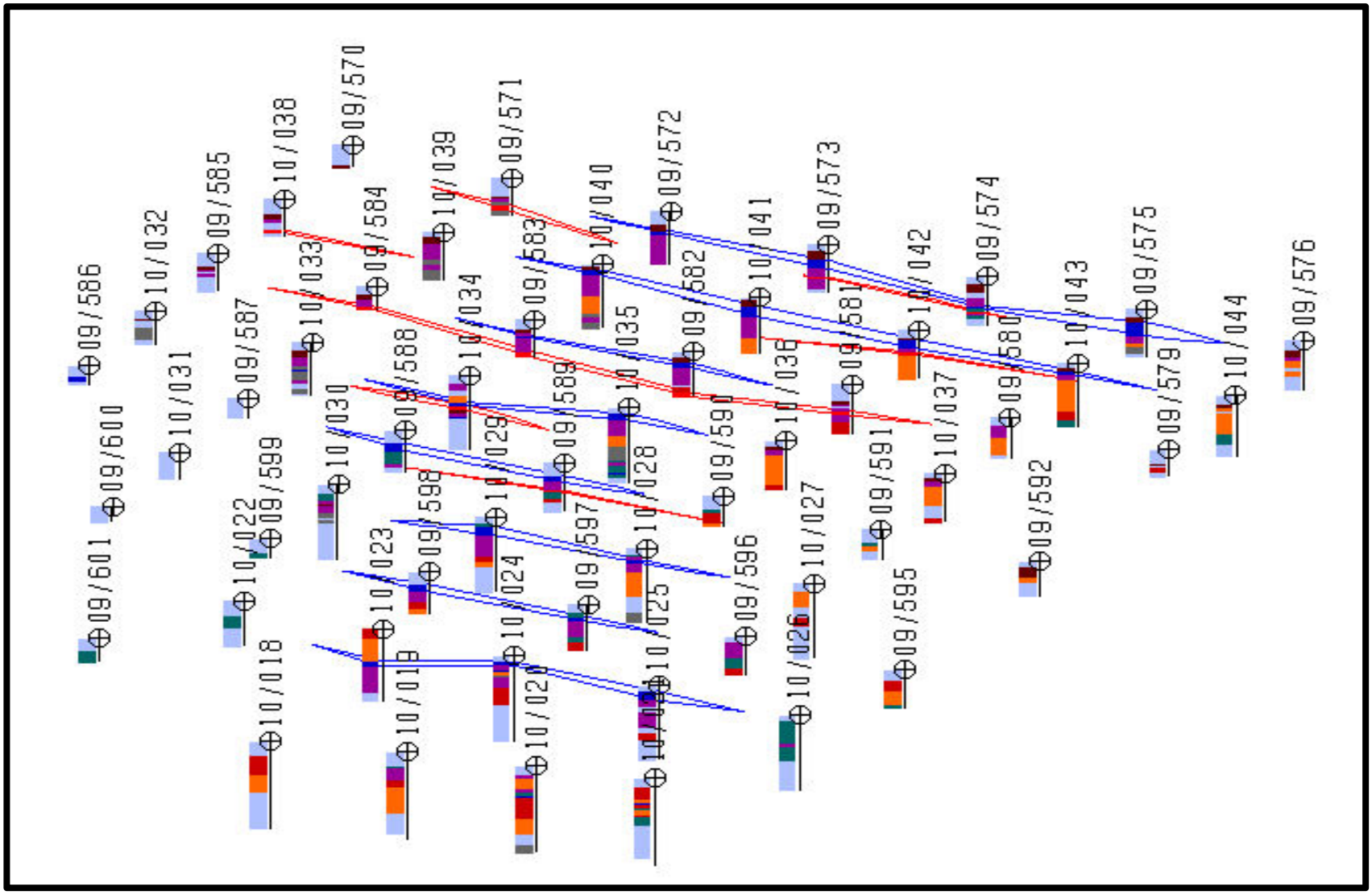


Figure 6-4. Top-face upper (blue) and lower (red) sections digitised from drill core to define each clay domain.

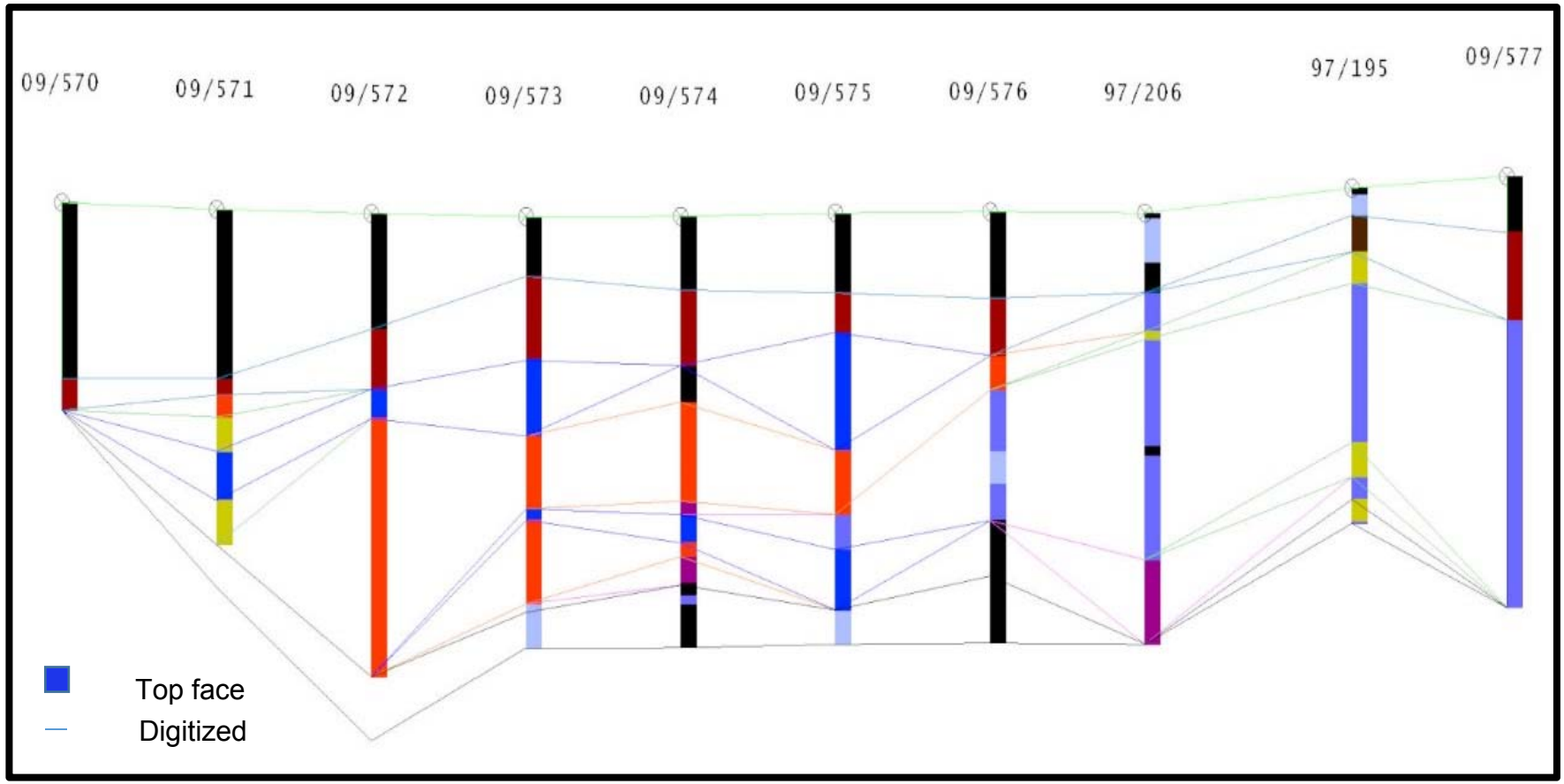


Figure 6-5. An illustration of a typical digitised section for domain creation, where top-face clay is demarcated blue.

6.3. Data analysis

Chemical analysis was done by the Council for Geoscience using X-ray fluorescence on fused beads. The data were then compared with the logged lithological domain. Samples were bulked for each lithological domain and re-analysed for their chemical composition. The bulked samples were further analysed by the Corobrik Central Laboratory for their physical properties, such as:

- Drying sensitivity
- Drying shrinkage
- Dry strength
- Fired shrinkage
- Fired strength
- Water absorption
- Fired colour.

6.4. Data validation

Corobrik makes use of the facilities of the Council for Geoscience for chemical analyses. The Council for Geoscience uses standards with each clay batch analysed and these are assessed by round robin tests with other laboratories. A typical example is given in Figure 6.6.

After data verification, the geological log sheets were used to compare the chemical analysis data according to the clay logs. Table 6.2 is a typical example of data that were re-evaluated. The chemical analysis should relate with the logged clay units. Spot checks were frequently conducted, as indicated in Table 6.2. If the chemical analyses are correct, the geological log sheet is edited and corrected. If the colours of the logged core do not correspond with the chemical analyses, the analyses were rejected and had to be repeated. Only after chemical data had been checked and validated, were the results loaded into the Surpac database for geological modelling.

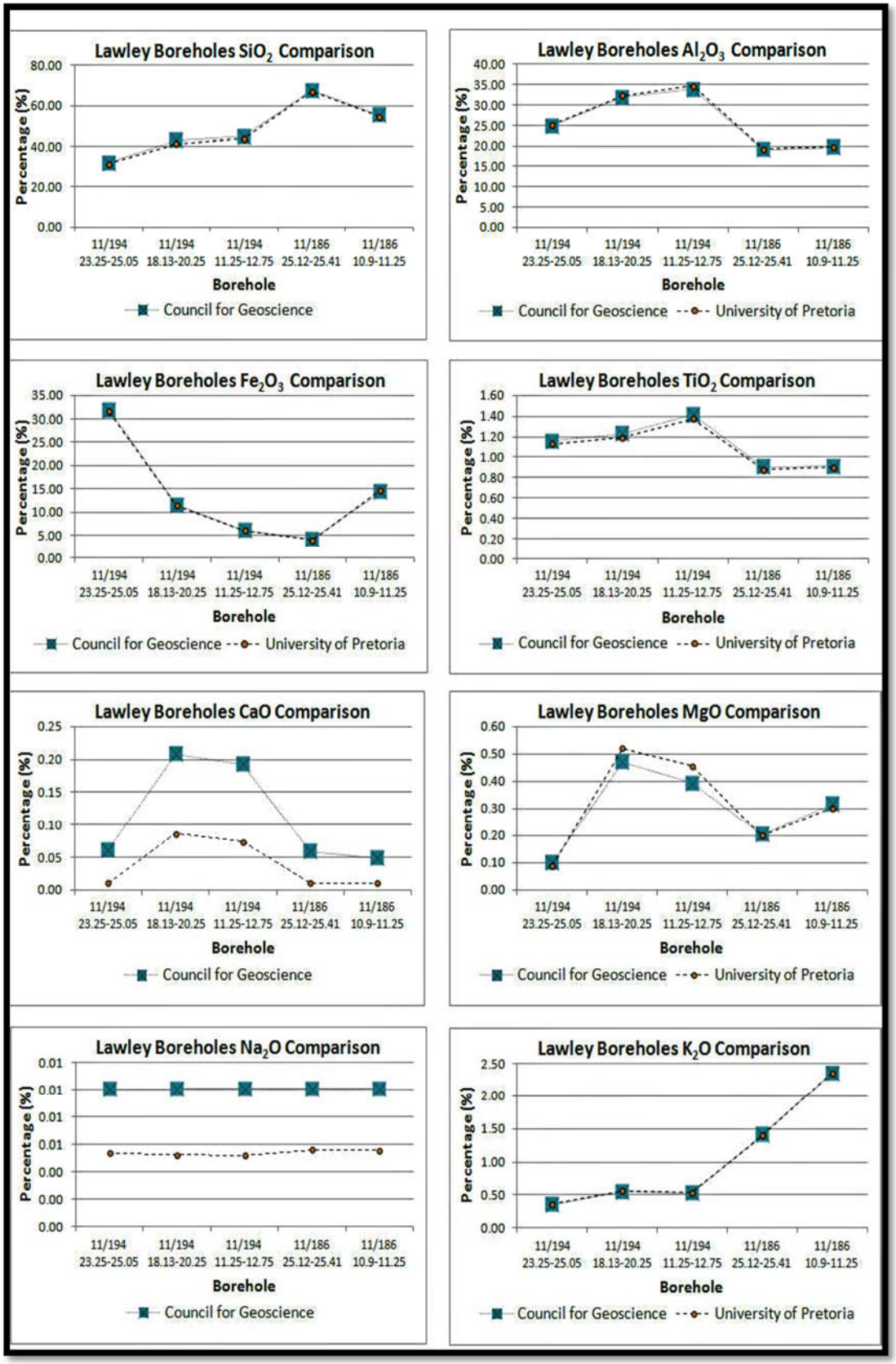


Figure 6-6. Illustration of chemical analysis verification results from round robin testing.

Table 6-3. Typical example of data validation of drilled core.

Sample	Hole ID	from	to	SiO_2	Al_2O_3	Fe_2O_3	TiO_2	CaO	MgO	Na_2O	K_2O	LoI	Total
Sandy Kaolin (M&L)	09/543	16.1	18.8	89.9	4.5	0.5	0.2	0.0	0.4	0.1	0.1	3.3	99.0
Sandy Kaolin (GEO)	09/543	16.1	18.8	92.5	4.4	0.5	0.1	0.2	0.4	0.1	0.1	1.7	100.0
Sandy Kaolin (Set Point)	09/543	16.1	18.8	91.4	4.0	1.6	0.2	0.2	0.5	0.1	0.1	2.3	100.4
Sandy Kaolin (M&L)	09/551	16.4	16.8	76.3	15.5	0.8	0.8	0.0	0.1	0.1	1.6	4.1	99.3
Sandy Kaolin (GEO)	09/551	16.4	16.8	77.5	15.3	0.8	0.7	0.1	0.1	0.1	1.7	4.1	100.4
Sandy Kaolin (Set Point)	09/551	16.4	16.8	75.7	15.5	1.3	0.7	0.1	0.1	0.1	1.7	4.5	99.7
Sandy Kaolin (M&L)	09/553	8.2	11.4	47.8	20.5	18.3	0.9	0.0	0.2	0.2	2.4	8.2	98.5
Sandy Kaolin (GEO)	09/553	8.2	11.4	50.3	20.0	17.6	0.9	0.1	0.1	0.1	2.5	7.9	99.5
Sandy Kaolin (Set Point)	09/553	8.2	11.4	49.4	20.8	16.1	0.8	0.1	0.1	0.1	2.4	8.2	98.0
Sandy Kaolin (M&L)	09/552	6.8	8.1	59.0	21.3	8.4	0.9	0.0	0.1	0.1	2.6	6.9	99.3
Sandy Kaolin (GEO)	09/552	6.8	8.1	59.4	20.8	9.0	0.9	0.1	0.1	0.1	2.7	6.9	100.0
Sandy Kaolin (Set Point)	09/552	6.8	8.1	59.2	21.1	8.0	0.9	0.1	0.1	0.1	2.7	6.9	99.1
Sandy Kaolin (M&L)	09/543	14.6	16.1	89.0	6.1	1.1	0.3	0.0	0.1	0.1	0.2	3.3	100.2
Sandy Kaolin (GEO)	09/543	14.6	16.1	89.3	6.4	1.1	0.3	0.2	0.1	0.1	0.3	2.4	100.2
Sandy Kaolin (Set Point)	09/543	14.6	16.1	87.9	6.0	1.7	0.3	0.2	0.1	0.1	0.3	2.8	99.4
Sandy Kaolin (M&L)	09/546	8.7	11.7	57.9	22.4	7.5	0.9	0.0	0.1	0.1	1.7	8.0	98.6
Sandy Kaolin (GEO)	09/546	8.7	11.7	50.6	31.8	2.9	1.4	0.2	0.1	0.1	1.5	10.7	99.3
Sandy Kaolin (Set Point)	09/546	8.7	11.7	48.9	32.2	3.1	1.3	0.3	0.1	0.1	1.4	11.3	98.7
Sandy Kaolin (M&L)	09/547	18.3	19.1	46.1	30.3	8.1	1.4	0.0	0.1	0.1	0.7	11.6	98.4
Sandy Kaolin (GEO)	09/547	18.3	19.1	48.5	30.1	7.3	1.4	0.2	0.1	0.1	0.8	11.2	99.7
Sandy Kaolin (Set Point)	09/547	18.3	19.1	46.8	30.9	6.7	1.3		0.1	0.1	0.8	11.9	98.6
Sandy Kaolin (M&L)	09/548	5.3	7.0	58.4	21.6	7.8	0.9	0.2	0.1	0.1	2.6	6.7	98.4
Sandy Kaolin (GEO)	09/548	5.3	7.0	58.5	20.6	9.9	0.9	0.1	0.1	0.1	2.7	6.9	99.8
Sandy Kaolin (Set Point)	09/548	5.3	7.0	58.6	21.1	8.4	0.8	0.1	0.1	0.1	2.7	6.9	98.8

Table 6-4. Example of chemical analysis data spot checks.

EXPLORATION DRILLHOLE PROJECT 2009													
Description	Borehole number	Depth in meters		CHEMICAL ANALYSES (%)									
		from	to	SiO_2	Al_2O_3	Fe_2O_3	TiO_2	CaO	MgO	Na_2O	K_2O	LoI	Total
	09/573	2.3	2.8	59.9	19.2	10.7	0.8	0.0	0.2	0.1	0.7	8.2	99.8
		2.8	6.7	56.2	24.6	6.6	1.1	0.1	0.3	0.1	0.9	9.5	99.4
		6.7	10.3	58.6	24.9	4.7	o.0	0.1	0.4	0.1	3.2	7.4	99.4
		10.3	12.0	52.2	30.9	2.6	1.6	0.1	0.3	0.4	1.0	11.1	100.2
		12.0	13.7	52.2	30.9	3.0	1.6	0.1	0.3	0.2	1.1	11.1	100.5
Fe spot check		13.7	14.3	63.1	25.2	1.2	1.0	0.1	0.2	<0.05	0.5	9.1	100.4
(Fesc)		14.3	16.3	59.6	27.8	1.1	1.1	0.1	0.2	<0.05	0.6	10.0	100.5
6.1		16.3	18.2	54.8	27.2	6.0	1.2	0.1	0.2	0.1	0.7	9.8	100.1
		18.2	20.3	43.3	26.9	16.7	1.1	0.1	0.2	0.1	0.5	10.5	99.4
	09/576	4.1	6.8	70.0	15.7	6.4	0.6	0.0	0.0	0.1	0.4	6.7	99.9
		6.8	8.7	57.9	27.7	2.4	1.1	0.1	0.2	0.1	0.4	10.4	100.3
3.2		8.7	11.3	60.3	22.1	7.4	1.0	0.1	0.1	0.5	0.8	8.2	100.5
		11.3	12.8	58.1	16.2	17.0	0.7	0.1	0.2	0.2	1.4	5.9	99.8
		12.8	14.5	54.7	21.9	12.6	0.9	0.1	0.1	0.9	0.6	8.4	100.2
		14.5	17.1	69.6	16.4	6.4	0.7	0.1	0.1	0.3	0.9	5.9	100.4
		17.1	20.3	55.7	23.3	9.6	1.1	0.1	0.2	<0.05	0.5	9.4	99.9
	09/581	2.3	3.9	73.4	12.9	6.1	0.7	0.0	0.1	0.2	0.4	5.5	99.3
		3.9	6.8	56.9	21.7	10.4	0.8	0.0	0.2	0.3	0.9	8.7	99.9
		6.8	8.3	53.9	28.2	4.8	1.3	0.1	0.3	0.3	0.9	10.3	100.1
		8.3	8.8	53.1	31.0	2.5	1.2	0.1	0.3	0.2	1.0	10.8	100.2
(Fesc)		8.8	9.4	53.8	26.2	7.6	1.3	0.1	0.3	0.2	0.7	9.8	100.0
3.4		9.4	10.8	51.9	30.9	3.3	1.5	0.1	0.2	0.2	0.4	11.4	99.9
2.3		10.8	12.8	66.3	21.9	3.2	1.0	0.1	0.1	0.3	0.8	7.5	101.2
3.2		12.8	15.0	55.1	29.0	3.0	1.1	0.1	0.2	0.2	0.5	10.7	99.9
		15.0	20.3	51.0	25.3	12.3	1.0	0.1	0.2	0.2	0.7	9.2	100.0
	09/584	3.8	5.3	49.9	31.0	3.8	1.4	0.1	0.3	0.2	0.6	11.5	98.8
4.1		5.3	5.6	50.1	31.6	4.0	1.5	0.1	0.3	0.2	0.8	11.5	100.1
2.7		5.6	6.5	49.3	32.7	2.7	1.4	0.1	0.4	0.6	0.7	12.1	100.0
2.4		6.5	8.5	49.8	31.4	3.2	1.4	0.1	0.3	0.5	0.8	11.6	99.1
3.2		8.5	9.8	60.9	25.5	2.5	1.1	0.1	0.2	0.1	0.5	9.4	100.3
9	09/604	5.5	8.7	52.1	26.9	8.9	0.9	0.0	0.2	<0.05	0.7	10.5	100.2
9.2		8.7	10.2	57.9	23.2	8.0	0.7	0.0	0.2	0.1	0.5	9.6	100.2

6.5. Descriptive statistics for the upper and lower top-face clays

Statistical analysis provides valuable information for describing the data. The descriptive statistics of SiO_2, Al_2O_3, Fe_2O_3, K_2O and loss on ignition for the top-face upper and lower clay domains are given in Tables 6.5 and 6.6. Figure 6.7 summarises the histograms for the top-face upper and lower clay domain variables and Figure 6.8 illustrates their corresponding quantile-quantile plots (QQ-plots).

Table 6-5. Descriptive statistics of the top-face upper layer.

Top-face upper clay layer					
N=24	**SiO_2**	**Al_2O_3**	**Fe_2O_3**	**K_2O**	**L.o.I.**
Measure of location	**Central tendency**				
Mean	57.61	27.17	3.28	1.80	8.50
Median	58.26	27.11	2.90	1.50	8.70
Mode	54.70	27.00	2.90	3.20	8.70
Measure of spread	**Dispersion of variability about the mean**				
Standard Deviation	3.34	2.70	1.57	1.00	0.95
Variance	11.14	7.30	2.46	0.99	0.90
Range	16.10	12.98	5.18	2.77	3.08
Minimum	50.38	19.69	0.95	0.43	6.80
Maximum	66.48	32.67	6.13	3.20	9.88

Table 6-6. Descriptive statistics of the top-face lower layer.

Top-face lower clay layer					
N=10	**SiO_2**	**Al_2O_3**	**Fe_2O_3**	**K_2O**	**L.o.I.**
Measure of location	**Central tendency**				
Mean	62.27	24.50	2.58	0.57	8.65
Median	62.05	24.75	2.38	0.50	8.74
Mode	#N/A	#N/A	3.90	0.50	#N/A
Measure of spread	**Dispersion of variability about the mean**				
Standard Deviation	1.97	1.32	1.29	0.18	0.67
Variance	3.90	1.75	1.66	0.03	0.45
Range	6.50	4.30	4.14	0.49	2.10
Minimum	59.80	21.90	0.60	0.31	7.50
Maximum	66.30	26.20	4.74	0.80	9.60

The drill holes indicate that the top-face upper clay domain is larger than the top-face lower clay domain.

Variable comparison between the top-face upper and lower clay domains.

Comparing the variables between the top-face upper and lower clay domains, the following observations can be made:

- The SiO_2 content in the top-face upper clay (57.61 %) is lower than in the top-face lower clay (62.27 %).
- The Al_2O_3 content in the top-face upper clay (27.17 %) is higher than in the top-face lower clay (24.50 %).
- The SiO_2/Al_2O_3 ratio is 2.12 for the top-face upper clay and 2.54 for the top-face lower clay.
- The Fe_2O_3 content (3.28 %) in the top-face upper clay is higher compared to the top-face lower clay (2.58 %).
- The K_2O content is higher in the top-face upper clay (1.80 %) than in the top-face lower clay (0.57%).
- Loss on ignition (L.o.I) is similar for both the top-face upper (8.50 %) and lower clay (8.65 %).
- The variance of all variables in the top-face upper clay is consistently higher than the variables in the top-face lower clay.

The statistical data indicate a higher clay (SiO_2/Al_2O_3 ratio) and flux content (Fe_2O_3 and K_2O) with greater variability in the top-face upper clay compared to the top-face lower clay.

The data distribution of the variables in the top-face upper and lower clay domains.

Limited data were obtained from drilling campaign for geostatistical data analysis. The top-face upper clay was present in 24 drill holes and the top-face lower layer in 10 drill holes. From the data presented in Tables 6.5 and 6.6 the following can be deduced:

- There are no repeating numbers for the SiO_2, Al_2O_3 and L.o.I variables in the top-face lower clay and therefore no mode.
- The mean, median and mode (central tendency) for the individual variables in the top-face upper and lower clays are very similar, except for Fe_2O_3 in the top-face upper layer with the median noticeably lower than the mean.
- It can be deduced that each of the above mentioned variables, in both clay layers, have symmetrical/normal data distributions.

The histograms presented in Figure 6.7 also illustrate the normal distributions of both the top-face upper and lower clay variables. The median for the Fe_2O_3 variable (2.90) in the top-face upper clay is slightly smaller than the mean (3.28), indicating positive skewness with a longer tail of high values to the right. A bimodal distribution is evident for K_2O in the top-face upper layer indicative of two populations. The QQ-plots presented in Figure 6.8 further illustrate that the variables plot close on a straight line and reflect the normal distribution of the data.

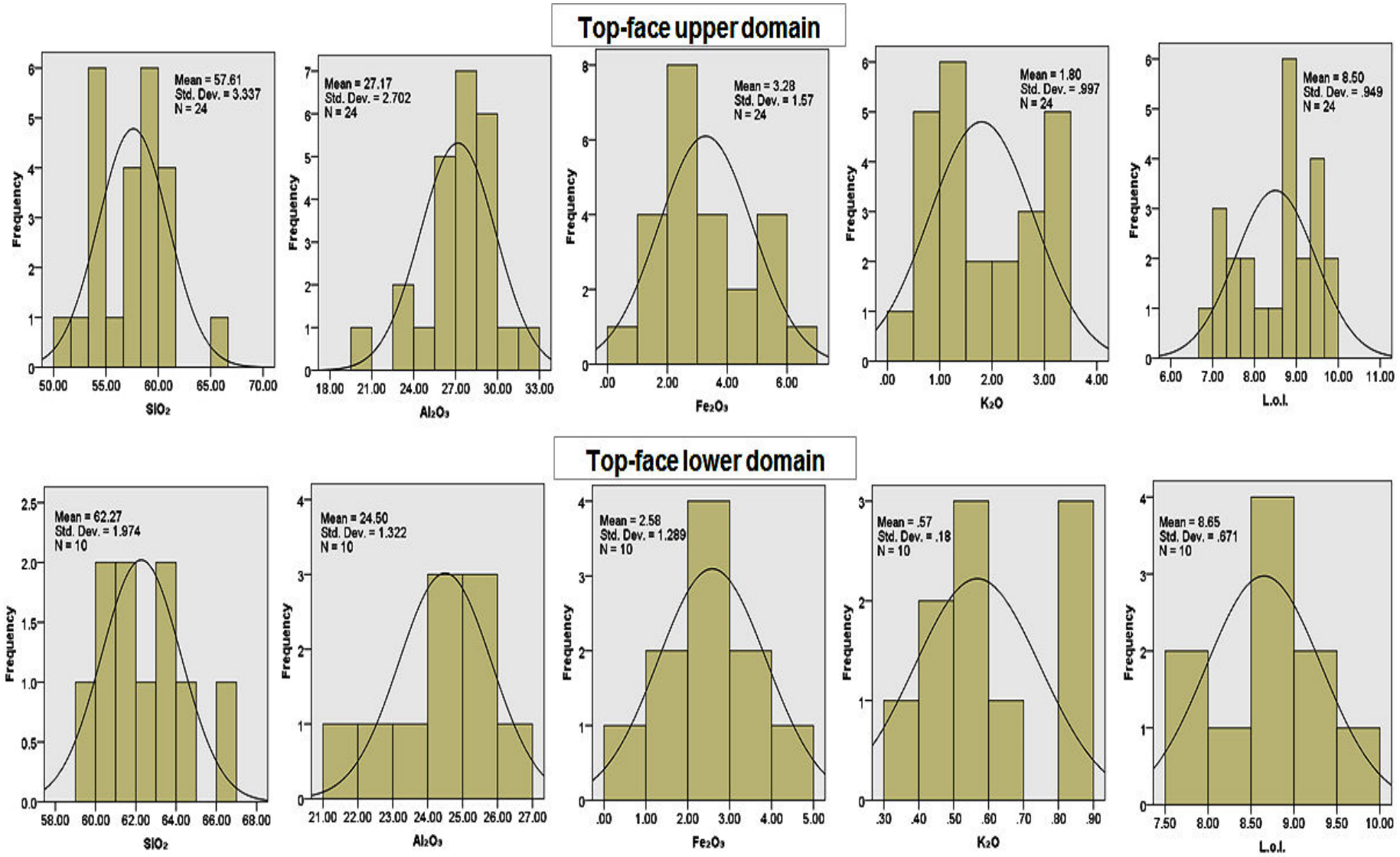


Figure 6-7. Histograms for top-face upper clay and lower clay.

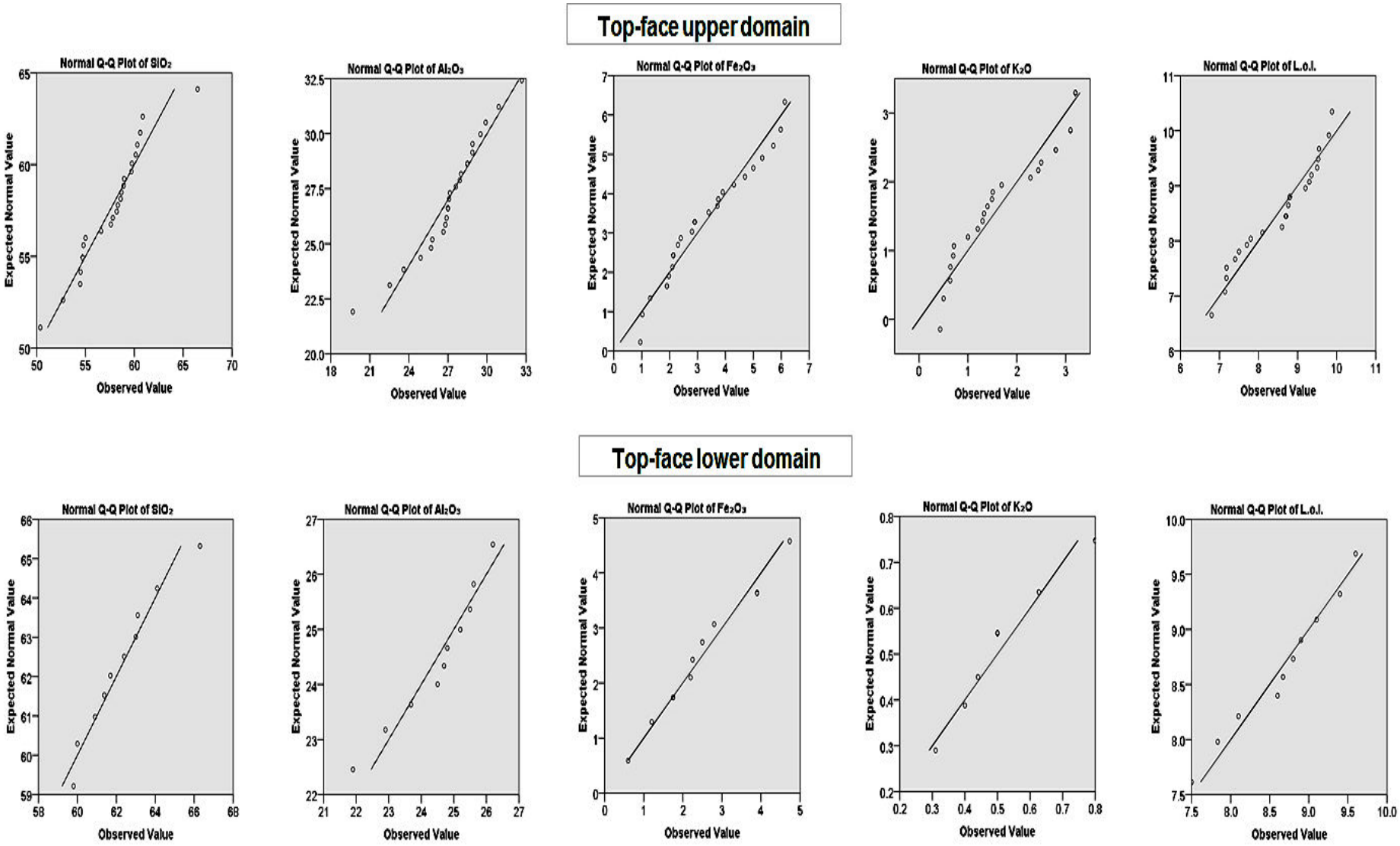


Figure 6-8. Probability plots for top-face upper clay and top-face lower clay.

6.6. Contour maps

6.6.1. Top-face upper clay

To illustrate the important spatial features, contour maps were constructed for the variables SiO_2, Al_2O_3, Fe_2O_3, K_2O and loss on ignition for the top-face upper clay using Surpac software. The chemical data obtained from the 24 drill hole samples (composited to 0.5m intervals) were used for contouring. These maps are summarised in Figure 6.9 and discussed in the following section.

SiO_2 contour map for top-face upper clay

The SiO_2 contour map indicates that the highest and steepest grade changes are towards the north and north-eastern corner of the map. Three distinct variations are noted. The variations are as follows:

- To the north between 58 percent and 64 percent.
- To the north-east corner between 52 percent and 58 percent.
- To the west between 54 percent and 58 percent.

The most prominent variation is that towards the north end of the map. This variation is adjacent to the variation towards the north-eastern corner of the map. These two variations, adjacent to one another, fluctuate widely with more than 10 percent. This is clearly an area of concern in terms of grade consistency. The eastern and southern parts of the map reveal subtle grade changes over a wider area that vary between 56 percent and 60 percent. This is mainly due to the absence of data in the southern region of the map, as data are constrained to top-face clay only.

Al_2O_3 contour map for top-face upper clay

Grade variations towards the north and north-eastern corner of the map vary between 22 percent and 27 percent, and 28 percent and 32 percent, respectively. These two variations, adjacent to one another, is an area of concern in terms of grade consistency. The grades vary up to 10 percent, similar to what was observed for the SiO_2 contour map. Another two variations, adjacent to one another, are noted towards the west. One variation varies

between 27 percent and 29 percent and the other between 24 percent and 25 percent. With regard to grade consistency, these two variations are also a cause for concern, albeit to a lesser extent than are those in north and north-east corner of the map.

Fe_2O_3 contour map for top-face upper clay

The contour map shows the highest concentration of Fe_2O_3 grades towards the north, with various smaller variations to the north-eastern corner of the map. To the north, the Fe_2O_3 varies between 4 percent and 5 percent. The smaller variations towards the north-eastern corner of the map vary between 2 percent and 3 percent, 4 percent and 5 percent, and 2 percent and 4 percent, respectively. These variations, adjacent to one another, will cause more drastic variance in the Fe_2O_3 grades compared with the other areas. Fe_2O_3 grade variation is small and more widely spread in an east–west direction and varies between 2 percent and 3 percent, and 3 percent and 4 percent, which will allow better grade control and quality consistency in this direction.

K_2O contour map for top-face upper clay

The K_2O contour map reveals several variations over the entire area. It is noteworthy that the highest values occurs in the centre of the map in an east–west direction and varies between 2 percent and 3 percent. To the north of the map in an east–west direction, grades vary between 0.5 percent and 2 percent. To the south of the map in an east–west direction, grades vary between 1.5 percent and 2 percent. It is clear that in terms of grade variability, the variability is higher in a north–south direction than it is in an east–west direction. The higher grades in the centre region of the map will cause more shrinkage of the brick during the firing process and, in the presence of high Fe_2O_3, will enhance the darker-colour of the brick. The grades are lowest in an east–west direction. These lower grade values will have a smaller effect on the fired shrinkage of the brick and will contribute to a lighter coloured brick, assuming the Fe_2O_3 grade remains consistent.

Loss on ignition contour map for top-face upper clay

The two variations at the northernmost part of the map reveal the steepest grade changes of between 7 percent and 8.5 percent, and 8 percent and 9.5 percent, respectively. Towards the eastern and south-eastern part of the map, grade changes of 7.5 percent to 9.0 percent are observed; however, these are not as steep as are those observed towards the northern-most part of the map. In the remaining areas of the map, grade changes are subtle and in the range of 8 percent to 9.5 percent. The loss on ignition grades to the most northern and south-eastern ends of the map will pose challenges in terms of grade consistency. Although loss on ignition does not contribute to the colour development of the brick, it does have an influence on the degasification properties of the brick during the firing stage. In the presence of high K_2O and Fe_2O_3 content and a reduced kiln atmosphere, severe bloating (expansion) can occur, causing sticking and deformed bricks.

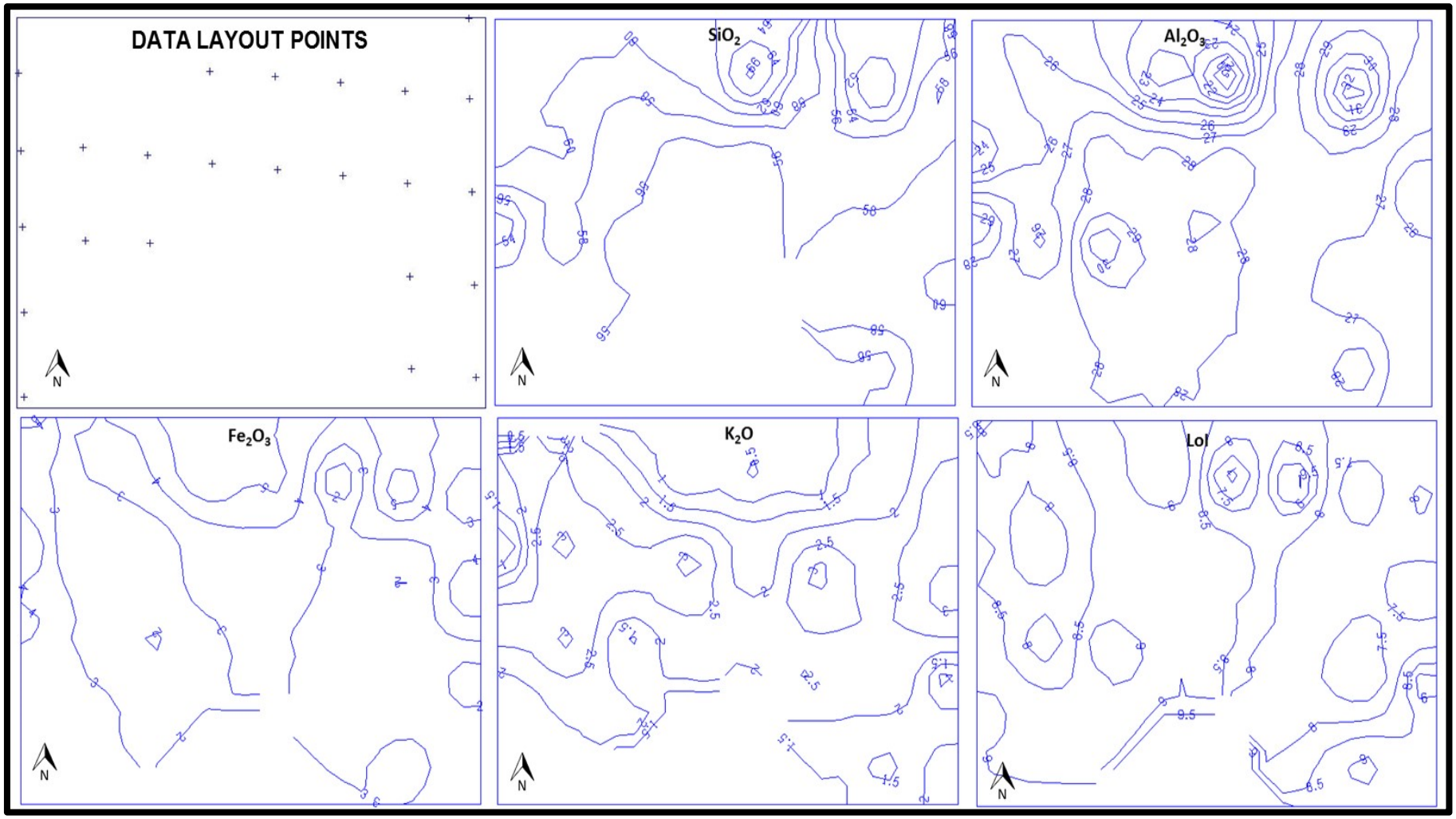


Figure 6-9. Contour maps for top-face upper clay variables.

6.6.2. Top-face lower clay

The spatial features for the top-face lower clay were constructed from the chemical data obtained from 10 drill holes, composited to 0.5m intervals. The contour maps that covered a smaller area than the top-face upper layer are depicted in Figure 6.5, and discussed below.

SiO_2 contour map for top-face lower clay

Variations were noted towards the southern part of the contour map, varying between 63 percent and 65 percent, and 61 percent and 63 percent, respectively. Another variation towards the centre of the map varies between 60 percent and 62 percent. The variability between these variations is not of major concern, since the difference between them is only about 5 %. The rate of change between these variations is subtle compared with the SiO_2 variations noted in the top-face upper clay. In terms of grade consistency, the lower top-face clay appears to be more consistent than the top-face upper clay.

Al_2O_3 contour map for top-face lower clay

Towards the north and north-west ends of the map, grade variation is almost non-existent at 25 percent. From the centre towards the south and south-western parts of the map, Al_2O_3 varies between 22 percent and 24 percent. Compared with the upper clay, the variations of the lower clay are not as prominent over the area.

Fe_2O_3 contour map for top-face lower clay

Towards the south-eastern corner of the map, the variation varies between 3 percent and 4.5 percent. Adjacent to this variation, towards the eastern side of the map, is another variation varying between 1.5 percent and 2.5 percent. Towards the west, grades very between 1 percent and 2.5 percent. The grade variability to the south-eastern corner and eastern area of the map is the steepest. Fe_2O_3 changes of up to 3 percent occur over a small area, which, in the presence of high K_2O, can cause a colour shift in the brick from light to dark. Apart from the south-eastern corner and easternmost part of the map, changes are subtle.

K_2O contour map for top-face lower clay

In contrast with the top-face upper clay, indicating various variations, none is detected in the lower clay. The grades in the lower clay vary between 0.3 percent and 0.8 percent. In terms of grade consistency, this clay is more continuous compared with the upper clay. Grade control for this clay should not be problematic.

Loss on ignition contour map for top-face lower clay

From the various contour maps studied, the loss on ignition map for the top-face lower clay appears to be continues. Grades very between 7.5 percent and 9.6 percent over the entire area of the map, with subtle changes. Similar to K_2O for the lower clay, grade control should not be problematic.

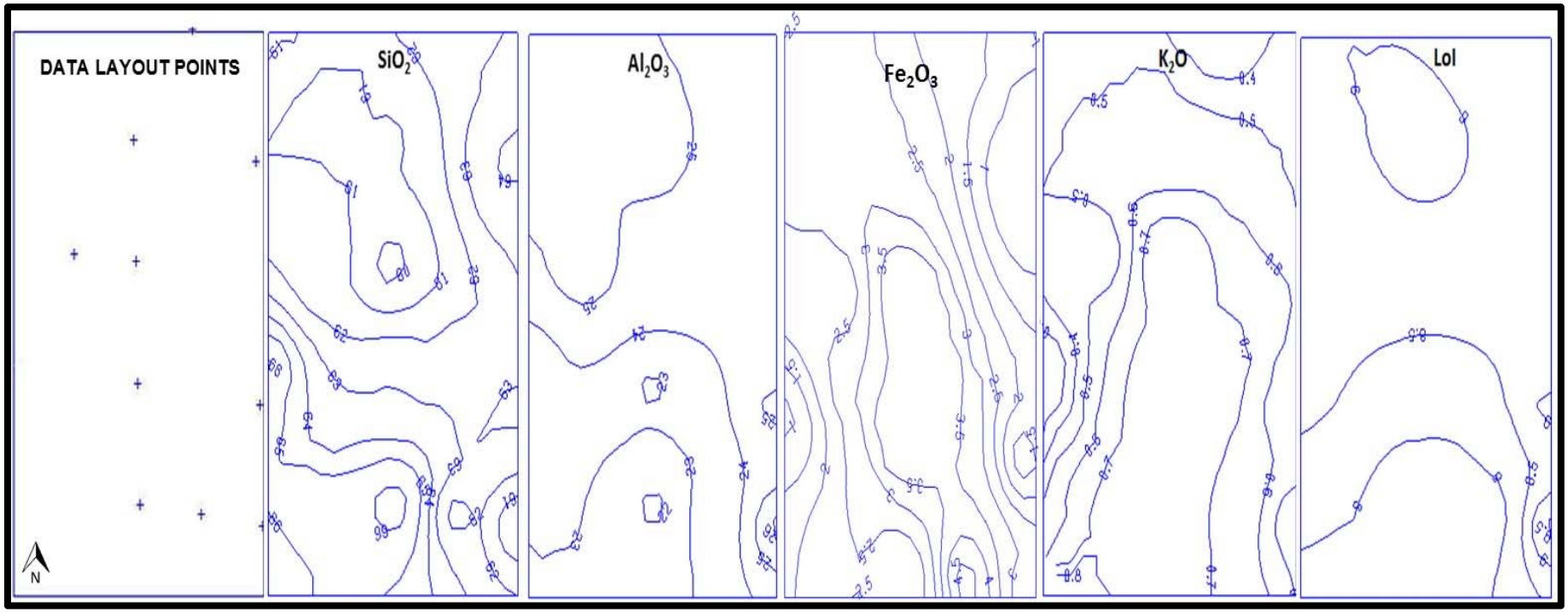


Figure 6-10. Contour maps for the top-face lower clay variables.

6.7. Summary

The statistical data analysis indicated key differences between the top-face upper and lower clays. From the descriptive statistics, it was noted that all the distributions were normal. The variables in the top-face upper layer showed the greatest inconsistency compared to the top-face lower layer. The Fe_2O_3 shows to be positively skewed for the top-face upper clay with a longer tail of small values to the right. The K_2O variable in the top-face upper layer appears to be bimodal, indicative of two populations.

The contour maps revealed that variations for the top-face upper clay variables SiO_2, Al_2O_3, Fe_2O_3 and loss on ignition were most evident towards the north and north-eastern parts of the map. In contrast, variations for the top-face lower clay variables were fewer and further apart, with a SiO_2 variation noted towards the southern part of the map and an Fe_2O_3 variation towards the south-eastern part of the map. The contour maps also indicated that for both the top-face upper and the lower clays, data were less constant in a north–south direction than they were in an east–west direction. Continuity appears to be in an east–west direction for both the clays.

CHAPTER 7

GEOSTATISTICS

7. INTRODUCTION

This chapter is devoted to the analysis of data continuity (variography). It relates to comparing the samples of the top-face upper and lower clay layers in terms of the distance and orientation between them. Understanding how the samples relate to one another in space can assist with using the information to estimate a block grade which is based on weighting the surrounding samples according to the variogram.

Chapters 5 and 6 described the collection and quality of the data, the geological context and the statistical properties of both the top-face upper and lower clay domains. The calculations of the variograms to follow are based on the following:

- Assumptions made as discussed in section 4.4.
- Data integrity as discussed in section 6.4.
- Statistical analysis of the data as discussed in section 6.5.

7.1. Compositing and preparation of variogram modelling

The data presented in chapter 6 illustrate the difference in thickness between the top-face upper and lower layer clay domains. The lengths of the core logged are illustrated in Figures 7.1 below. The minimum core length was 0.34m and the maximum 4.16m. The samples were composited to 0.5m intervals to include all possible samples. Compositing was done to ensure equal influence on the statistics and to minimise the introduction of a bias. Compositing was constraint within the domains and it was done to weight the sample grades to equivalent interval lengths. Variogram modelling was done on distances of pairs between holes in the horizontal plane. After compositing, there were 109 data points for the top-face upper layer and 32 data points for the top-face lower layer used for variogram mapping.

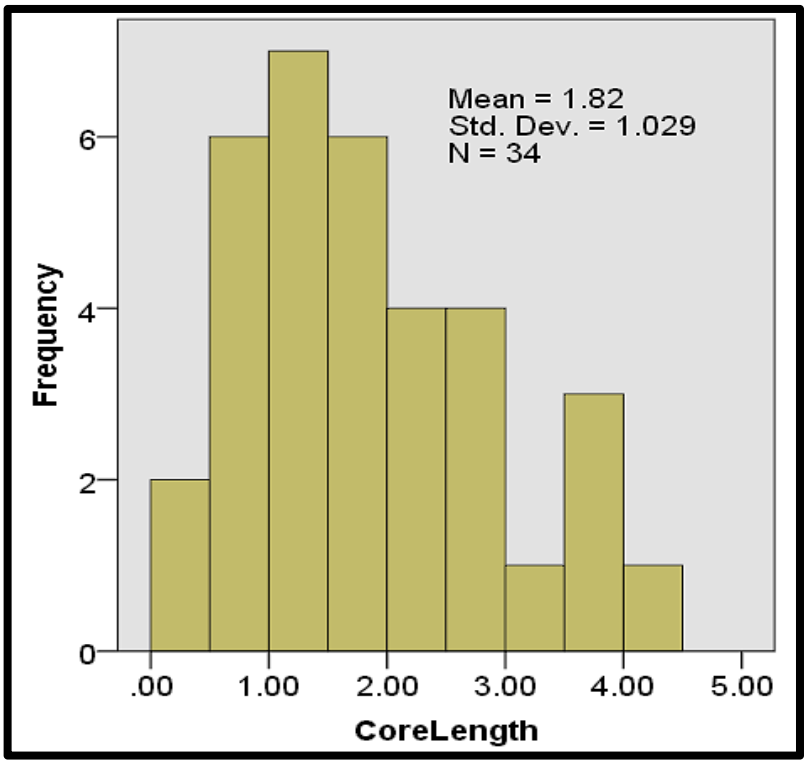


Figure 7-1, Lengths of top-face core samples logged

The statistical data discussed in Chapter 6 indicated that the data were normally distributed and therefore no transformation was applied for variogram modelling.

Variograms were created for both the upper and lower top-face clays and were modelled, using the spherical model. The model variogram is a curve that was mathematically fitted to the geological data. This was done to illustrate the grade variance plotted against the distance separating the samples. The variograms and variogram maps for the top-face upper clay are given in Figures 7.2 to 7.6, and those for the top-face lower clay in Figures 7.7 to 7.12. Table 7.1 summarises the variogram parameters for the five top-face upper clay variables, and Table 7.2 those for the top-face lower clay variables.

7.2. Variography for the top-face upper clay

Short-scale variance

The nugget effect symbolises discontinuity at the starting point equivalent to short-scale variability. The variability can be ascribed to measurement

inaccuracy or geological structures with correlation ranges shorter than the sampling resolution. The nugget (Table 7.1) is extremely small for all five the top-face upper clay variables, representing limited short-scale variability.

Large-scale variance

The distance at which the spherical model flattens out is known as the range. Variables are spatially auto-correlated by distances closer than the range, whereas locations beyond the range are not. As is noted in Table 7.1 and Figures 7.2 to 7.6, the longest range, for distances of pairs between holes, is reached for the Al_2O_3 variable (128.05) and the shortest range for the SiO_2 variable (54.42). This finding indicates that more Al_2O_3 variables were auto-correlated than were the SiO_2 variables. The Fe_2O_3 and loss on ignition variable ranges are very similar and were auto-correlated to a range value of approximately 75, while that of K_2O was auto-correlated to a range value of 65.

The sill was reached on the y-axis at the range value of the semi-variogram (the value at which the variogram levels off). For the top-face upper clay variables (Figs 7.2 to 7.3, and Table 7.1) the highest sill value obtained was for SiO_2 at 9.81, followed in decreasing order by Fe_2O_3 at 1.98, Al_2O_3 at 1.54, loss on ignition at 0.93, and K_2O at 0.9. These sill values indicate the radius of the region of impact (range).

Table 7-1. Variogram parameters for the five top-face upper clay variables.

	Top face upper layer				
Paramater	**SiO_2**	**Al_2O_3**	**Fe_2O_3**	**K_2O**	**Lol**
Model Type	Spherical	Spherical	Spherical	Spherical	Spherical
Nugget	0.11	0.01	0.02	0.01	0.01
Structure	1	1	1	1	1
Sill	9.81	1.54	1.98	0.90	0.93
Range	54.42	128.05	75.03	64.99	77.80

Continuity of mineralisation

An attempt was made to determine the orientation of mineralisation, variogram maps (Figs 7.2 to 7.6) were constructed for the SiO_2, Al_2O_3, Fe_2O_3, K_2O and Lol variables. The variogram maps were created, for distances of pairs between holes, in order to assess the bearing of the lowest change over the longest range. The direction with the smallest change over this range is the direction of maximum continuity. Table 7.2 provides the parameter values obtained for the top-face upper clay variogram maps.

Table 7-2. Top-face upper clay variogram map parameters.

	Top face upper layer				
Paramater	**SiO_2**	**Al_2O_3**	**Fe_2O_3**	**K_2O**	**Lol**
Ellipsoid plunge	0.00	0.00	0.00	0.00	0.00
Ellipsoid bearing	40.27	71.87	35.72	39.78	30.09
Ellipsoid dip	10.73	8.72	-6.09	0.00	-12.15
Major:semi-major	1.01	1.12	1.00	1.00	1.22
Major:minor	9.29	5.50	3.24	6.77	5.62

The orientation of the major axis is given as the horizontal azimuth, plunge (major axis dip) and dip (roll around the major axis). The ratio between the length of the major axis and the semi-major axis is the major/semi-major anisotropy ratio, whereas the ratio between the length of the major axis and the minor axis is the major/minor anisotropy ratio (Table 7.2). The major/semi-major anisotropy ratio was highest for the loss on ignition variable at 1.22, and lowest for the Fe_2O_3 and K_2O variables at 1.00. The major/semi-major anisotropy ratios were very similar, ranging between 1.00 and 1.22. If an area displays anisotropy, the anisotropy ratio could assist in determining the need for the interpolation of an anisotropic variogram model. The closer the major/semi-major ratio is to one, the less is the need for interpolation. In the instance of the top-face upper clay variables, the variable ratios were all close to one and therefore interpolation was not necessary.

All the variogram maps displayed (Figs 7.2 to 7.6) plot all the azimuths in a plane. The cold colours indicate low variance and ‘goodness of fit’, whereas

the warm colours indicate higher variance. The white areas indicate the nonexistence of samples in that azimuth over that distance. The variogram maps were used as a tool for attempting to find the orientation and range of the major axis of anisotropy, followed by the lengths and ranges of the other two axes.

In the variograms displayed in Figures 7.2 to 7.6, the number of samples in the blue area of the variogram map over the greatest range is taken into account, at the same time staying below or at the intersection of the variance line (green). The parameters obtained from the omni-directional variogram maps were used for estimation by means of ordinary kriging, which is further discussed in Chapter 8, to follow.

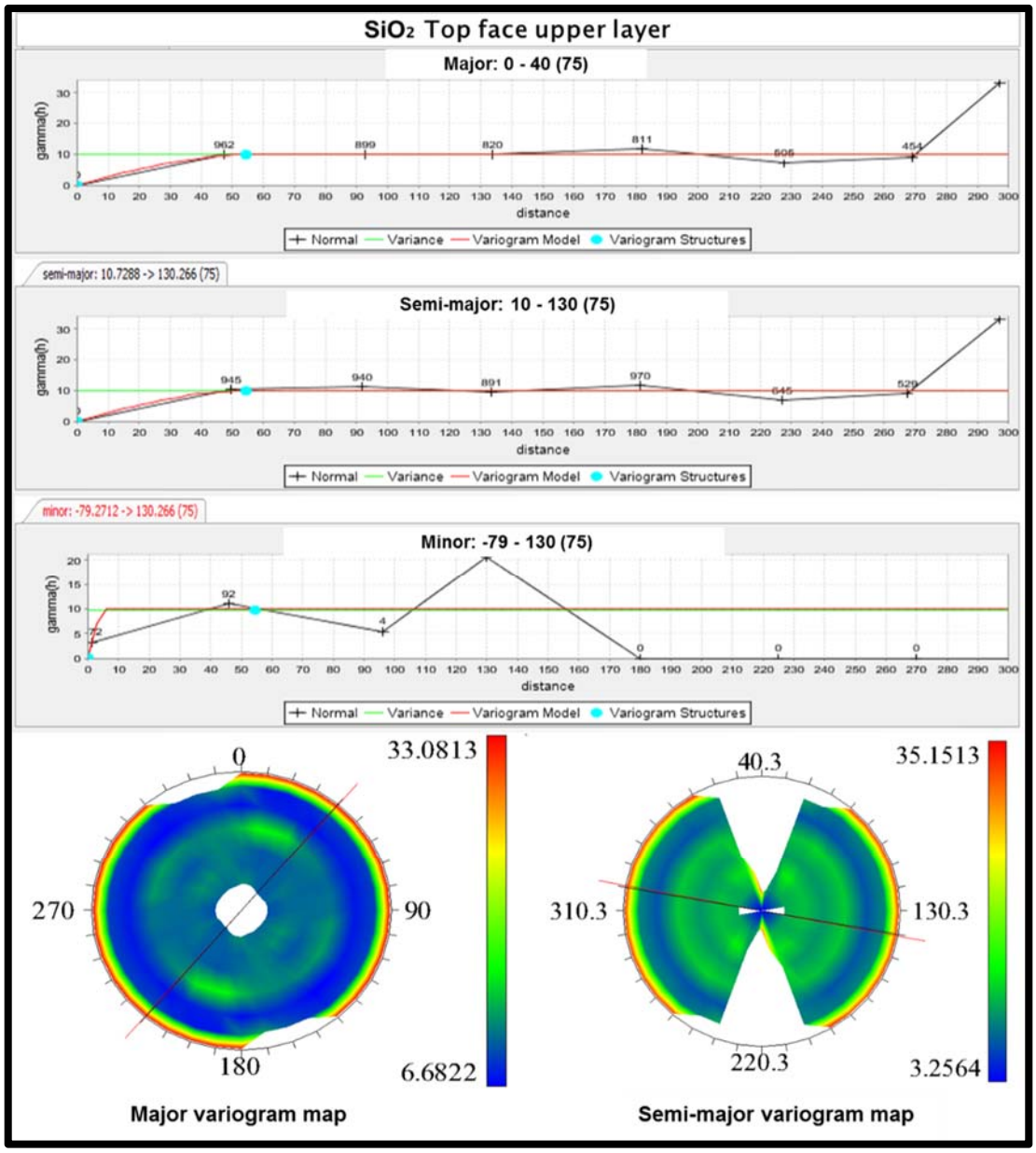


Figure 7-2. Major, semi-major and minor variograms, including the major and semi-major variogram maps for SiO_2 in the top-face upper clay.

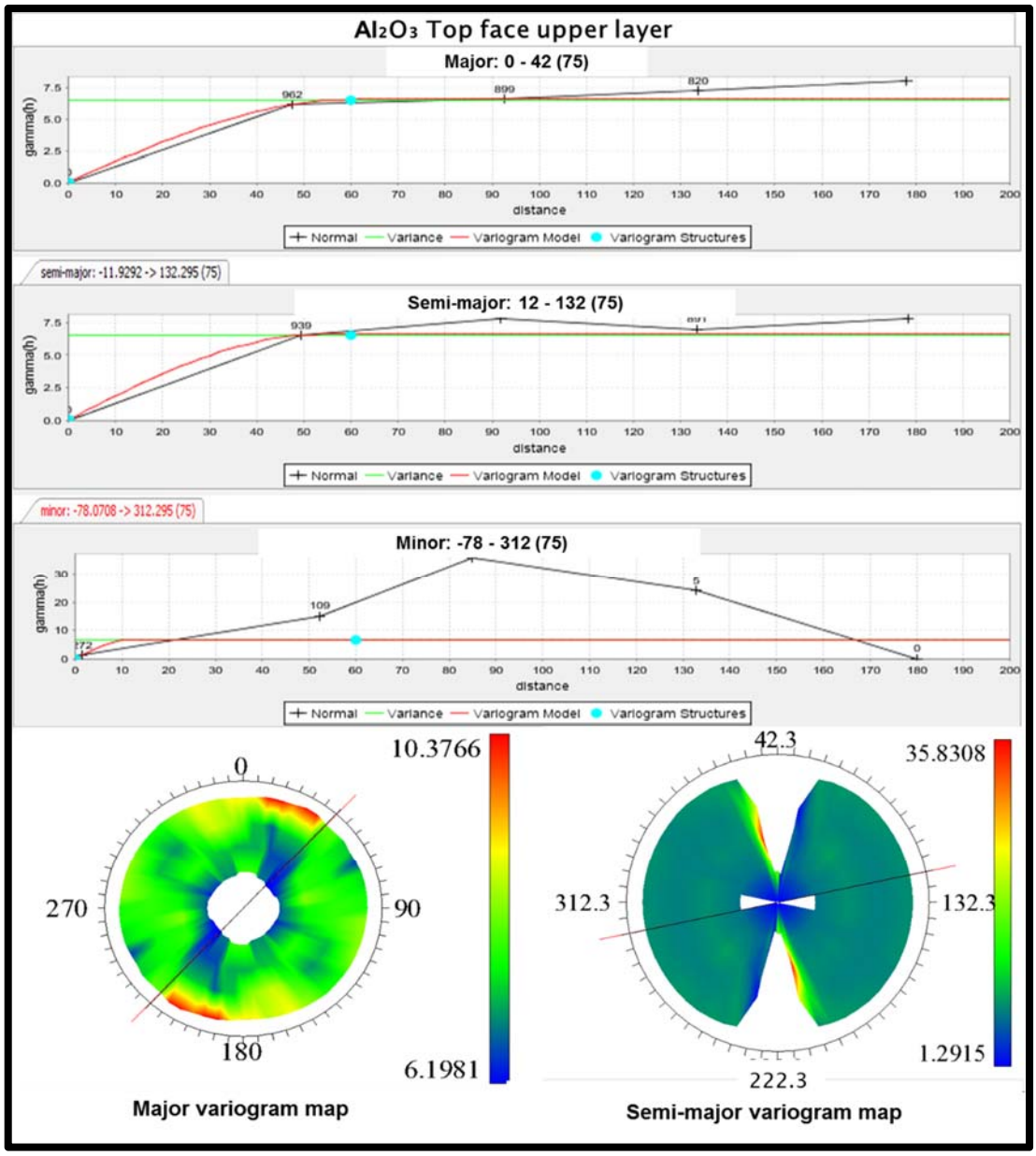


Figure 7-3. Major, semi-major and minor variograms, including the major and semi-major variogram maps for Al_2O_3 in the top-face upper clay.

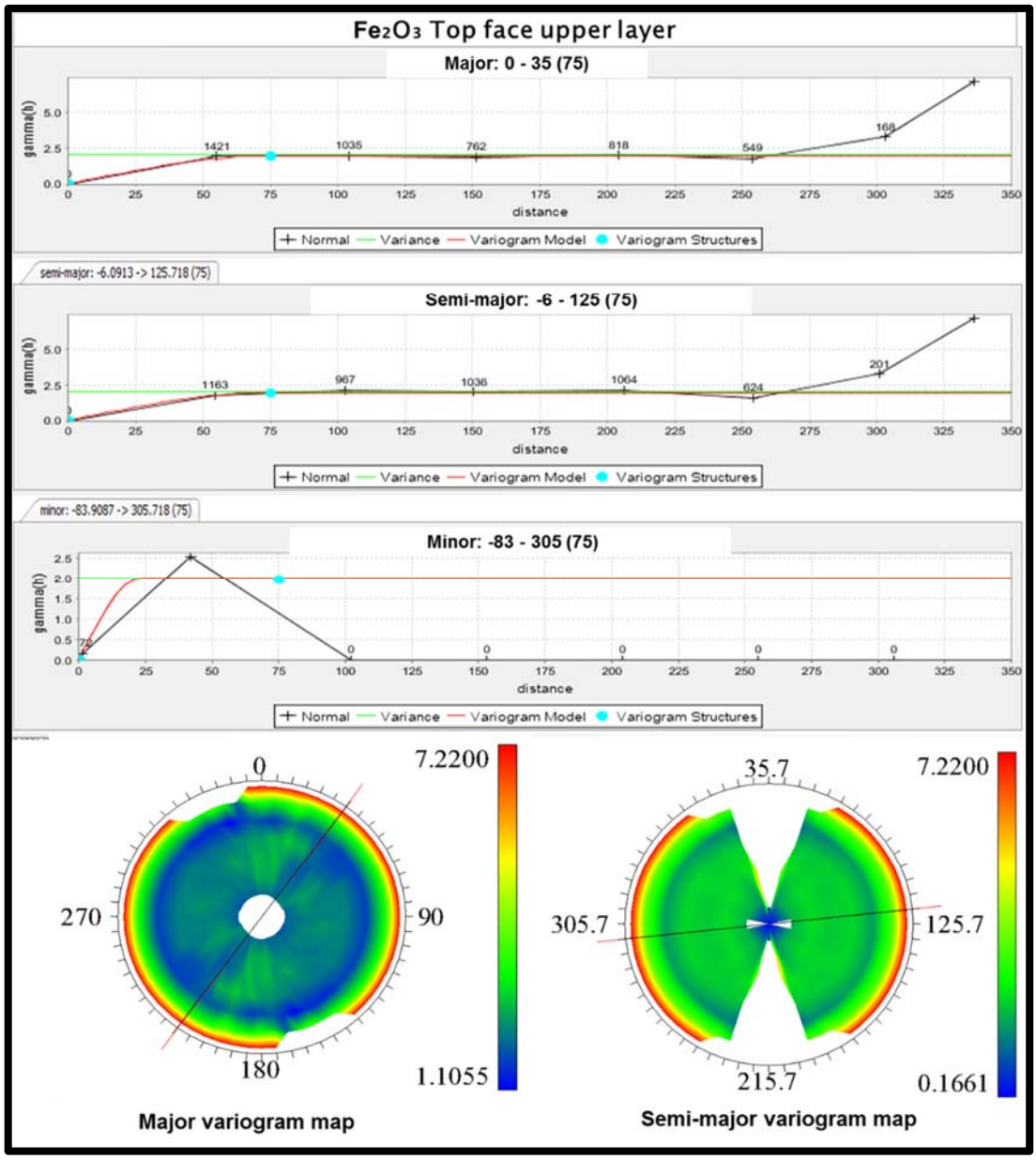


Figure 7-4. Major, semi-major and minor variograms, including the major and semi-major variogram maps for Fe_2O_3 in the top-face upper clay.

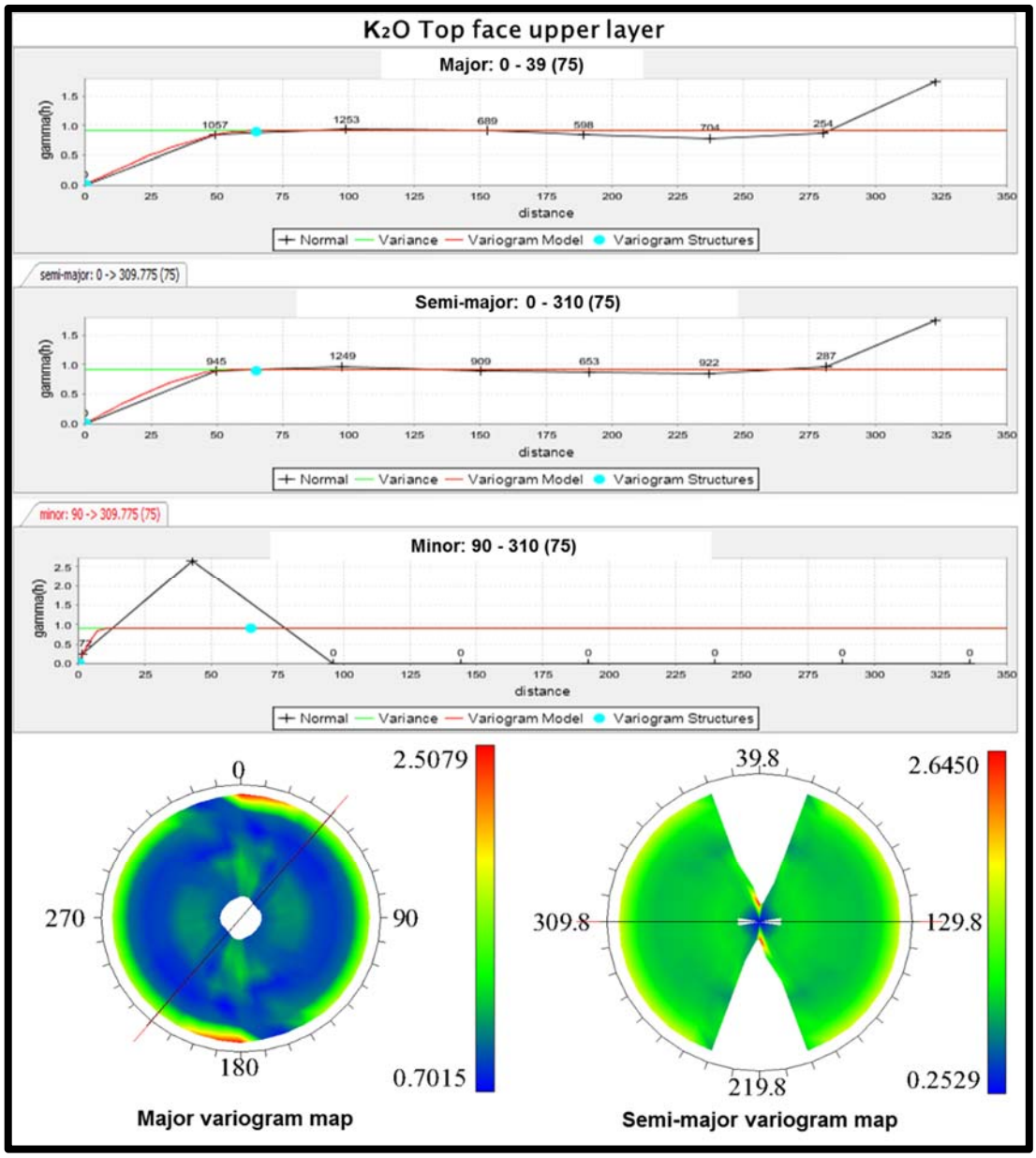


Figure 7-5. Major, semi-major and minor variograms, including the major and semi-major variogram maps for K_2O in the top-face upper clay.

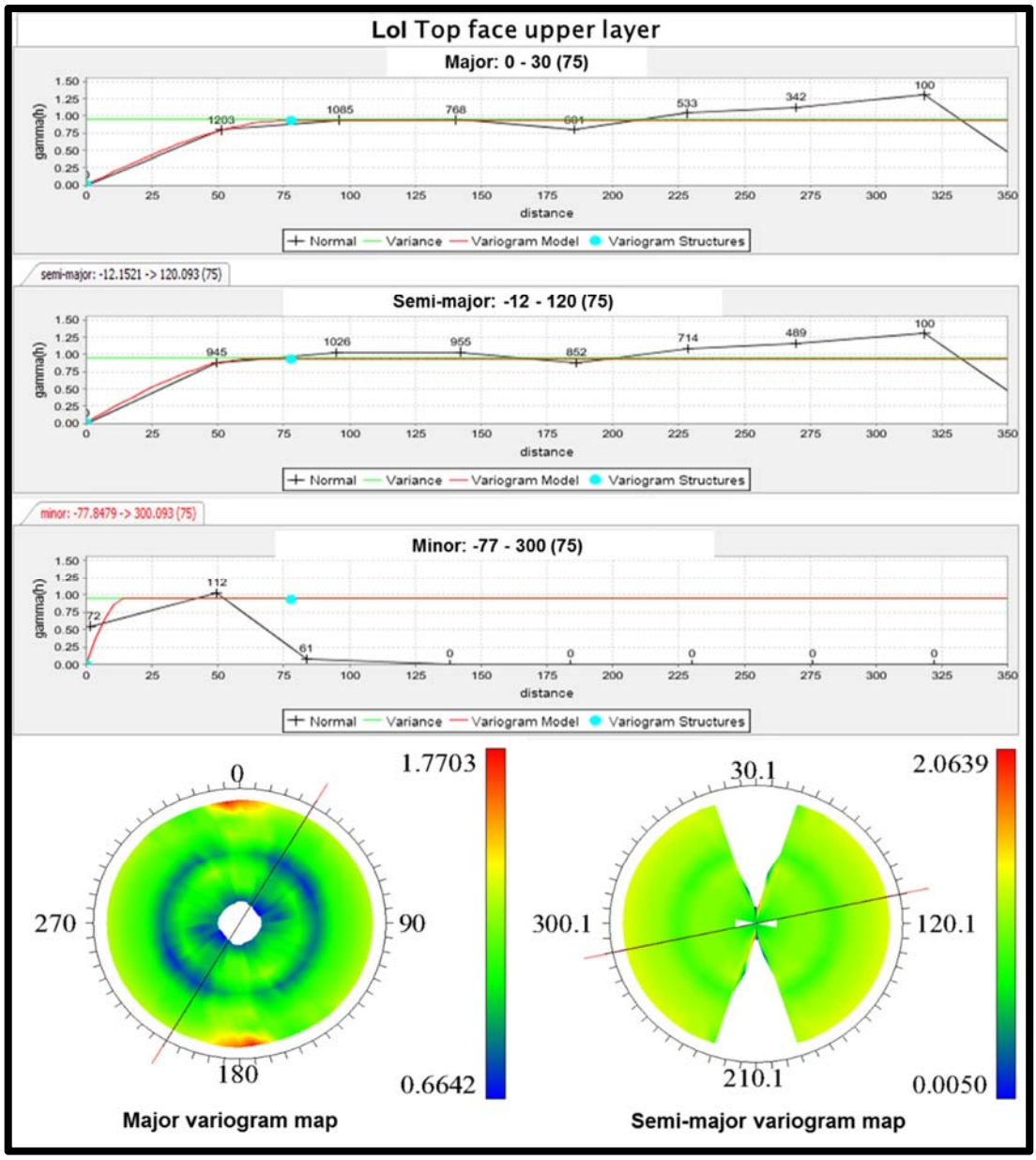


Figure 7-6. Major, semi-major and minor variograms, including the major and semi-major variogram maps for L.o.I in the top-face upper clay.

7.3. Variography for the top-face lower clay

Short-scale variance

Similar to the top-face upper clay, the variogram parameters for the top-face lower clay are summarised in Table 7.5. The nugget is even smaller than was that observed for the top-face upper clay, indicating limited short-scale variability.

Large-scale variance

As noted from Table 7.5 and Figures 7.11 to 7.15, the longest range was reached for the Al_2O_3 variable at 128.05 (similar to the top-face upper clay), and the shortest for the first Fe_2O_3 variogram structure at 74.5. This indicates that more Al_2O_3 variables were auto-correlated than were any one of the other four variables. The first Fe_2O_3 structure range is very similar to the K_2O range at between 75 and 80. The second Fe_2O_3 structure range is very similar to the loss on ignition range, both approximately 123, indicating auto-correlation up to these range values.

For the top-face lower clay variables (Figs 7.11 to 7.15, and Table 7.5) the highest sill value obtained was for SiO_2 at 4.91, followed in decreasing order by Al_2O_3 at 1.55, Fe_2O_3 at 1.13, loss on ignition at 0.34, and K_2O at 0.04. These sill values indicate the radius of the region of impact.

Table 7-3. Variogram parameters for the five top-face lower clay variables.

	Top face lower layer					
Paramater	**SiO_2**	**Al_2O_3**		**Fe_2O_3**	**K_2O**	**Lol**
Model Type	Spherical	Spherical		Spherical	Spherical	Spherical
Nugget	0.04	0.01		0.01	0.00	0.00
Structure	1	1		2	1	1
Sill	4.91	1.55	1) 0.53	1.13	0.04	0.34
Range	89.73	128.05	2) 74.57	122.47	80.77	123.37

Continuity of mineralisation

An attempt was made to determine the orientation of mineralisation, variogram maps (Figs 7.10 to 7.15) were also constructed for the SiO_2, Al_2O_3, Fe_2O_3, K_2O and Lol top-face lower clay variables. Table 7.6 depicts the parameter values for the top-face lower clay variogram maps.

Table 7-4. Top-face lower clay variogram map parameters.

	Top face lower layer				
Paramater	**SiO_2**	**Al_2O_3**	**Fe_2O_3**	**K_2O**	**Lol**
Ellipsoid plunge	0.00	0.00	0.00	0.00	0.00
Ellipsoid bearing	150.12	71.87	150.23	139.94	70.35
Ellipsoid dip	-10.38	8.72	-19.85	-19.82	-10.01
Major:semi-major	1.00	1.00	1.00	1.00	1.13
Major:minor	1.00	1.00	1.27	8.94	1.46

The major/semi-major anisotropy ratio was the highest for the loss on ignition variable at 1.14 and was the same for SiO_2, Al_2O_3, Fe_2O_3 and K_2O variables at 1.00, comparable with the top-face upper clay. These anisotropy ratios were also very similar, ranging between 1.00 and 1.13. For the top-face lower clay variables, the major/semi-major variable ratios were all also close to one, indicating no interpolation was required.

In the variograms displayed in Figures 7.6 to 7.10, the number of samples in the blue area of the variogram map over the greatest range is taken into account, at the same time staying below or at the intersection of the variance line (green). The parameters obtained from the omni-directional variogram maps were used for estimation by means of ordinary kriging.

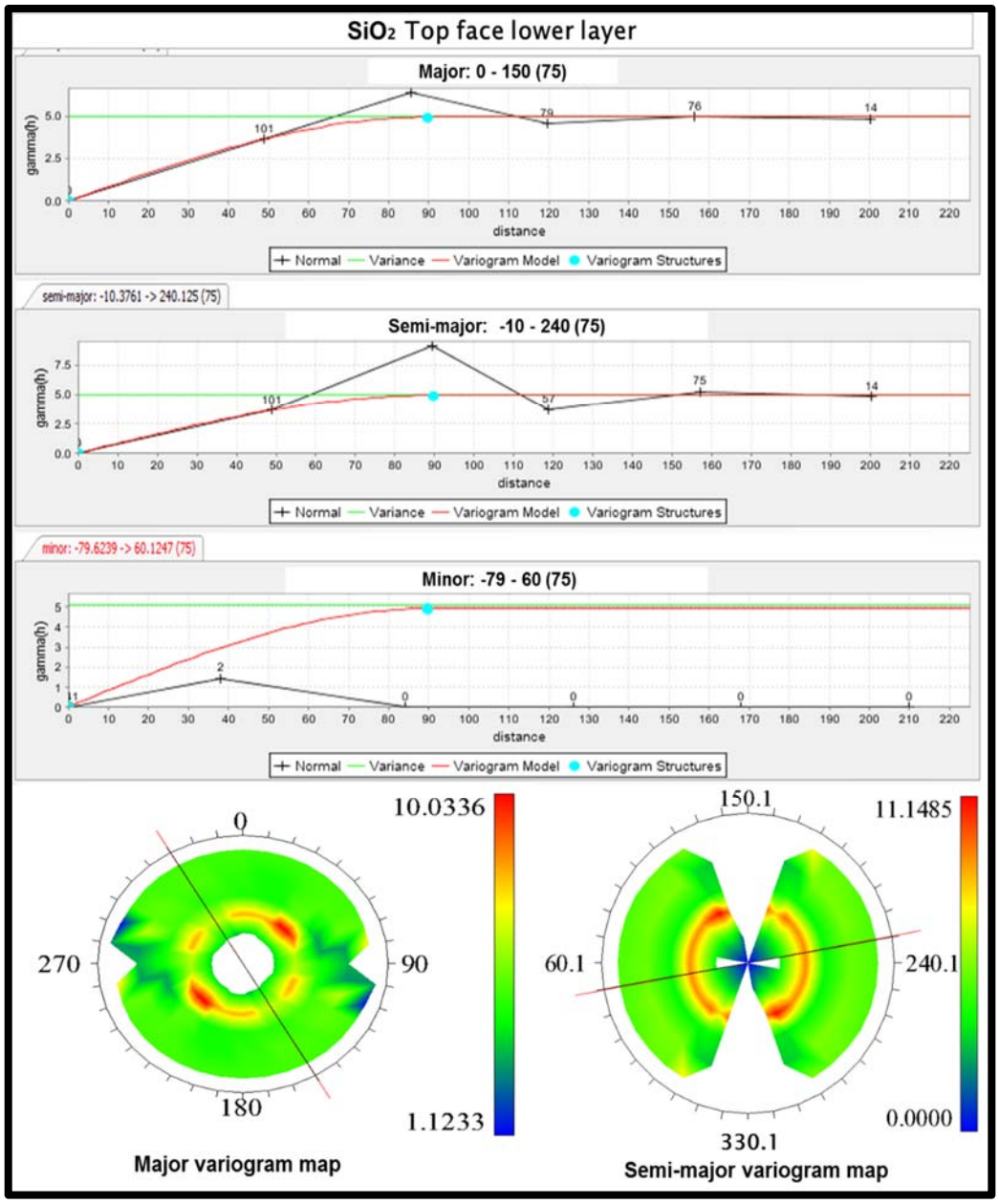


Figure 7-7. Major, semi-major and minor variograms, including the major and semi-major variogram maps for SiO_2 in the top-face lower clay.

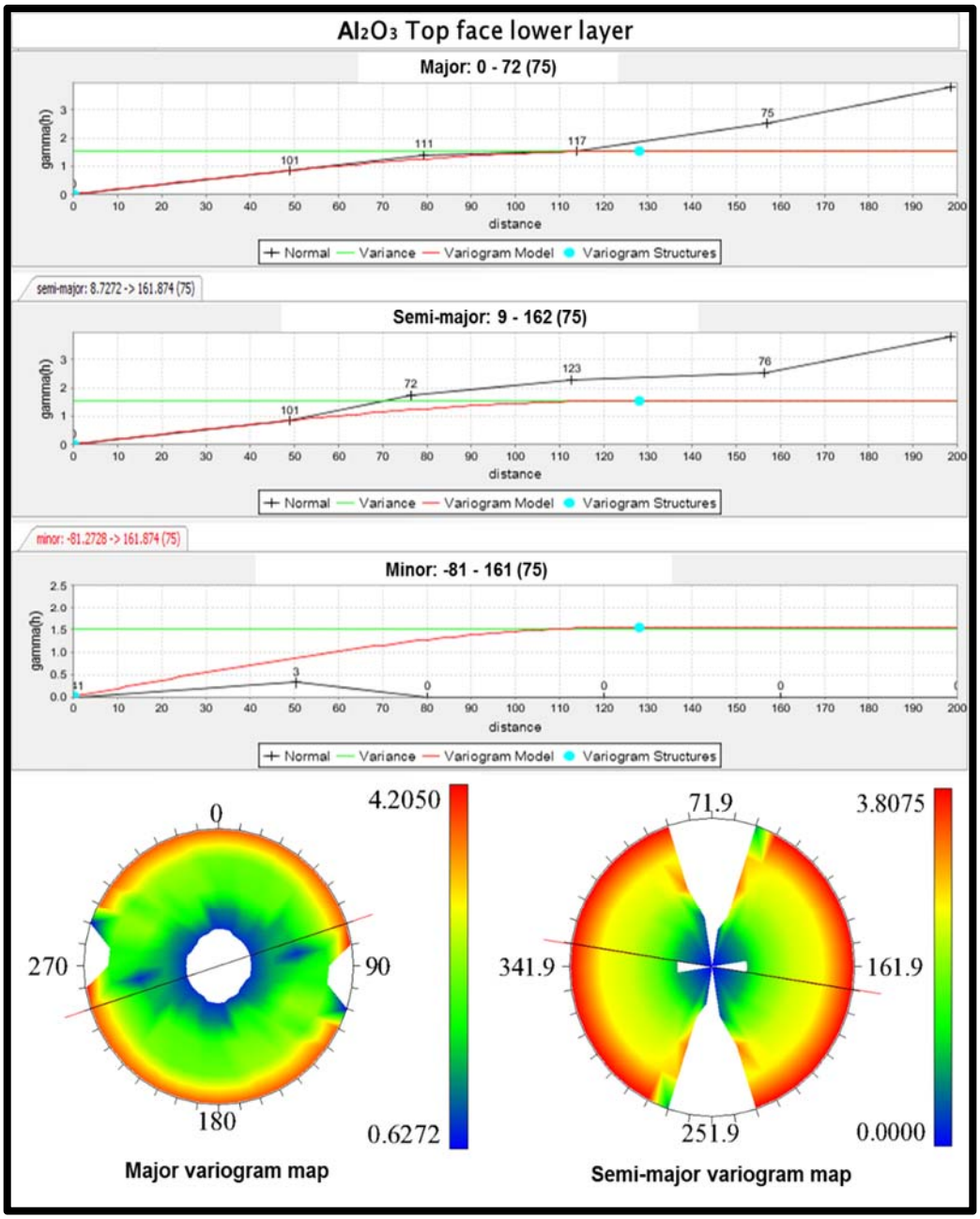


Figure 7-8. Major, semi-major and minor variograms, including the major and semi-major variogram maps for Al_2O_3 in the top-face lower clay.

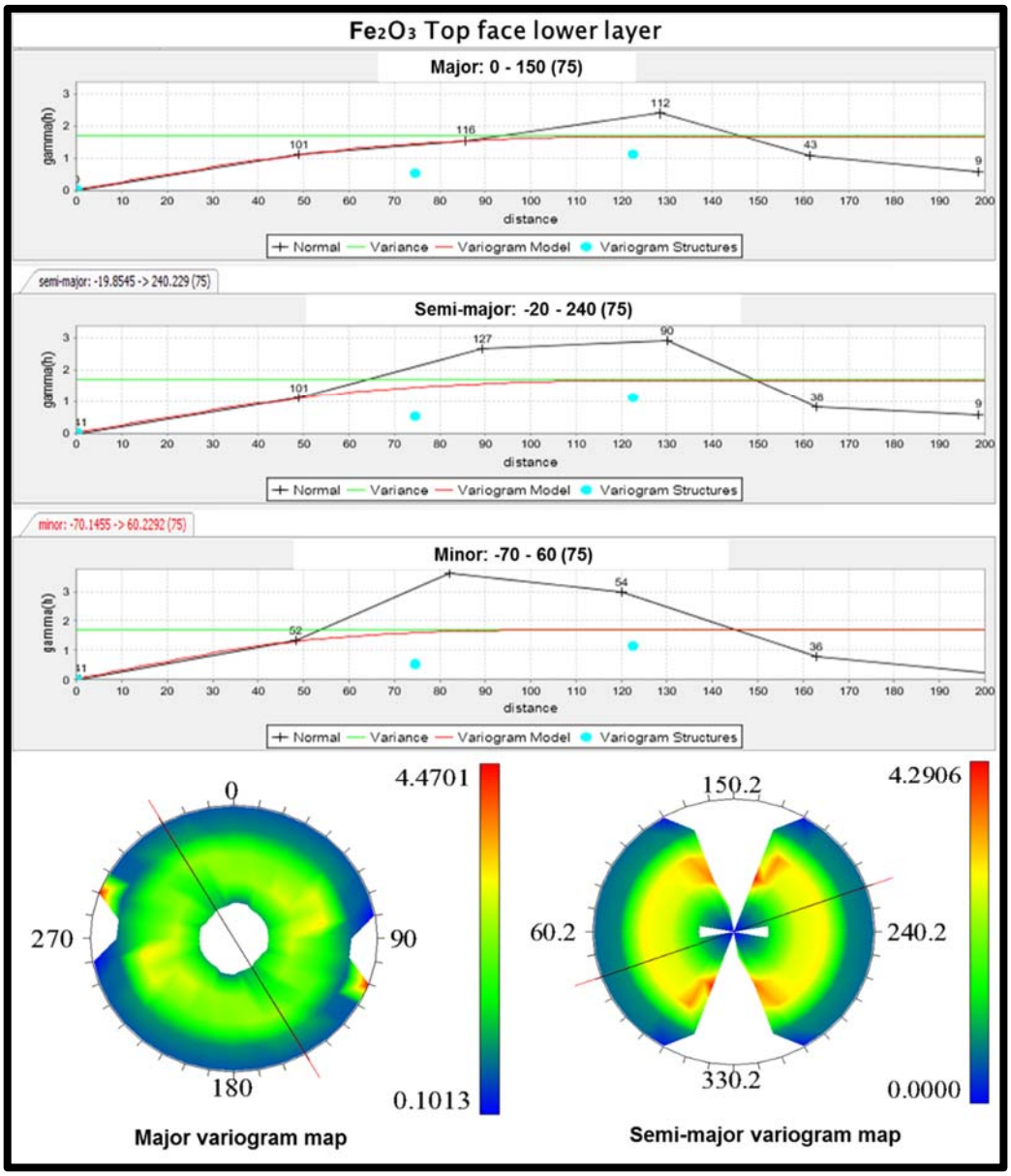


Figure 7-9. Major, semi-major and minor variograms, including the major and semi-major variogram maps for Fe_2O_3 in the top-face lower clay.

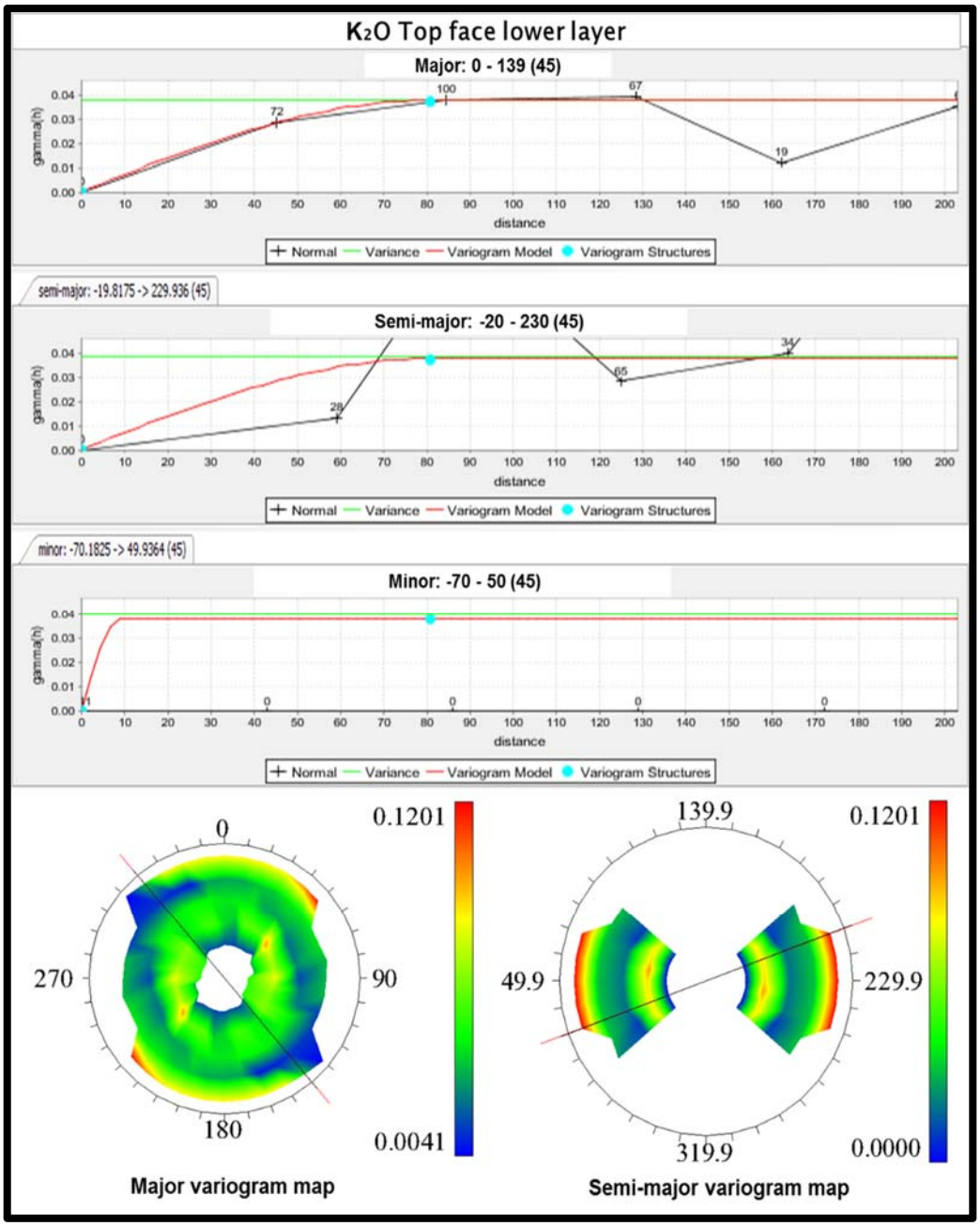


Figure 7-10. Major, semi-major and minor variograms, including the major and semi-major variogram maps for K_2O in the top-face lower clay.

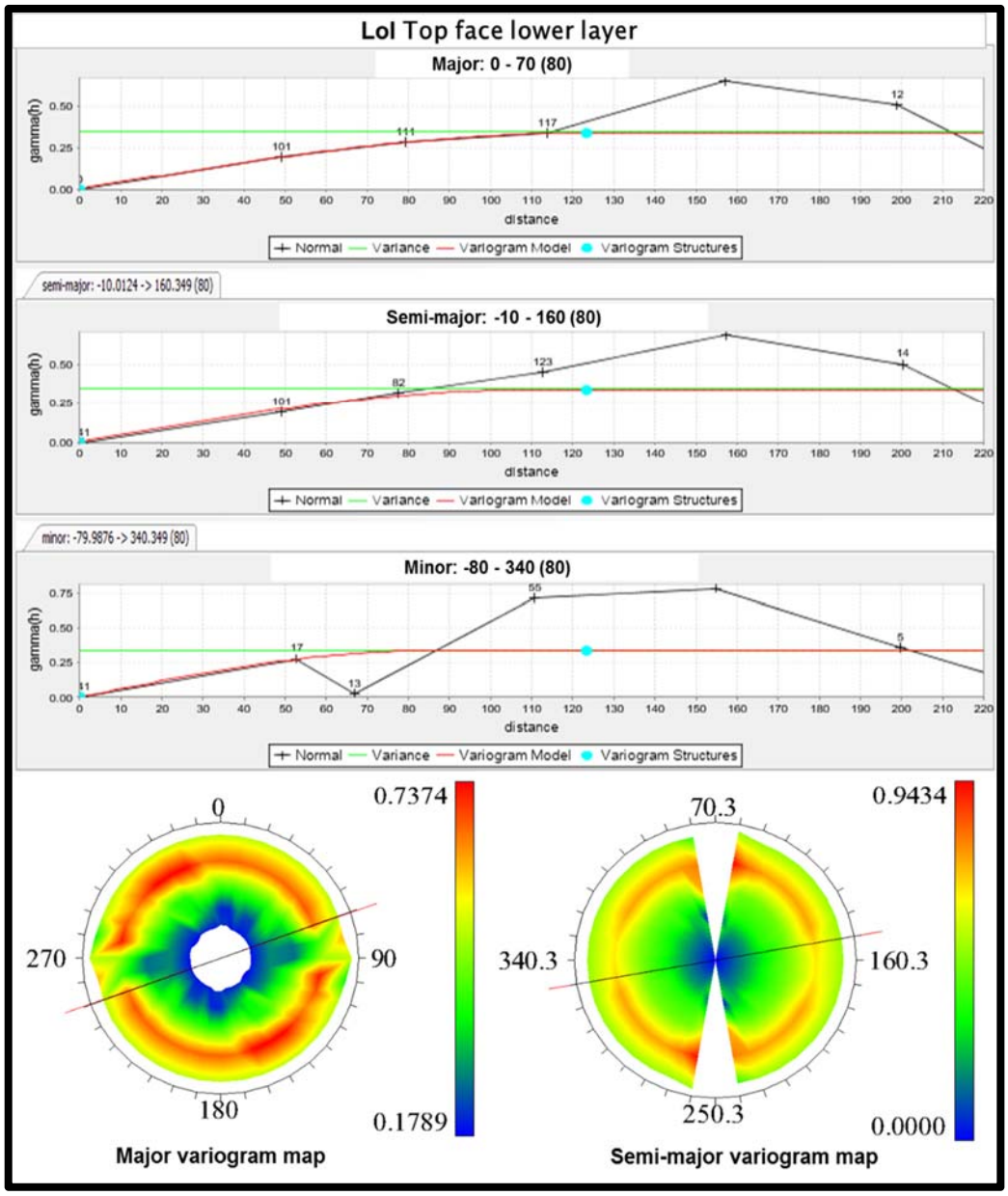


Figure 7-11. Major, semi-major and minor variograms, including the major and semi-major variogram maps for L.o.I in the top-face lower clay.

7.3.1 Comparing variogram parameters between the top-face upper and lower clays

Nugget

The variogram parameters for the top-face upper and lower clays are summarised and compared in Figure 7.16, below. The nugget was low for both the top-face upper and the lower clays. Between the ten variables, the nugget was the highest for the SiO_2 top-face upper clay variable, followed by the SiO_2 top-face lower clay variable, the Fe_2O_3 top-face upper clay variable, the Fe_2O_3 lower clay variable, the Al_2O_3 lower clay variable and Al_2O_3, K_2O, and loss on ignition for the top-face upper clay variables.

Sill

The sill followed the same pattern as the nugget. The sill for the SiO_2 top-face upper clay was the highest, followed by the SiO_2 top-face lower clay variable. The sill was the lowest for both the top-face upper and the lower K_2O variable.

Range

The range for the Al_2O_3 top-face upper and lower variables, including the top-face lower clay loss on ignition variable, revealed the longest modelled range. The longest range was in the order of 125 m and the shortest range in the order of 60 m for the SiO_2 top-face upper clay variable.

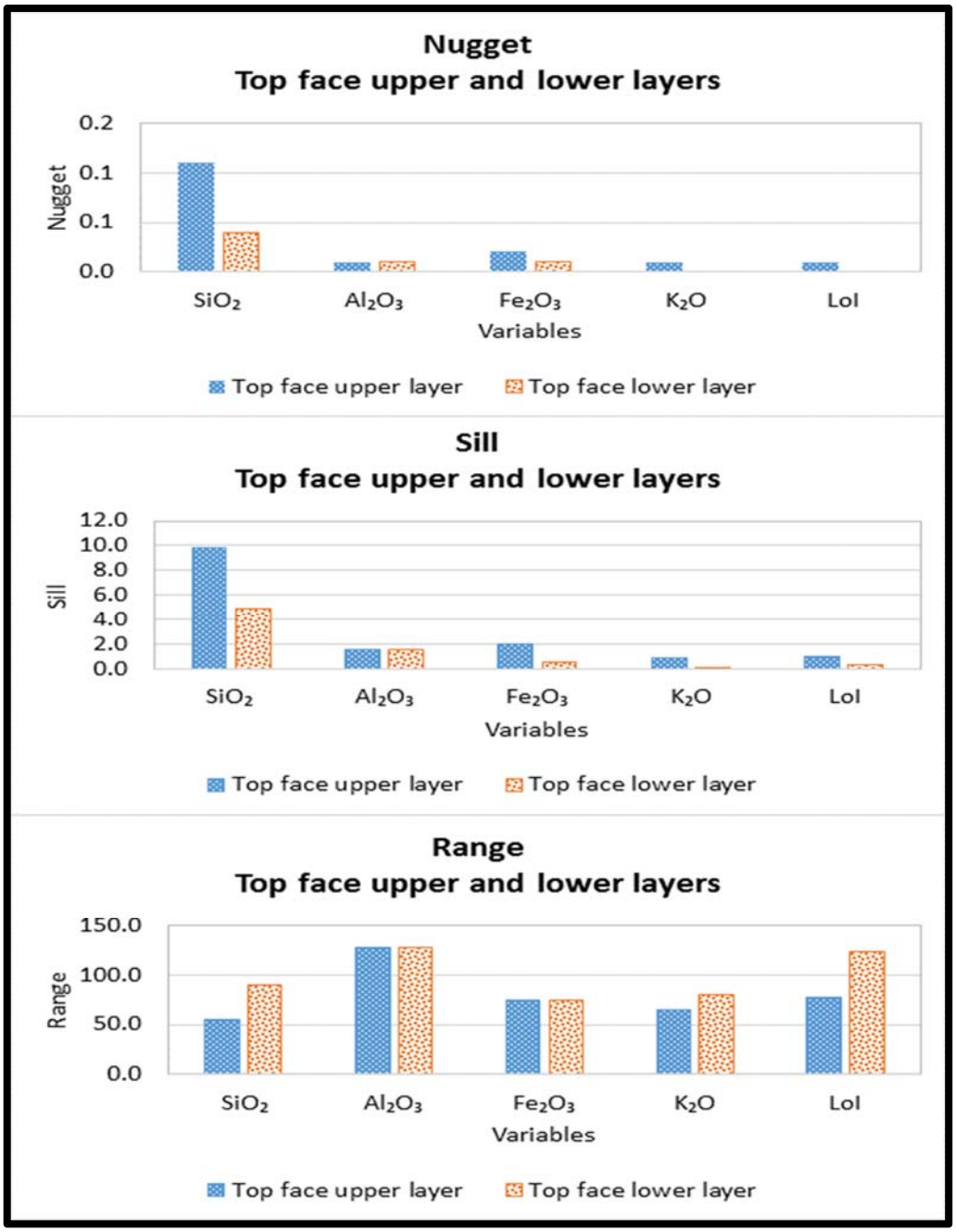


Figure 7-12. The nugget, sill and range parameters, comparison between the top-face upper and lower clays.

The variogram models created for both the five top-face upper and the lower clay variables are the most important geostatistics to guide the outcome of the estimation. These variogram models also define the weights of the kriging function estimations. The next chapter will be dedicated to the estimations of both the top-face upper and the lower clay variables.

CHAPTER 8

ESTIMATION

8. ESTIMATION OF THE TOP-FACE UPPER AND LOWER CLAY VARIABLES

8.1. Introduction

Different techniques such as inverse distance, ordinary kriging and indicator kriging can be used for estimations. These techniques are based on statistical methods. Kriging is the only interpolation method that gives the interpolated and output error reports with the standard errors of the estimations. The exceptionally flexible ordinary kriging prediction method can be used for data showing a trend. This method can use either semi-variograms or covariances, transformations to remove trends, and provides for measurement error.

As a predictor, kriging does not require normally distributed data, but normal distributed data are required for quantile and probability maps. Kriging is the best unbiased predictor when predictors formed from weighted averages are considered, regardless of whether the data are normally distributed. The kriging assumption relies on all the random errors being second-order stationarity. This assumes that the random errors have a zero covariance and mean between random errors pairs, with the only dependence between them being not their location, but the distance and direction separating them.

The kriging assumption accepts that the distance and direction between sample points reveal spatial correlation, which could be used to explain surface variations. The method applies a mathematical function to an identified number of points within a certain radius in order to produce output values for each location. In addition, it employs exploratory statistical analysis, variogram modelling, surface creation, and a variance surface. For data having spatially correlated distances or directional data biases, kriging is the most appropriate method to use. The weights allocated to the kriging method are generated

based on the distance between the samples and their spatial arrangements. The weights in ordinary kriging depend on the model fitted to the data, as was done for the top-face upper and lower clays discussed in Chapter 7. Applying a model to the variogram quantifies the spatial autocorrelation between the variables for each clay in terms of the measured points, the distance to the prediction location, and their spatial relationship around the prediction location.

The estimation method chosen for the top-face upper and lower clay variables is ordinary kriging, for the reasons discussed and because this method ensures an unbiased linear estimate that has the least variability between the predicted and actual values (Dohm, 2012).

8.2. Estimation methodology

To enable estimation, two solids were created for the top-face upper and lower clay domains, as is illustrated in Figures 8.1, 8.2 and 8.3. The top-face upper and lower clay volume ratio was 3:1.

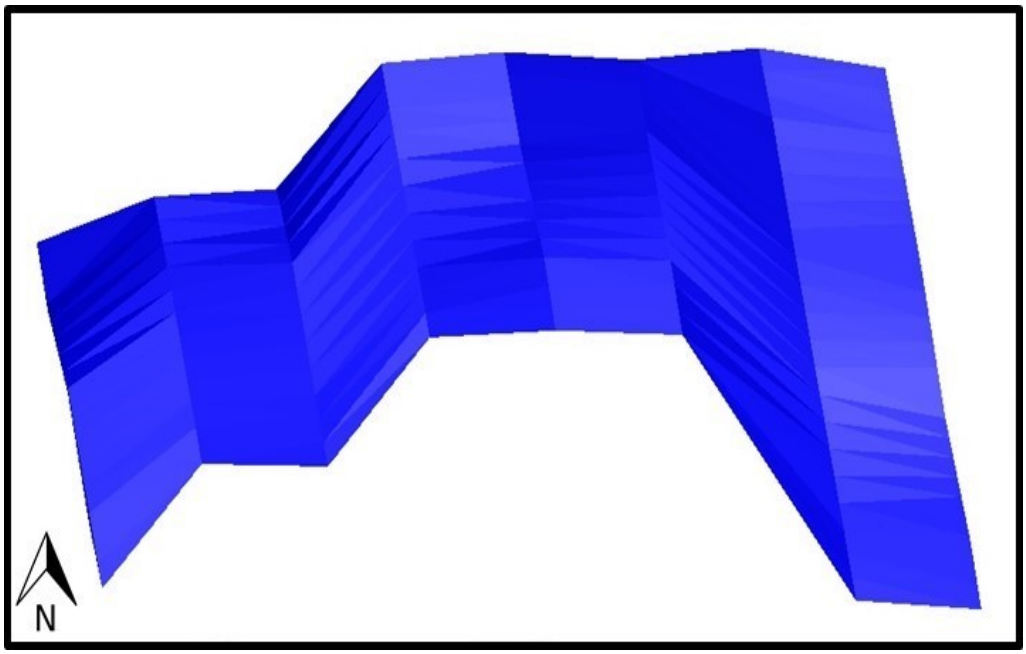


Figure 8-1. Solid created for the top-face upper clay domain.

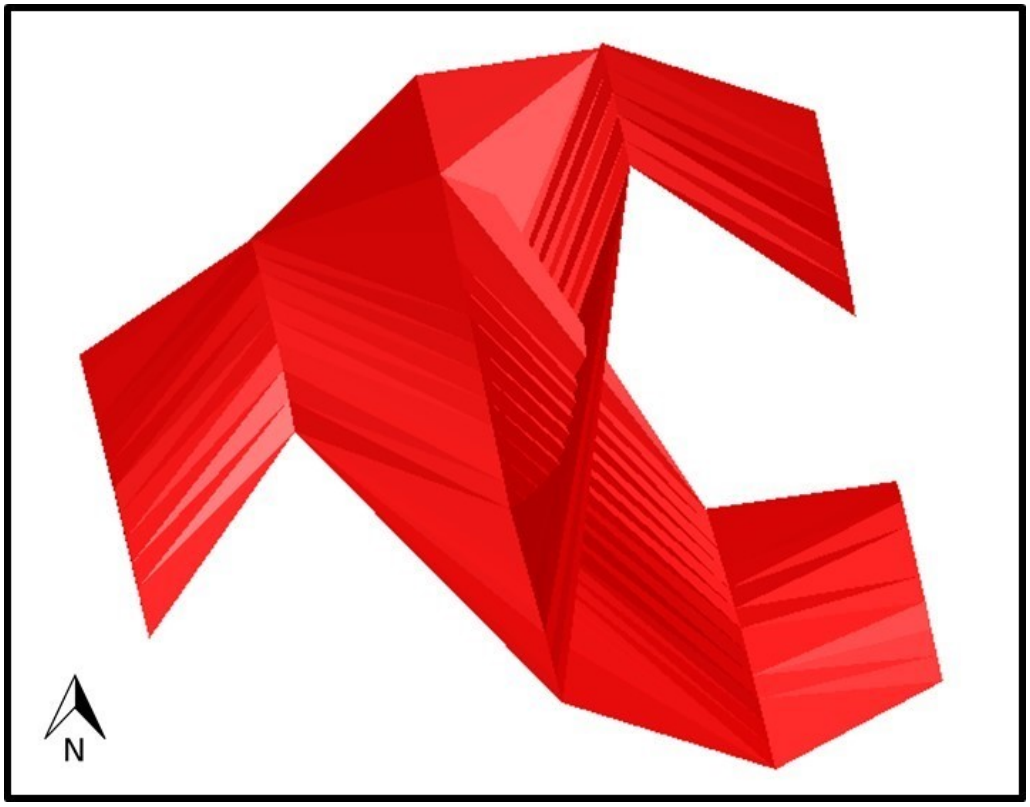


Figure 8-2. Solid created for the top-face lower clay domain.

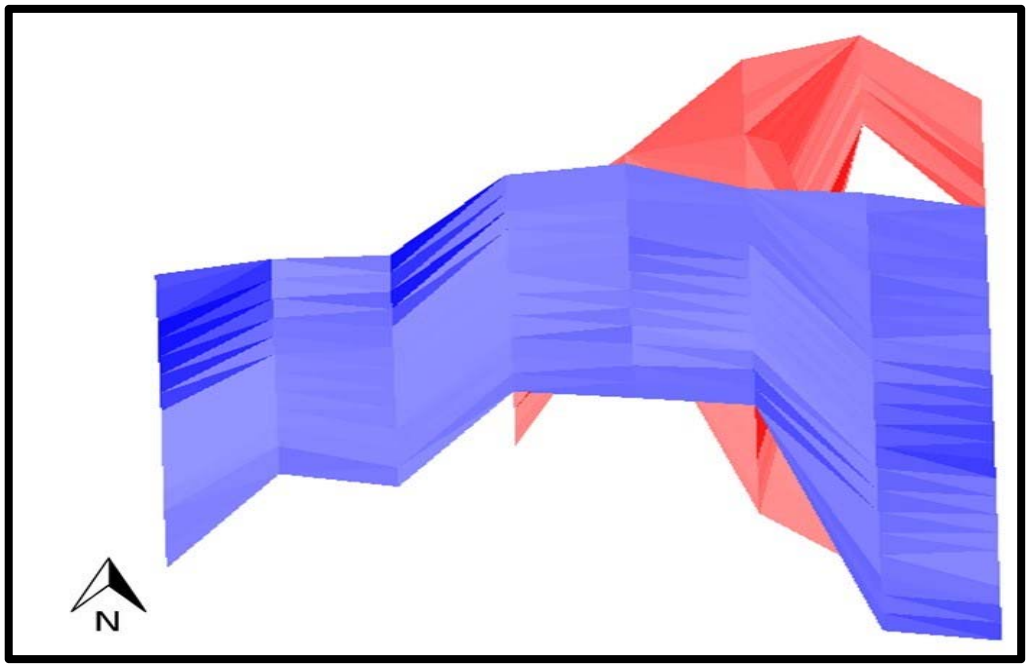


Figure 8-3. Solid created for the top-face upper and lower clay domains.

Subsequent to the solids, a block model was created with constraints for the top-face upper and lower clays. To determine the correct block size for the

block model, various block models were created, with the discretisation, block size and maximum number of samples varied. The kriging variance and conditional bias for these different block models were calculated, as is summarised in Table 8.1. A block size of 25 x 25 x 3 was chosen after the first step, as the conditional bias and kriging variance was the lowest. Using a constant block size of 25 x 25 x 3, but varying discretisation, revealed that a discretisation size of 3 x 3 x 3 resulted in the lowest conditional biased and kriging variance. During the last step, varying the minimum and maximum sample numbers indicated that a minimum sample size of 10 and a maximum sample size of 35 resulted in the lowest conditional bias and kriging variance.

The block model created for estimation purposes had a block size of 25 x 25 x 3, a discretisation size of 3 x 3 x 3 and a minimum/maximum sample size of 10 and 35.

Table 8-1 Optimising block size for estimation.

Determining Factors used for Block Model Size						
Block Size	BV	Cond.Bias	KV	Lagrange	Disc	MIN_MAX
Step 1						
10x10x3	0.779	0.997	0.225	-0.002	3x3x3	3_15
20x20x3	0.706	0.974	0.253	-0.012	3x3x3	3_15
25x25x3	0.669	0.943	0.16	-0.033	3x3x3	3_15
50x50x3	0.494	0.888	0.203	-0.042	3x3x3	3_15
Step 2						
25x25x3	0.888	0.979	0.373	-0.011	1x1x1	3_15
25x25x3	0.691	0.949	0.162	-0.03	2x2x2	3_15
25x25x3	0.669	0.943	0.16	-0.33	3x3x3	3_15
25x25x3	0.66	0.941	0.147	-0.034	4x4x4	3_15
25x25x3	0.66	0.941	0.147	-0.034	5x5x5	3_15
Step 3						
25x25x3	0.669	0.943	0.15	-0.03	3x3x3	3_15
25x25x3	0.669	0.969	0.146	-0.017	3x3x3	4_20
25x25x3	0.669	0.98	0.144	-0.011	3x3x3	6_25
25x25x3	0.669	0.994	0.142	-0.003	3x3x3	8_30
25x25x3	0.669	1.003	0.141	0.001	3x3x3	10_35
25x25x3	0.669	1.004	0.141	0.002	3x3x3	15_40
Model Criteria used for Estimation						
Block Model Size: 25x25x3 Discretisation: 3x3x3 Min_Max Samples: 10_35						

8.3. Estimated grades

Grade estimations, using ordinary kriging and the variogram model parameters determined in Chapter 7, were performed for both the five top-face upper and the lower clay variables.

8.3.1. Top-face upper clay variable estimations

The ordinary kriging estimation values for the top-face upper clay are given in Table 8.2. In Figure 8.4 the kriging variance between the variables of the discretised blocks is compared, while in Figure 8.5 the kriging efficiency is compared, and in Figure 8.6 the conditional bias. The estimated grade for SiO_2 varied between 56.06 percent and 58.25 percent, for Al_2O_3 between 27.35 percent and 28.52 percent, for Fe_2O_3 between 2.94 percent and 3.75 percent, for K_2O between 2.29 percent and 2.94 percent, and for loss on ignition between 7.97 percent and 8.86 percent. The estimated grades for the top-face upper clay variables are depicted in Figures 8.7 to 8.11.

Kriging variance

The kriging variance allows for the assessment of the reliability of the estimate and gives a statistical synopsis of how significant the observed changes in variable concentrations are. Unusually high variances require higher sampling densities, as localised geochemical processes can cause unusual local variance. From Figure 8.4, it is evident that the highest kriging variance was obtained for SiO_2, followed by Al_2O_3, Fe_2O_3, K_2O, and loss on ignition, in descending order. SiO_2 is undoubtedly the variable with the highest kriging variance in all five the discretisation zones of the deposit. The kriging variance increased as the variance of the variable data increased, or as the data became gradually redundant. The closer the data are to the estimation location, the lower the kriging variance.

The kriging variance is independent of the estimated data values. It is a function of spatial configuration and the distribution of the data variables. The link between the variable data and the kriging variance is the variogram, which is global and not local. With this in mind, the kriging variance is not necessarily

an accurate reflection of the local variation. Although it does not provide for assessing uncertainty, it is used primarily to find the optimum set of weights for the kriging function. It is a good measure of how the data are spatially configured and arranged.

Kriging efficiency

Kriging efficiency is a measure of how effective the kriging estimate correctly predicts the block grade. The measure ranges between -1 and one, -1 being a very poor estimate and one being a very good estimate. Figure 8.5 depicts the kriging efficiency of the top-face upper clay variables. The kriging efficiency was positive for all the top-face upper clay variables, which varied between as low as 0.0 for SiO_2 to as high as 0.8 for Al_2O_3. Low kriging efficiency, as seen for SiO_2, indicates a high degree of smoothing, and high kriging efficiency, as seen for Fe_2O_3, indicates a low degree of smoothing. The kriging efficiency for the top-face upper clay variables was acceptable.

Conditional bias

The aim of kriging is to eliminate the conditional bias. A conditional bias that remains is usually the result of a limited search routine. The conditional bias for the top-face upper clay variables is summarised in Table 8.2 and illustrated in Figure 8.6. The conditional bias slope indicates the reliability of the estimates and is measured on a scale of zero (poor relationship between estimates and true grades) and one (strong relationship between estimates and true grades), equivalent to the regression slope.

From the estimated values (Table 8.2, Fig. 8.6), the conditional bias slope was the lowest for SiO_2 (0.5) and the highest for loss on ignition (1.0). The reliability of the SiO_2 is not as good as is that of Al_2O_3, Fe_2O_3, K_2O, and loss on ignition. Very good estimation reliability was obtained for Al_2O_3 (on average above 0.85), Fe_2O_3 (on average above 0.9), K_2O (on average above 0.85), and loss on ignition (on average above 0.85). The estimation reliability of SiO_2, on average, had a conditional bias of 0.6. It can be concluded from the kriging

exercise that reliable estimate values were obtained for the Al_2O_3, Fe_2O_3, K_2O, and loss on ignition, and to a lesser extent for SiO_2.

Coefficient of variation and the LaGrange multiplier

The coefficient of variation between the top-face upper clay variables were all very similar and below 0.3. The low coefficient of variation indicated that there were few residuals relative to the predicted value, and a good model of fit was obtained. The LaGrange multiplier was negative for most of the variables and was the highest for the SiO_2 variable. The LaGrange multiplier was used to minimise the kriging variance.

Table 8-2. Block estimation of the top-face upper clay variables.

SiO_2 block estimation						Average
Estimated grade	57.01	56.22	58.25	56.06	56.89	56.89
Kriging variance	2.66	4.65	2.36	3.56	3.77	3.40
Block variance	4.65	4.65	4.65	4.65	4.65	4.65
Kriging efficiency	0.43	0.00	0.49	0.24	0.19	0.27
Coefficient of variation	0.03	0.04	0.03	0.03	0.03	0.03
Lagrange multiplier	-1.19	-1.27	-1.60	-1.72	-1.26	-1.41
Slope of regression (Conditional bias slope)	0.73	0.50	0.71	0.62	0.63	0.64
Al_2O_3 block estimation						Average
Estimated grade	27.45	27.77	28.52	27.66	26.67	27.61
Kriging variance	2.33	1.61	1.40	3.71	0.77	1.96
Block variance	3.85	3.85	3.85	3.85	3.85	3.85
Kriging efficiency	0.39	0.58	0.64	0.04	0.80	0.49
Coefficient of variation	0.06	0.05	0.04	0.07	0.03	0.05
Lagrange multiplier	-0.40	-0.12	-0.08	-0.52	-0.16	-0.25
Slope of regression (Conditional bias slope)	0.83	0.95	0.97	0.56	0.95	0.85
Fe_2O_3 block estimation						Average
Estimated grade	3.26	3.27	3.75	3.22	2.94	3.29
Kriging variance	0.64	0.47	0.35	1.03	0.20	0.54
Block variance	1.39	1.39	1.39	1.39	1.39	1.39
Kriging efficiency	0.54	0.66	0.75	0.26	0.86	0.61
Coefficient of variation	0.25	0.21	0.16	0.31	0.15	0.22
Lagrange multiplier	-0.10	-0.02	-0.01	-0.12	-0.04	-0.06
Slope of regression (Conditional bias slope)	0.89	0.98	0.99	0.81	0.97	0.93
K_2O block estimation						Average
Estimated grade	2.29	2.40	2.86	2.53	2.94	2.60
Kriging variance	0.31	0.22	0.19	0.49	0.12	0.27
Block variance	0.59	0.59	0.59	0.59	0.59	0.59
Kriging efficiency	0.48	0.62	0.67	0.16	0.79	0.55
Coefficient of variation	0.24	0.20	0.15	0.28	0.12	0.20
Lagrange multiplier	-0.11	-0.02	-0.01	-0.10	-0.03	-0.05
Slope of regression (Conditional bias slope)	0.79	0.96	0.97	0.66	0.94	0.86
Loss on ignition block estimation						Average
Estimated grade	8.80	8.86	8.62	8.54	7.97	8.56
Kriging variance	0.34	0.16	0.16	0.48	0.10	0.25
Block variance	0.62	0.62	0.62	0.62	0.62	0.62
Kriging efficiency	0.46	0.75	0.75	0.24	0.85	0.61
Coefficient of variation	0.07	0.05	0.05	0.08	0.04	0.06
Lagrange multiplier	-0.14	0.00	0.00	-0.10	-0.02	-0.05
Slope of regression (Conditional bias slope)	0.75	1.00	1.01	0.71	0.97	0.89

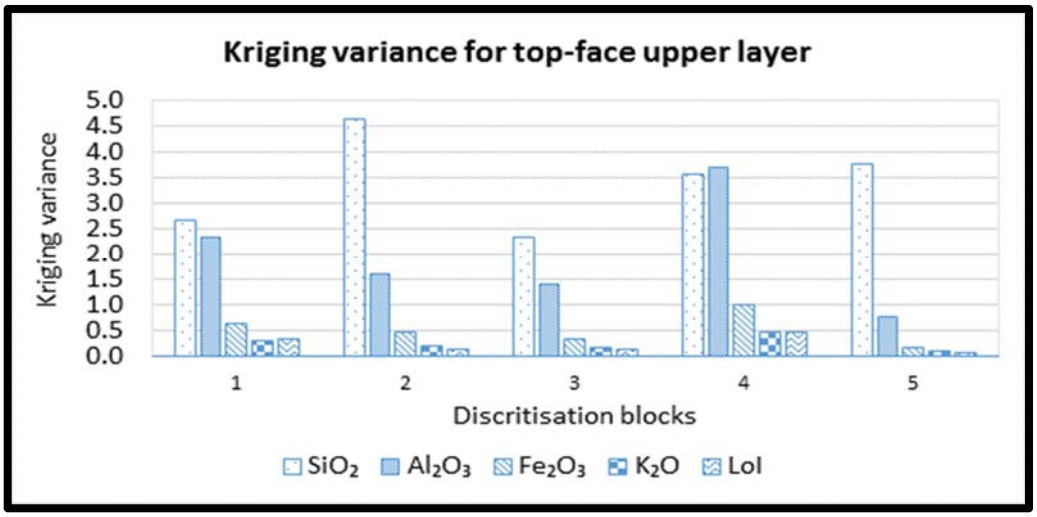


Figure 8-4. Kriging variance for the top-face upper clay variables.

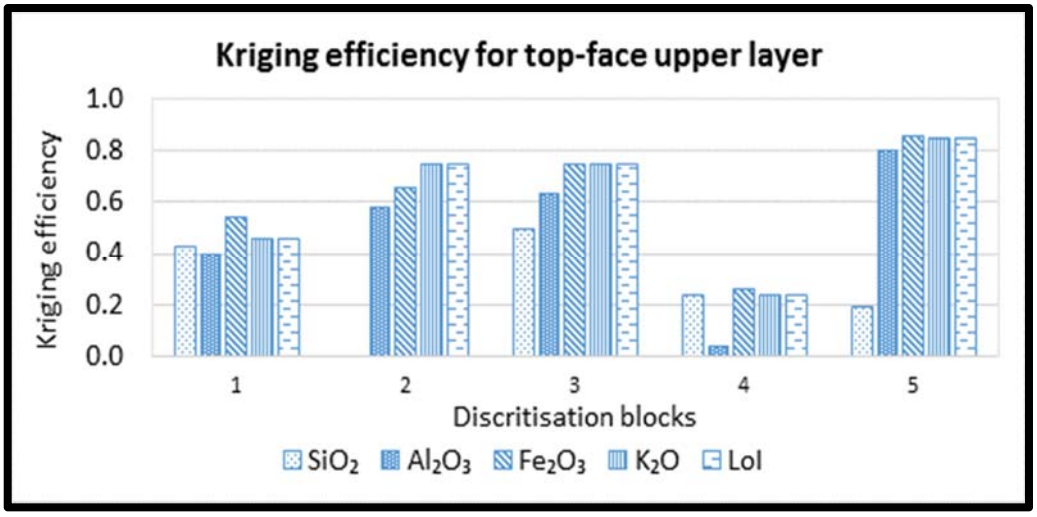


Figure 8-5. Kriging efficiency for the top-face upper clay variables.

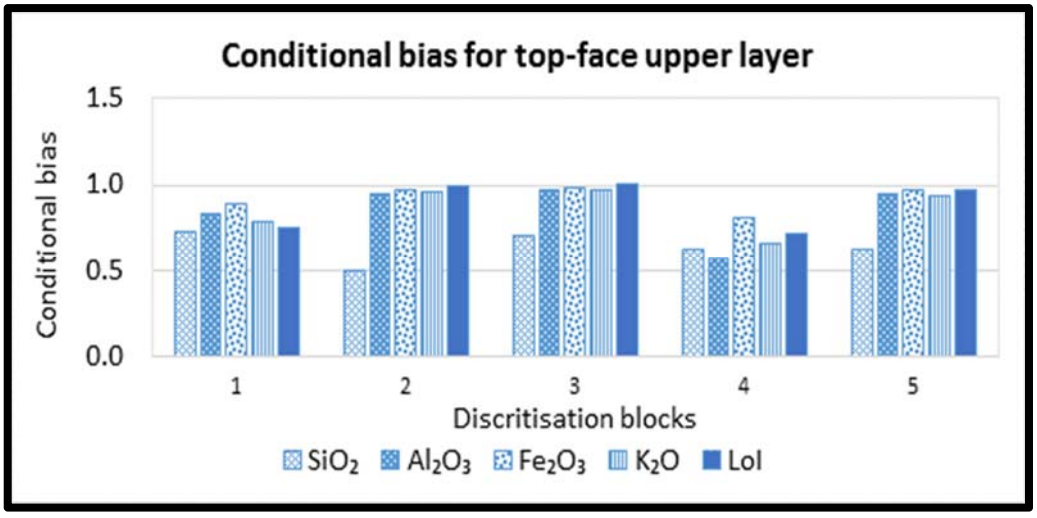


Figure 8-6 Conditional bias for the top-face upper clay variables.

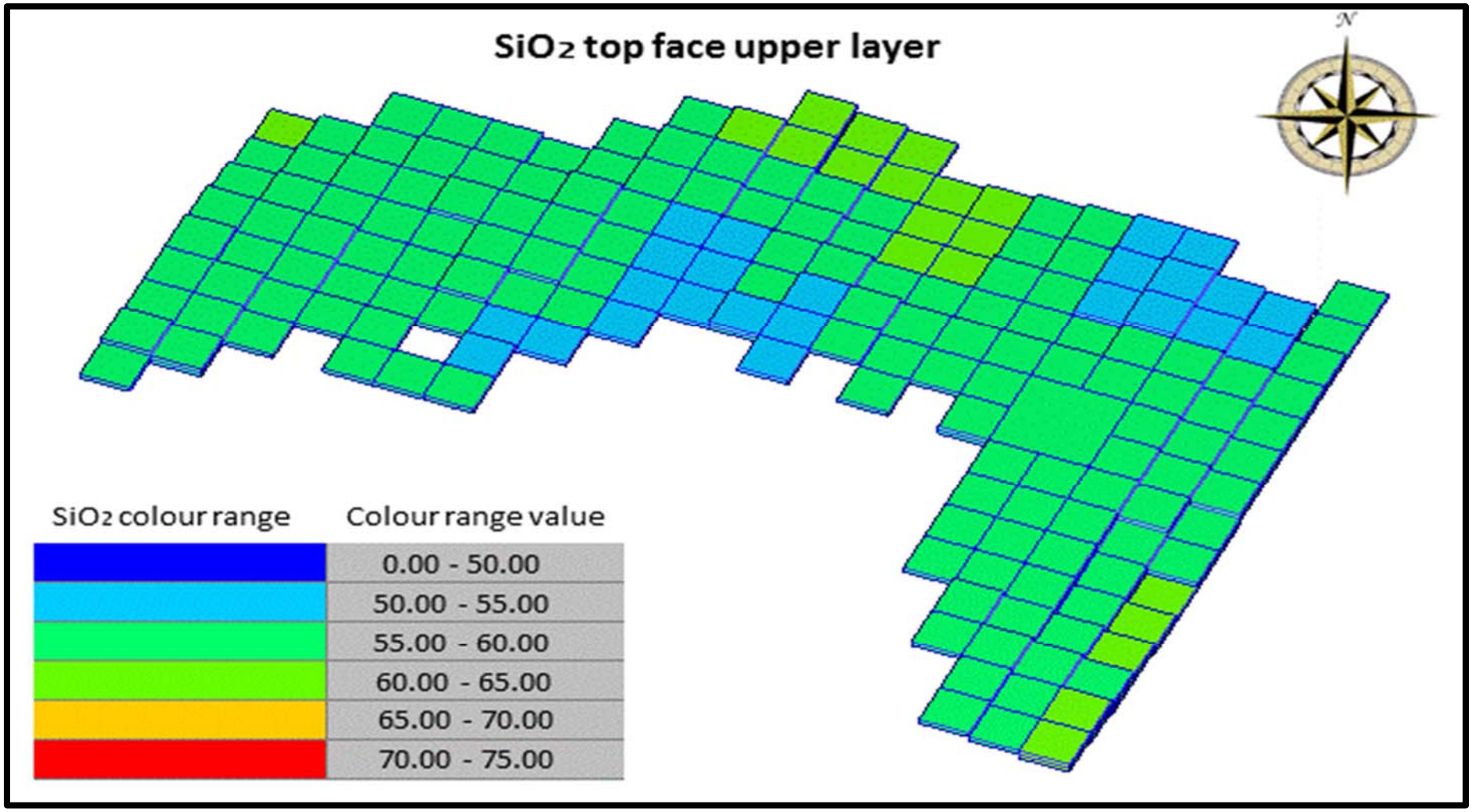


Figure 8-7 Estimated SiO_2 top-face upper clay grades.

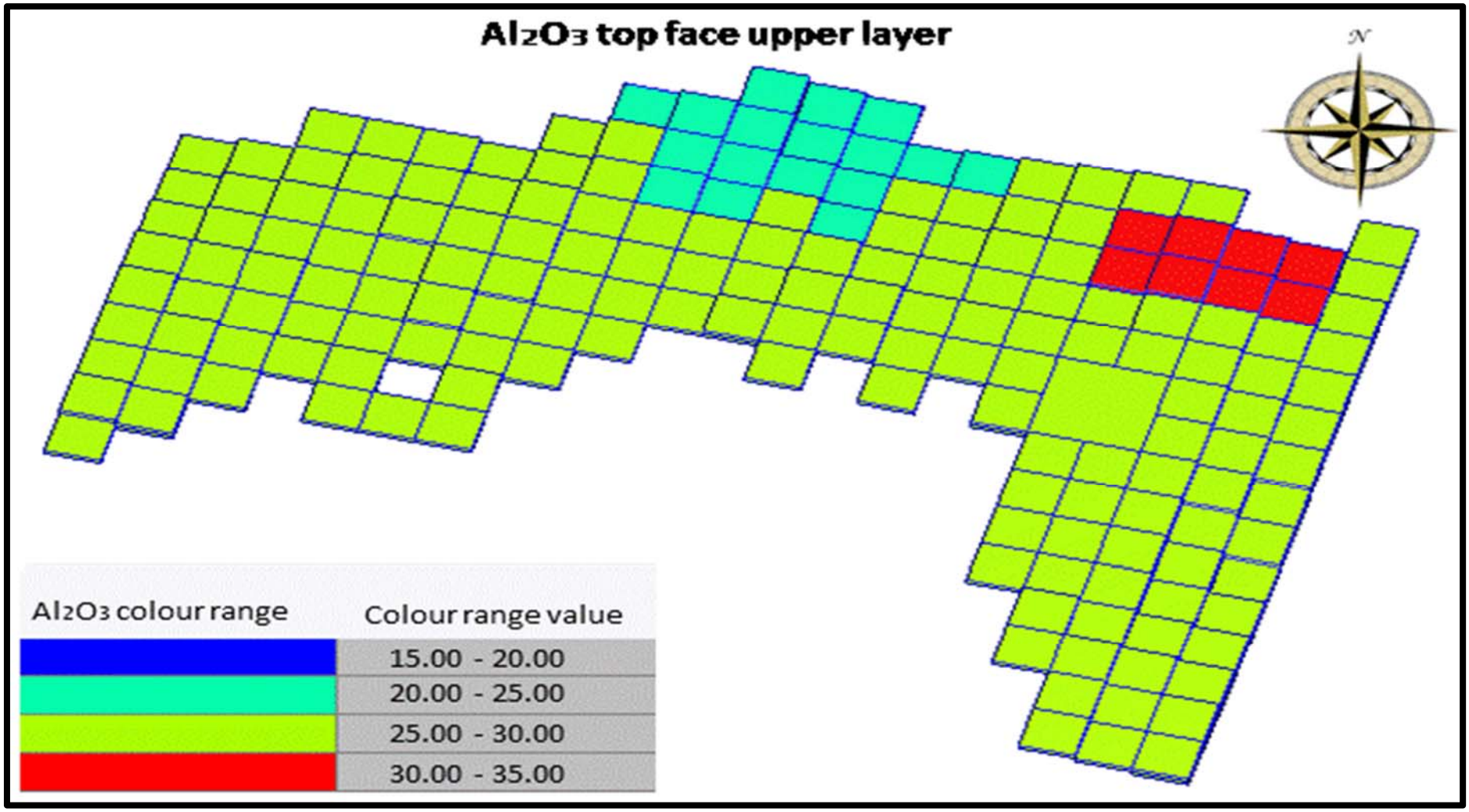


Figure 8-8 Estimated Al_2O_3 top-face upper layer grades.

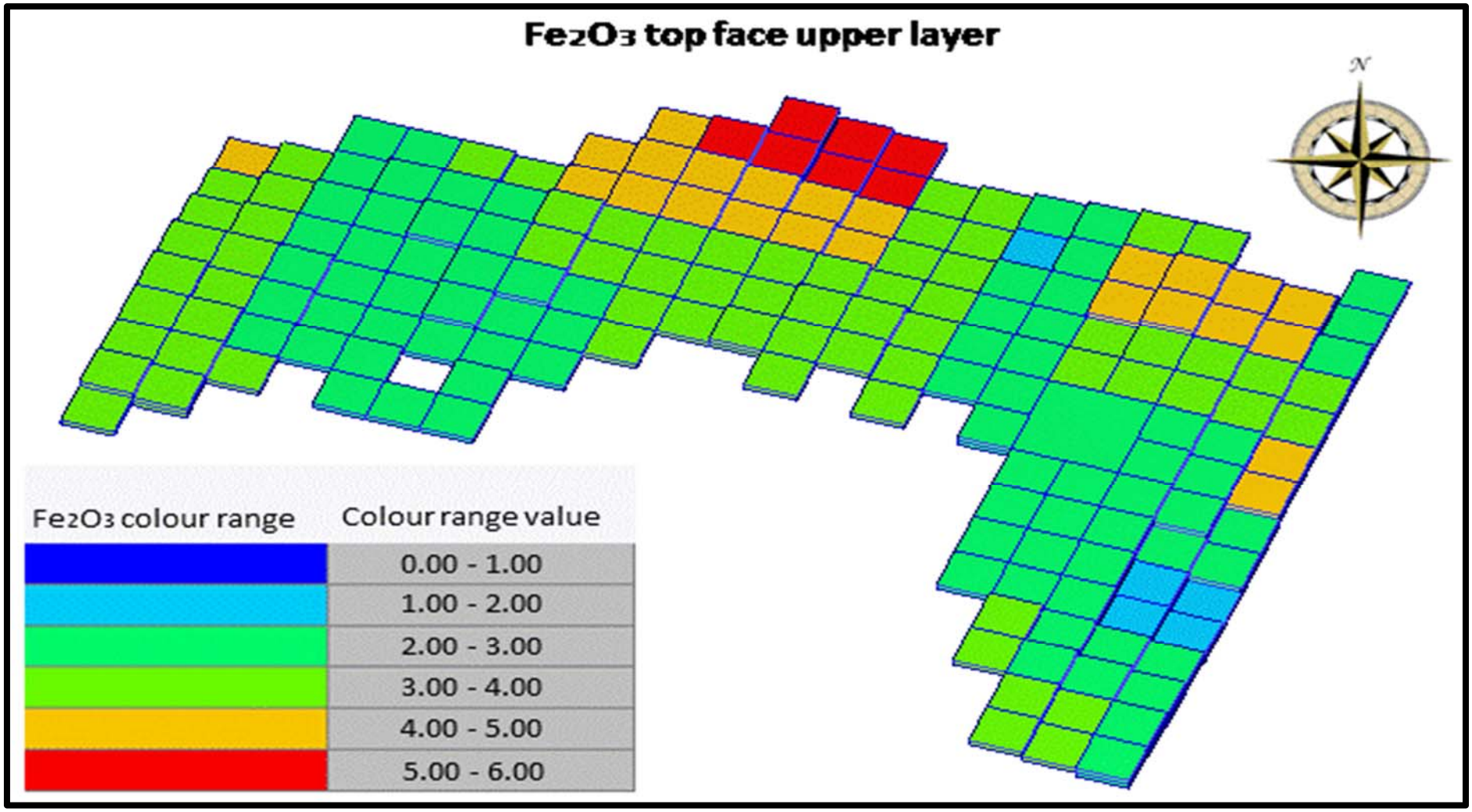


Figure 8-9 Estimated Fe_2O_3 top-face upper layer grades.

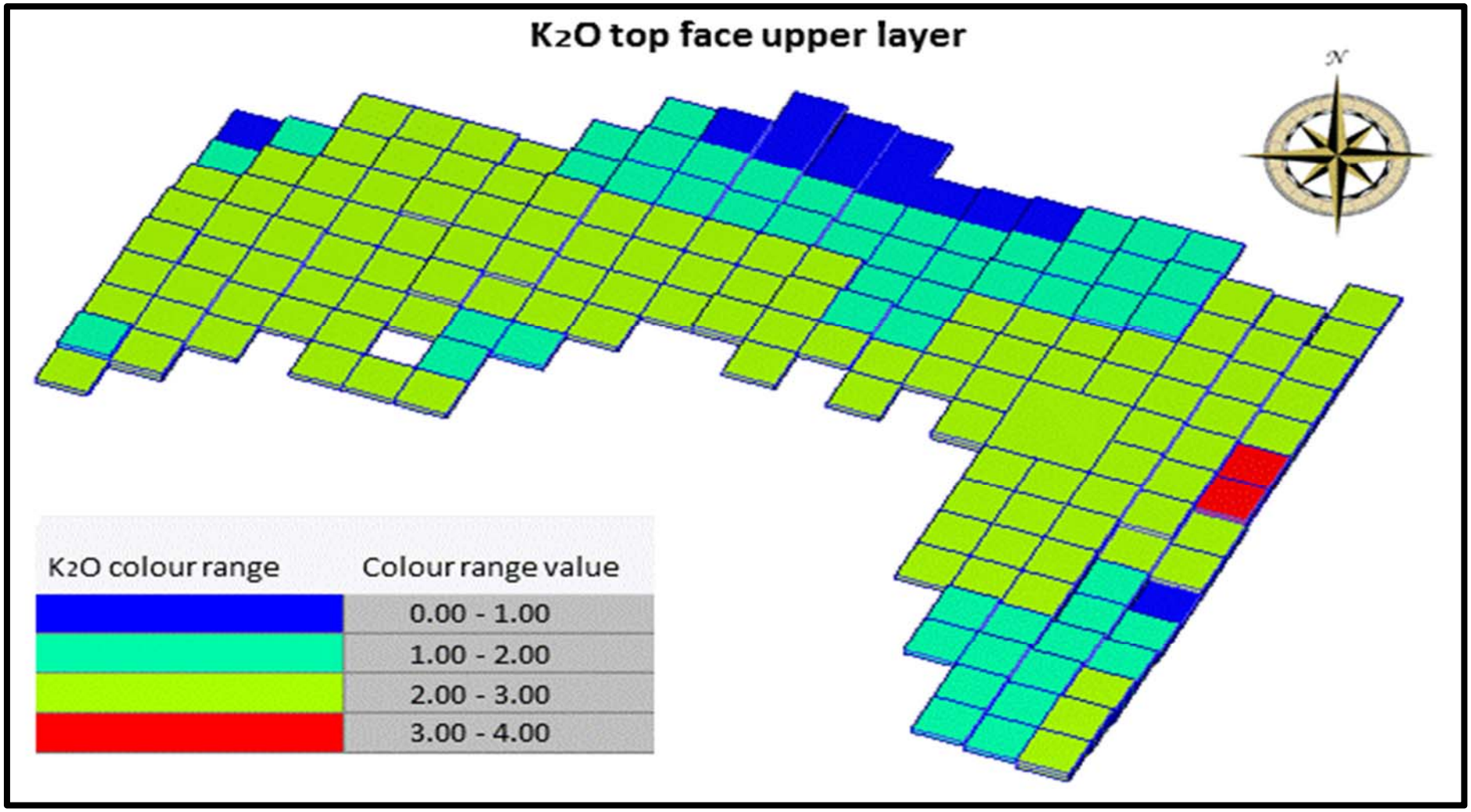


Figure 8-10 Estimated K_2O top-face upper layer grades.

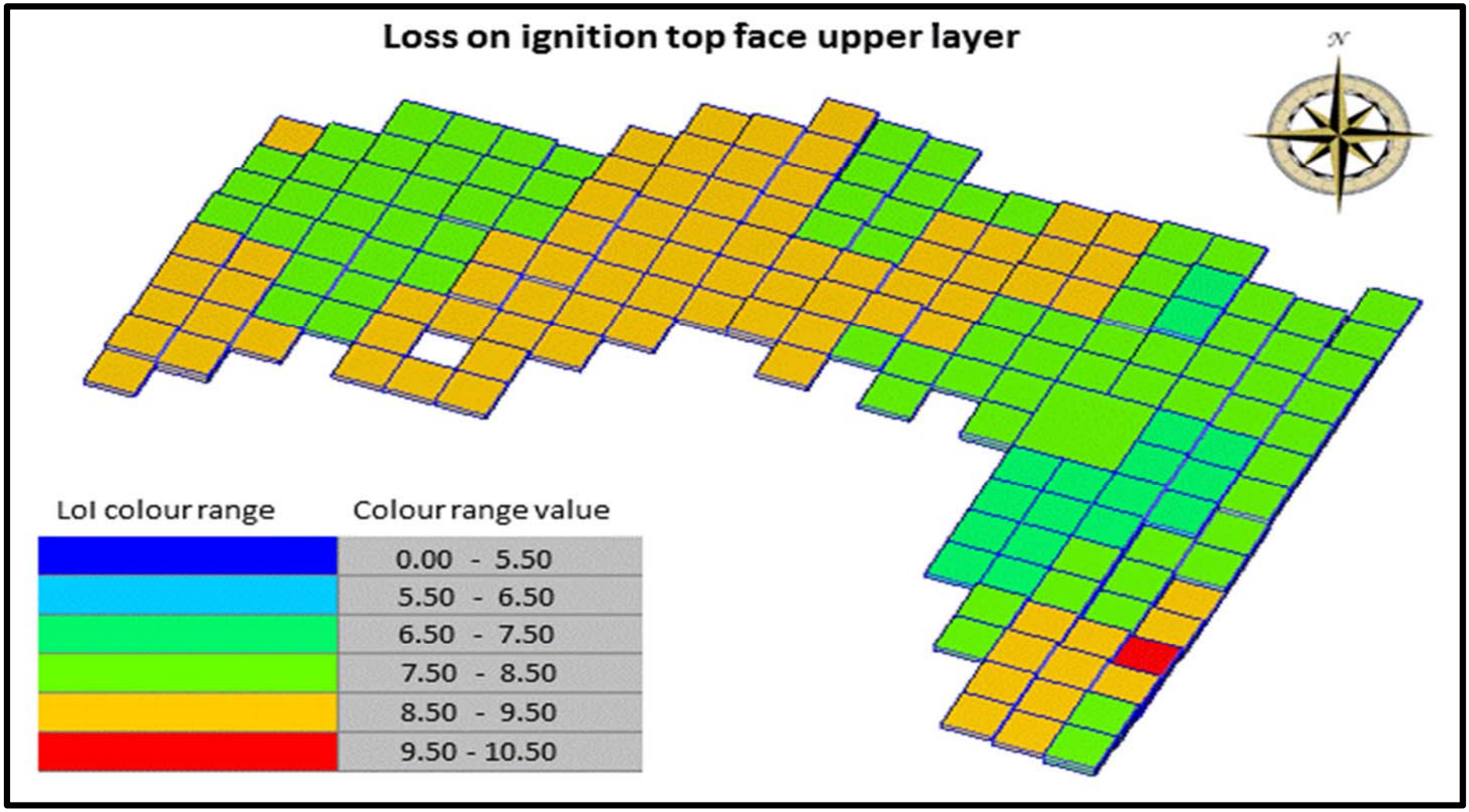


Figure 8-11. Estimated loss on ignition top-face upper clay grades.

8.3.2. Top-face lower clay variable estimations

The top-face lower clay variable estimations are summarised in Table 8.3 and Figures 8.12 to 8.14, to follow. The average estimated grade for SiO_2 varied between 65.33 percent and 65.37 percent, for Al_2O_3 between 23.37 percent and 24.34 percent, for Fe_2O_3 between 1.98 percent and 2.04 percent, for K_2O between 0.60 percent and 0.75 percent, and loss on ignition between 7.63 percent and 7.66 percent. The highest range estimated was for the Al_2O_3 variable at 0.97 percent, which is considered as minor. The estimated grades for the top-face upper clay variables are depicted in Figures 8.15 to 8.19.

Kriging variance

The kriging variance of the top-face lower clay variables was extremely low. On average, it was the lowest for K_2O at 0.01, and the highest for Fe_2O_3 at 1.83 (Table 8.3, Fig. 8.12). These low kriging variance values indicated that the data were close to the estimation location, which was also used to find the optimum set of weights for the kriging function. With regard to spatiality, the values indicated that the data were spatially well configured and arranged.

Kriging efficiency

The kriging efficiency was positive for the SiO_2, K_2O, and loss on ignition variables and negative for the Al_2O_3 and Fe_2O_3 variables (Table 8.3, Fig. 8.13). On average, the lowest kriging efficiency was similar for both the Al_2O_3 and Fe_2O_3 variables, which varied on average between -0.32 and -0.29. Considering that a measuring range of -1 is a poor estimate and that one is a very good estimate, it is clear that the estimations for both Al_2O_3 and Fe_2O_3 were poor. The negative values were as a result of the kriging variance that were greater than the true block variance, which could be ascribed to an variation. In such an instance, it would be more efficient to use the mean as the estimate, assuming it was accurate. In contrast, SiO_2, K_2O and loss on ignition were very good estimations, where loss on ignition had the best average estimate of 0.81, followed by SiO_2 at 0.76.

Conditional bias

The conditional bias (Table 8.3, Fig. 8.14) for the loss on ignition variable was on average closest to one at 0.96, followed by SiO_2 at 0.94, K_2O at 0.78, Al_2O_3 at 0.20, and Fe_2O_3 at 0.15. These results indicated that for the SiO_2, K_2O and Al_2O_3 variables, a strong relationship existed between the estimates and the true grades, whereas a weak relationship existed between the Al_2O_3 and Fe_2O_3 estimated variables. The conditional bias therefore indicated the reliability of the SiO_2, K_2O and Al_2O_3 variables and the unreliability of the Al_2O_3 and Fe_2O_3 estimated variables.

Coefficient of variation and the LaGrange multiplier

The coefficient of variations between the top-face lower clay variables were all similar at below 0.2, except for Fe_2O_3, which was 0.67. The coefficient of variation indicated that there were few residuals relative to the predicted value, and a good model of fit was obtained (albeit not as good as for Fe_2O_3). The LaGrange multiplier was negative for almost all the discretised variables and the highest for the K_2O variable (zero). A zero LaGrange multiplier implied an inactive constraint, and removing the constraint would not change the solution to the optimisation problem.

Table 8-3 Block estimation of the top-face lower clay variables.

SiO_2 block estimation						Average
Estimated grade	65.33	65.37	65.36	65.36	65.35	65.36
Kriging variance	0.94	1.02	1.04	0.89	0.92	0.96
Block variance	3.92	3.92	3.92	3.92	3.92	3.92
Kriging efficiency	0.76	0.74	0.74	0.77	0.76	0.76
Coefficient of variation	0.02	0.02	0.02	0.01	0.02	0.02
Lagrange multiplier	-0.10	-0.44	-0.45	-0.09	-0.10	-0.23
Slope of regression (Conditional bias slope)	0.97	0.88	0.88	0.97	0.97	0.94
Al_2O_3 block estimation						Average
Estimated grade	23.52	23.52	23.37	23.37	24.23	23.60
Kriging variance	1.66	1.66	1.40	1.41	1.67	1.56
Block variance	1.21	1.21	1.21	1.21	1.21	1.21
Kriging efficiency	-0.37	-0.37	-0.16	-0.17	-0.38	-0.29
Coefficient of variation	0.06	0.06	0.05	0.05	0.05	0.05
Lagrange multiplier	-0.50	-0.50	-0.37	-0.37	-0.58	-0.46
Slope of regression (Conditional bias slope)	0.10	0.10	0.32	0.32	0.17	0.20
Fe_2O_3 block estimation						Average
Estimated grade	2.04	2.02	2.00	1.98	1.95	2.00
Kriging variance	1.83	1.81	1.79	1.76	1.73	1.78
Block variance	1.35	1.35	1.35	1.35	1.35	1.35
Kriging efficiency	-0.35	-0.34	-0.32	-0.30	-0.28	-0.32
Coefficient of variation	0.66	0.66	0.67	0.67	0.67	0.67
Lagrange multiplier	-0.54	-0.53	-0.52	-0.51	-0.50	-0.52
Slope of regression (Conditional bias slope)	0.11	0.13	0.15	0.17	0.20	0.15
K_2O block estimation						Average
Estimated grade	0.75	0.75	0.60	0.69		0.70
Kriging variance	0.01	0.01	0.01	0.02		0.01
Block variance	0.02	0.02	0.02	0.02		0.02
Kriging efficiency	0.42	0.63	0.51	0.23		0.45
Coefficient of variation	0.15	0.12	0.17	0.18		0.15
Lagrange multiplier	0.00	0.00	0.00	-0.01		0.00
Slope of regression (Conditional bias slope)	0.77	0.85	0.84	0.65		0.78
Loss on ignition block estimation						Average
Estimated grade	7.63	7.63	7.66	7.66		7.65
Kriging variance	0.05	0.06	0.05	0.05		0.05
Block variance	0.29	0.29	0.29	0.29		0.29
Kriging efficiency	0.81	0.80	0.83	0.82		0.81
Coefficient of variation	0.03	0.03	0.03	0.03		0.03
Lagrange multiplier	-0.02	-0.02	0.00	0.00		-0.01
Slope of regression (Conditional bias slope)	0.93	0.92	0.99	0.99		0.96

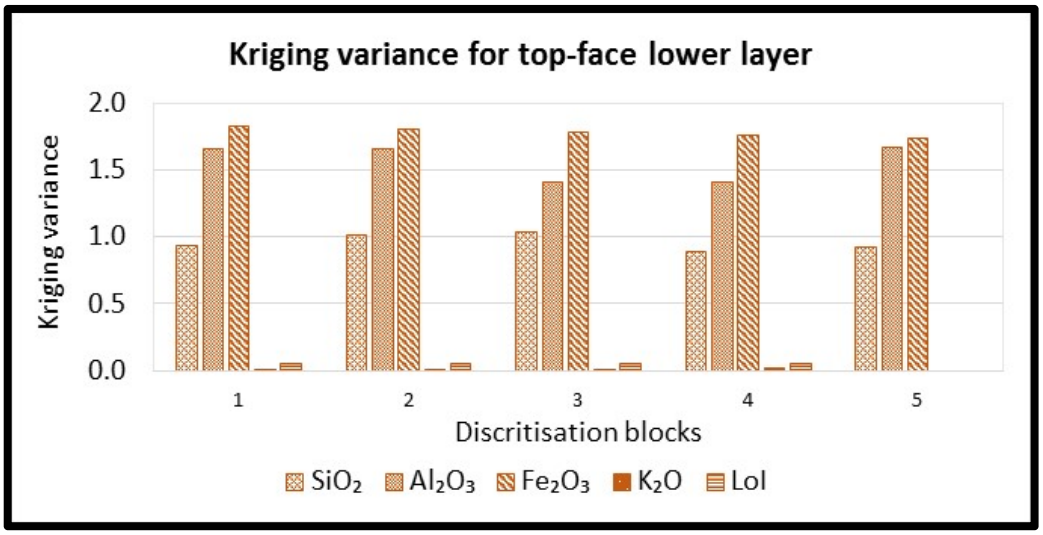


Figure 8-12. Kriging variance for the top-face lower clay variables.

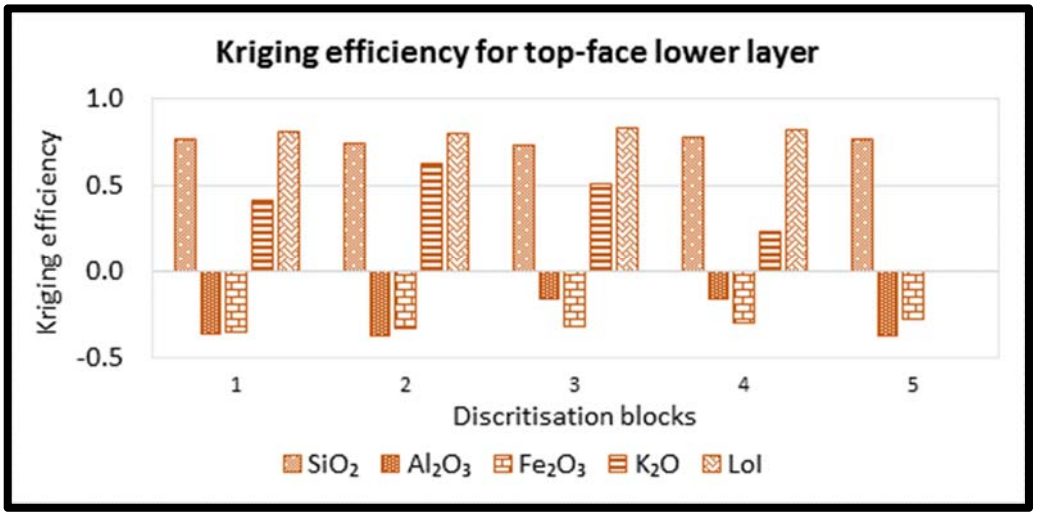


Figure 8-13 Kriging efficiency for the top-face lower clay variables.

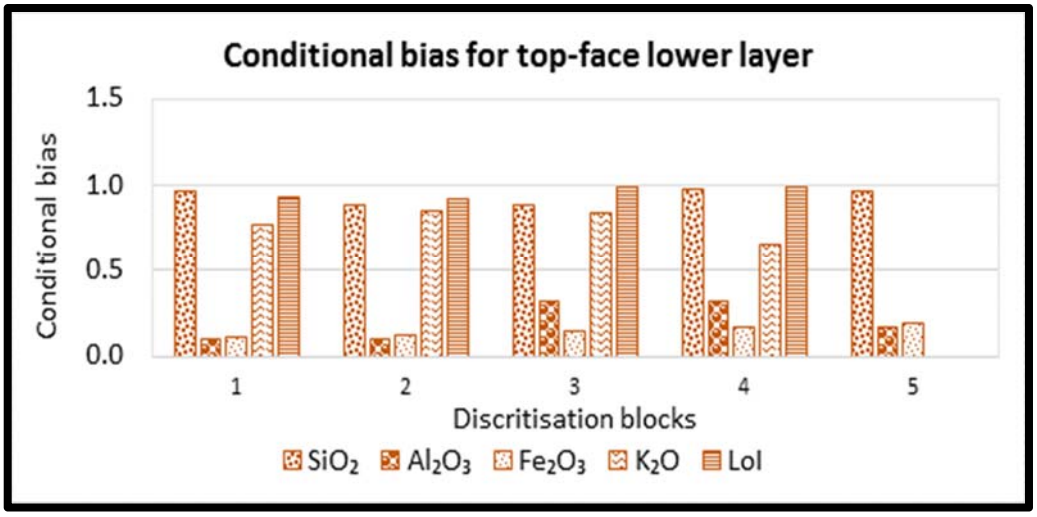


Figure 8-14. Conditional bias for the top-face upper clay variables.

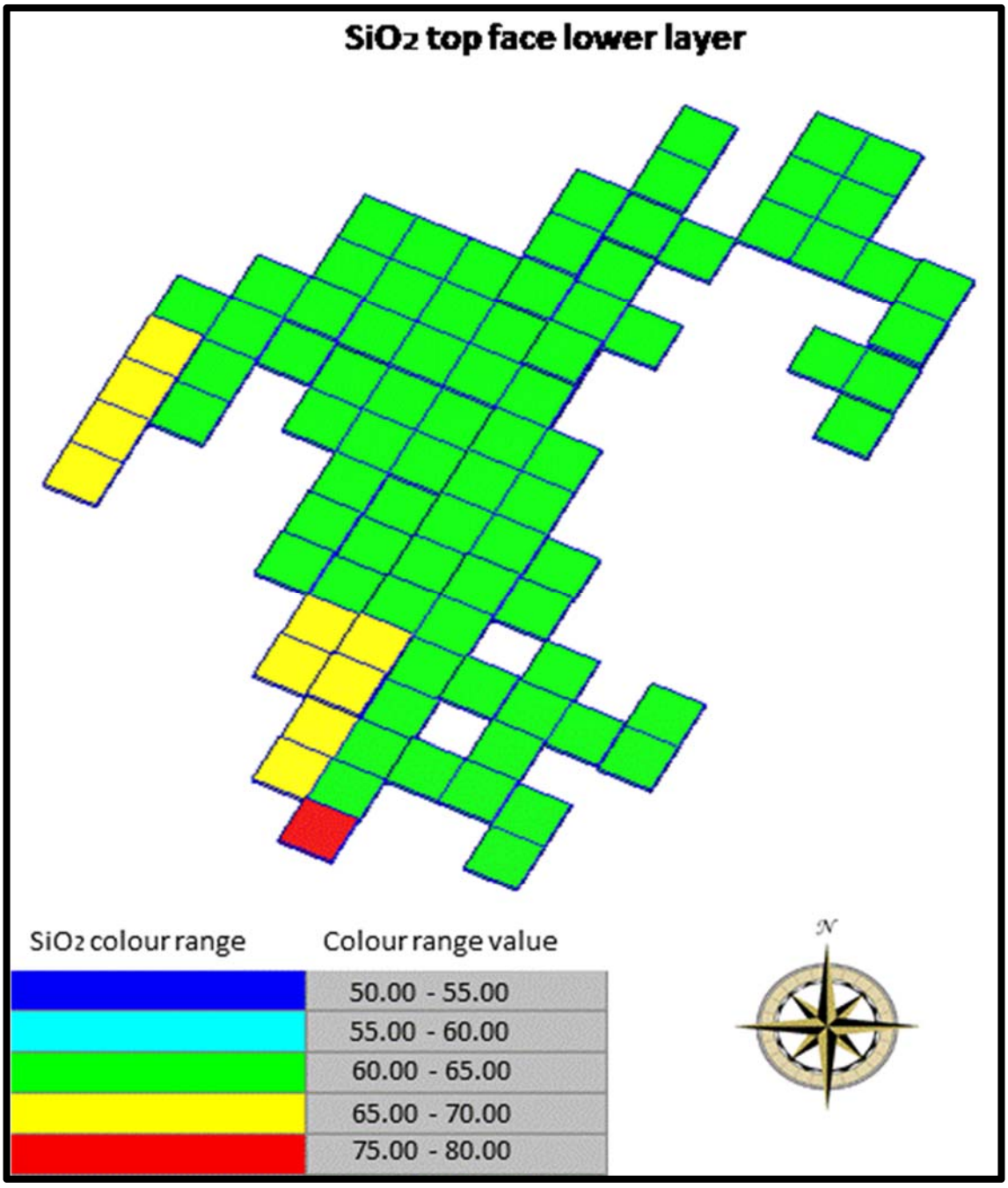


Figure 8-15 Estimated SiO_2 top-face lower clay grades.

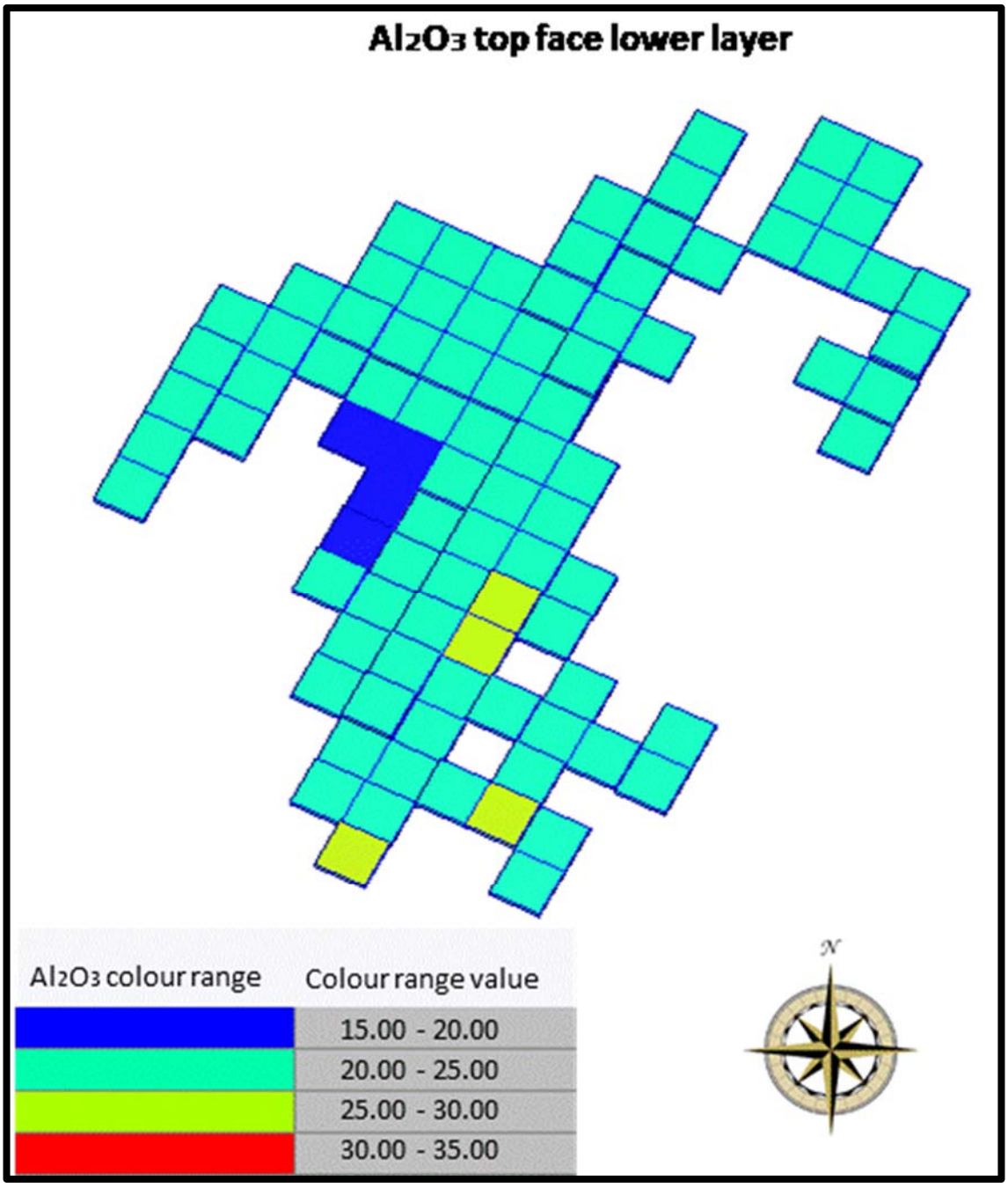


Figure 8-16 Estimated Al_2O_3 top-face lower clay grades.

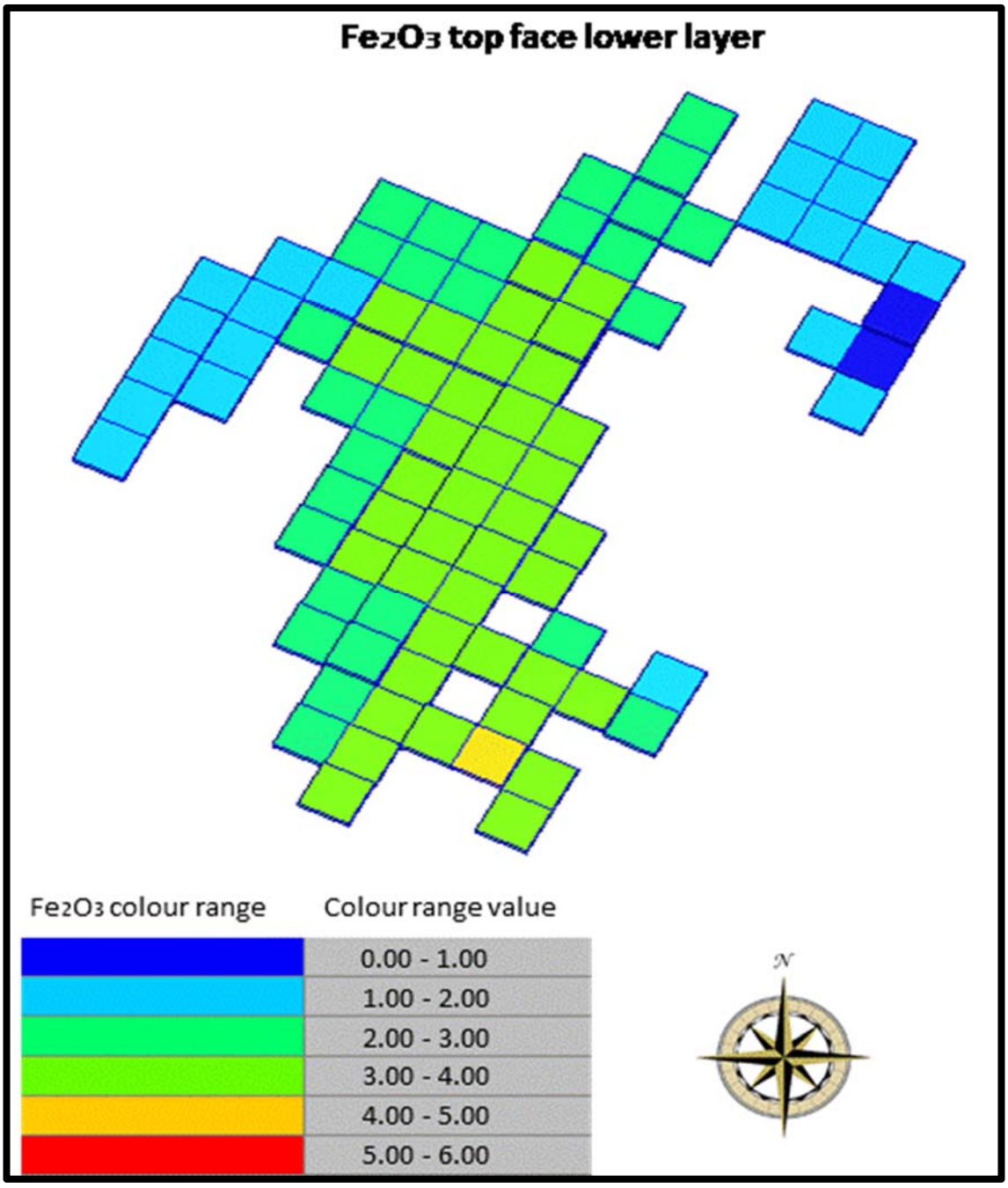


Figure 8-17 Estimated Fe_2O_3 top-face lower clay grades.

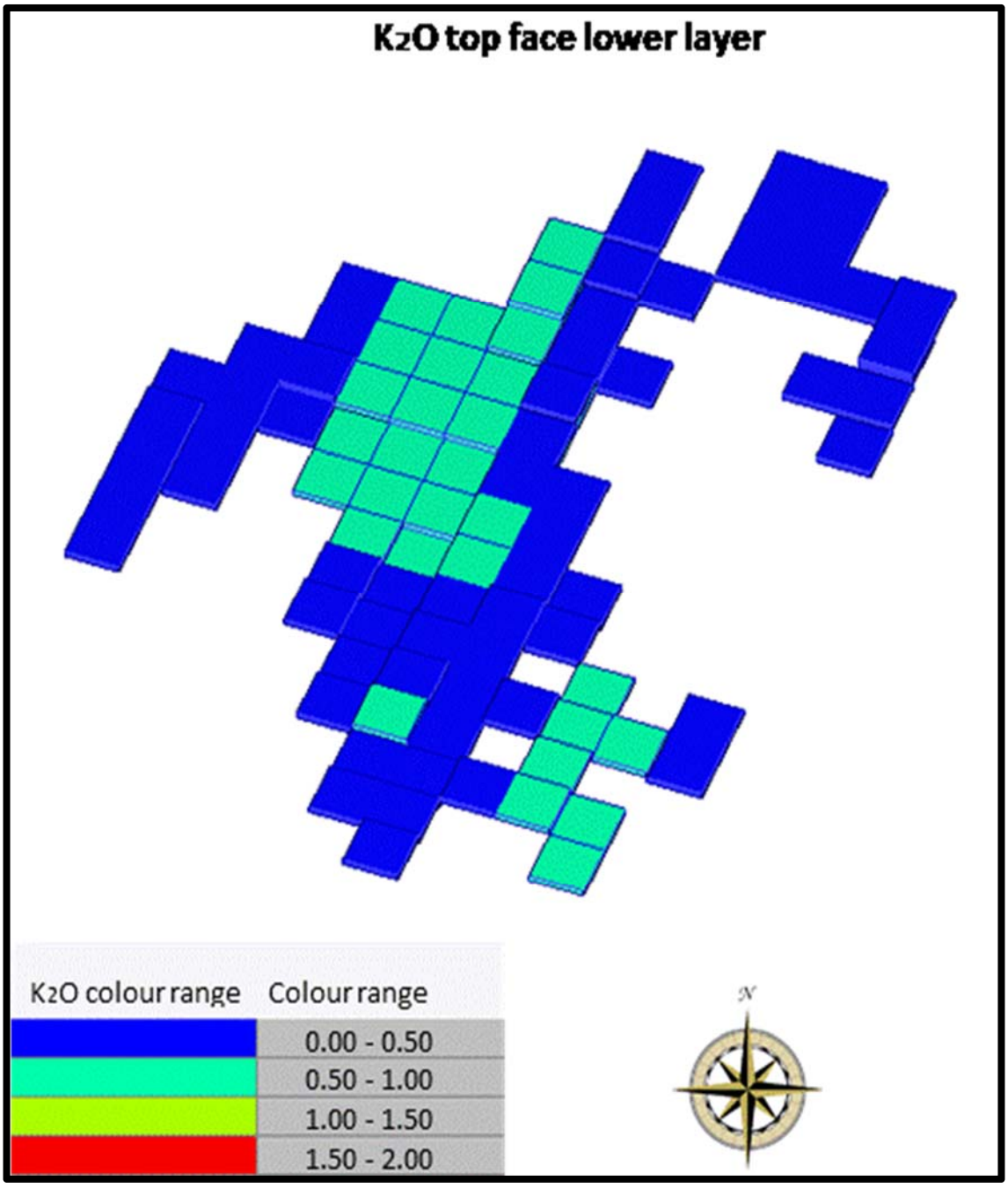


Figure 8-18 Estimated K_2O top-face lower clay grades.

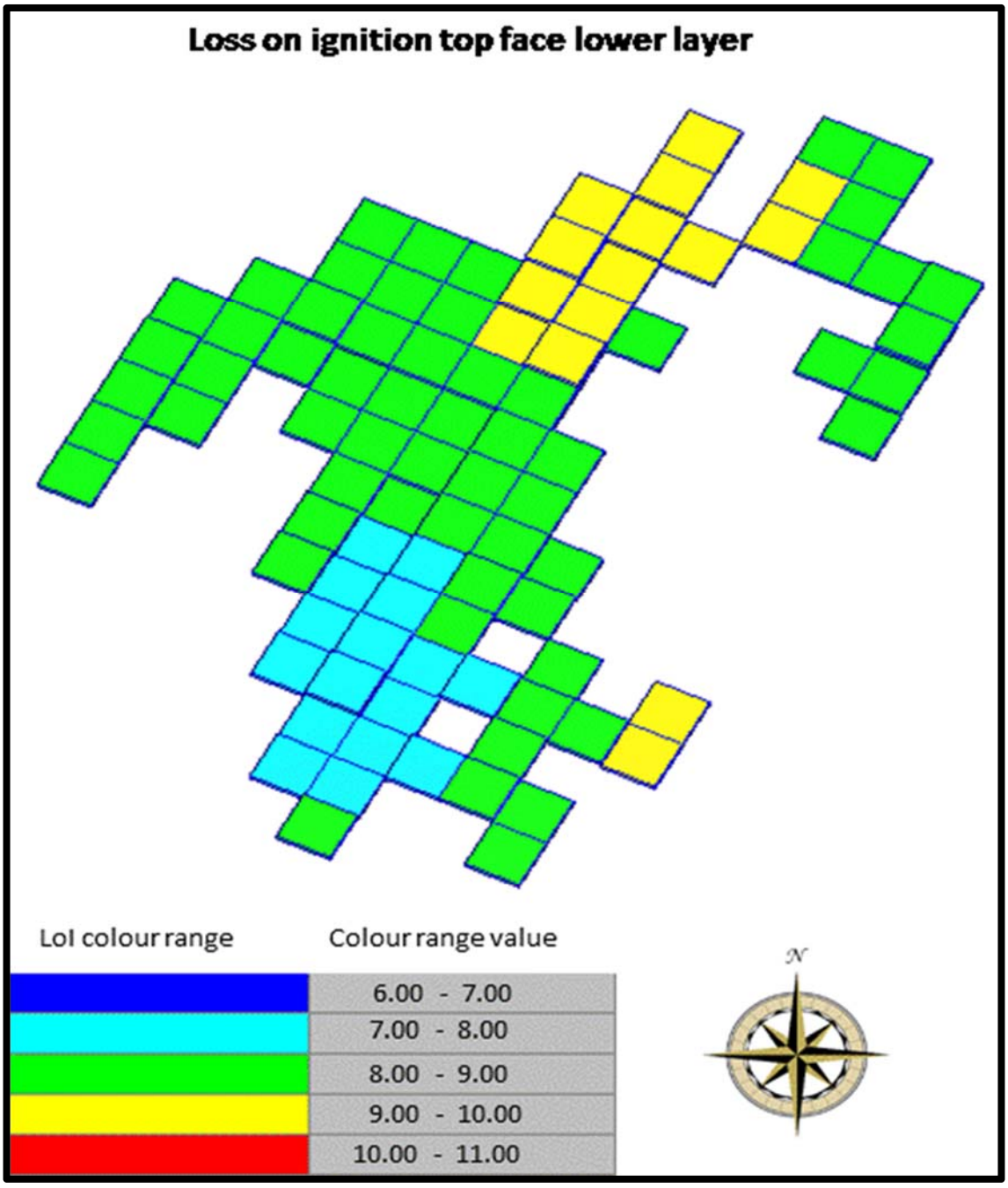


Figure 8-19 Estimated loss on ignition top-face lower clay grade.

8.3.3. Comparison between the top-face upper and lower clay estimated variables.

In comparing the kriging variance (Fig. 8.20), kriging efficiency (Fig. 8.21), and conditional bias (Fig. 8.21) between the top-face upper and the top-face lower clays, it is noted that:

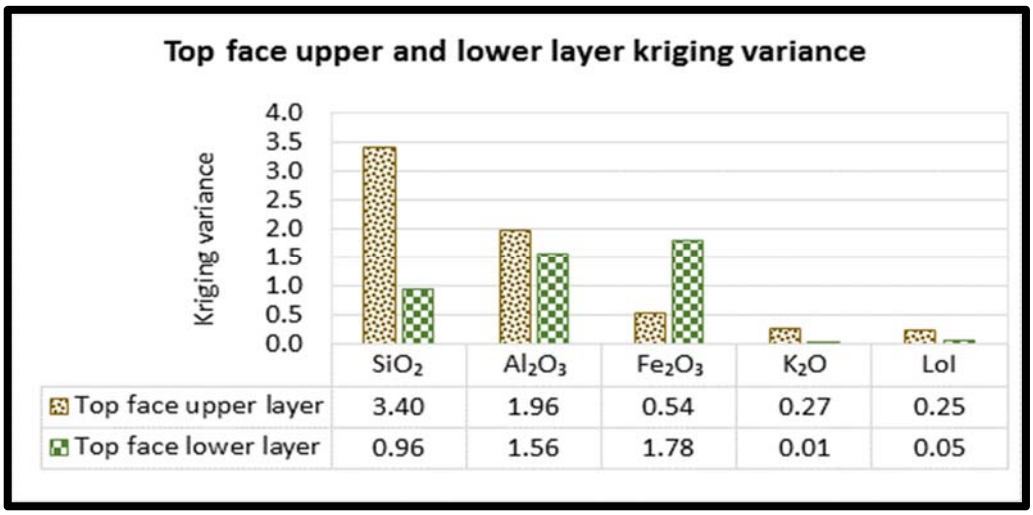
- The kriging variance was the highest for the top-face upper clay variables, except for the Fe_2O_3 variable that was higher for the top-face lower clay.
- The kriging efficiency was higher for the top-face Al_2O_3, Fe_2O_3 and K_2O upper clay variables, and lower for the SiO_2 and loss on ignition variables compared with the lower clay variables.
- The conditional bias for all the top-face upper clay variables was above 0.8, except for SiO_2 (0.64). The conditional bias for SiO_2 and loss on ignition were the only two variables above 0.7.

From the above it is clear that the local variance (kriging variance) of SiO_2 and Al_2O_3 in the top-face upper clay was more significant than were the Fe_2O_3, K_2O and loss on ignition variables. In the top-face lower clay, Al_2O_3 and Fe_2O_3 proved to be more significant than the SiO_2, K_2O and loss on ignition variables.

Kriging efficiency measures how effectively the kriging estimate correctly predicts the block grade. In other words, the percent overlap that can be expected between the estimated block histogram and that of the true block grades. A kriging efficiency of 100% indicates a perfect match between estimated and true grade distributions. The slope of regression equation is used to estimate the slope of the regression between the true and estimated block grades. A slope of “1” indicates that the estimated low and high grades correspond accurately to the true high and low grades. The block grades were well predicted for the Al_2O_3, Fe_2O_3, K_2O and loss on ignition top-face upper clay variables (good overlap between estimated and true grades), except for SiO_2, which was not as good. The grades were poorly predicted for the Al_2O_3

and Fe_2O_3 top-face lower clay variables and well predicted for the SiO_2, K_2O and loss on ignition variables.

The conditional bias indicates the over and under estimation of grades and an estimated value of one is a perfect prediction. For both the top-face upper and lower clays, the estimated values were slightly smaller than one. For a perfect prediction the kriging variance should be zero and the kriging efficiency one. A perfect prediction for the variables were not obtained. The conditional bias calculated for the variables indicate that Al_2O_3 and Fe_2O_3 for the top-face lower clay is more prone to over and under estimation than any of the other variables. Generally, the upper clay variables were better predicted than the lower clay variables. Except for the Al_2O_3 and Fe_2O_3 top-face lower clay variables, the overall variable grades were well predicted.



	SiO_2	Al_2O_3	Fe_2O_3	K_2O	LoI
Top face upper layer	3.40	1.96	0.54	0.27	0.25
Top face lower layer	0.96	1.56	1.78	0.01	0.05

Figure 8-20 Comparison between the top-face upper and lower clay kriging variance.

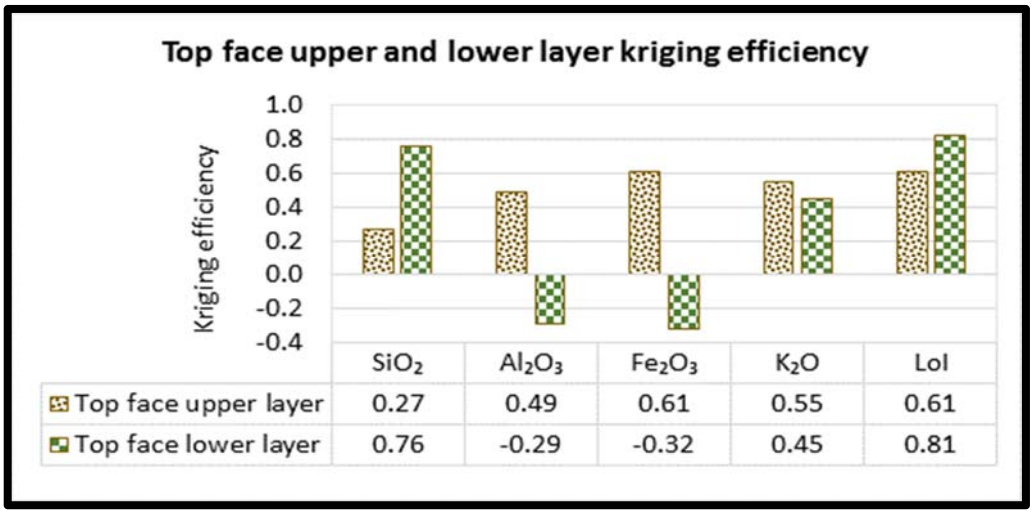


Figure 8-21 Comparison between the top-face upper and lower clay kriging efficiency.

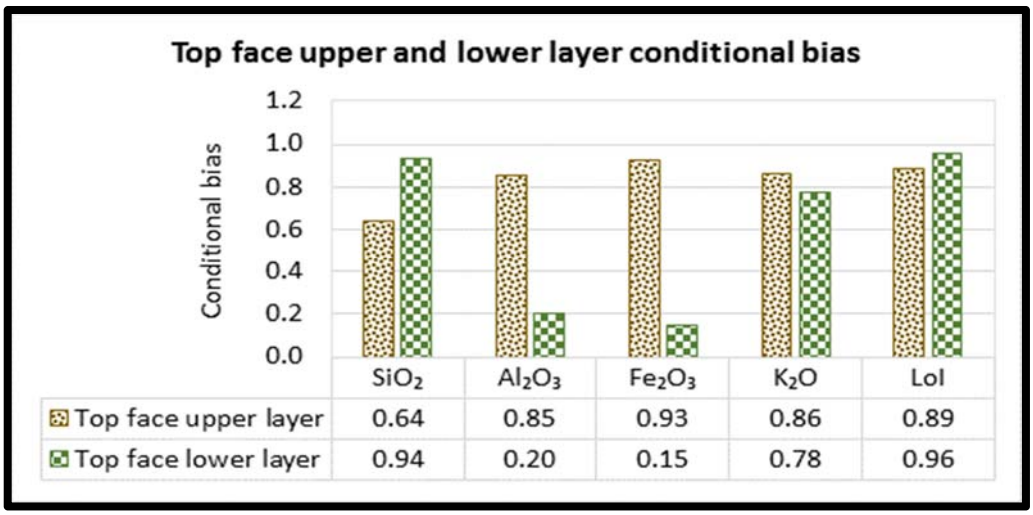


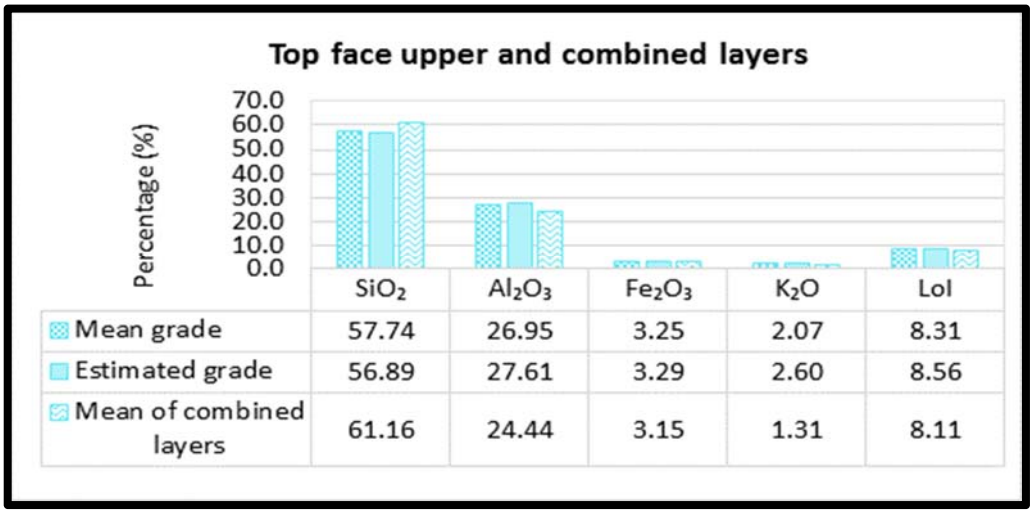
Figure 8-22 Comparison between the top-face upper and lower clay conditional bias.

8.3.4. Comparison between the mean of the combined top-face clays, as well as the mean and estimated grades of both the individual top-face upper and the lower clays

The mean grade for the combined top-face upper and lower clays is given in Figures 8.23 and 8.24, respectively. In Figure 8.23, the mean grade of the top-face upper clay is compared with the estimated grade and the mean grade of both the top-face upper and the lower clays combined. Similarly, in Figure 8.24 the mean grade of the top-face lower clay is compared with the estimated

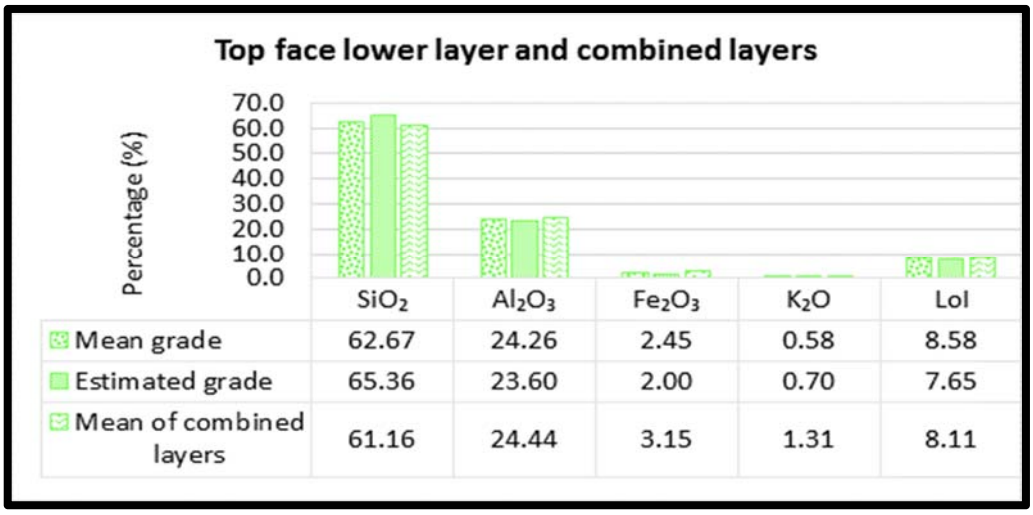
grade and mean grade of both the top-face upper and the lower clays combined.

There was a notable difference between the mean and the estimated grades of the top-face upper clay compared with the mean of the combined top-face clays. The SiO_2 variable for the combined clays was significantly higher than was the top-face upper clay, with Al_2O_3 and K_2O significantly lower (Fig. 8.23). In contrast to the top-face upper clay, the SiO_2, Al_2O_3, Fe_2O_3 and K_2O were significantly higher than for the combined top-face clays (Fig. 8.24). This important finding shows that combining the two top-face clays will definitely not reduce variability, but would rather exacerbate the variability in the grades, as these are two different clay populations.



	SiO_2	Al_2O_3	Fe_2O_3	K_2O	LoI
Mean grade	57.74	26.95	3.25	2.07	8.31
Estimated grade	56.89	27.61	3.29	2.60	8.56
Mean of combined layers	61.16	24.44	3.15	1.31	8.11

Figure 8-23 Comparison between the mean of the combined top-face clays and the top-face upper clay mean and estimated grades.



	SiO_2	Al_2O_3	Fe_2O_3	K_2O	LoI
Mean grade	62.67	24.26	2.45	0.58	8.58
Estimated grade	65.36	23.60	2.00	0.70	7.65
Mean of combined layers	61.16	24.44	3.15	1.31	8.11

Figure 8-24 Comparison between the mean of the combined top-face clays and the top-face lower clay mean and estimated grades.

CHAPTER 9

CONCLUSION AND RECOMMENDATION

9. SUMMARY

The aim of this dissertation was to determine whether a geostatistical technique, such as ordinary kriging, could be used to improve the quality consistency of a stockpile, which, in turn, could assist in improving the quality and colour consistency of the final brick product, year after year.

9.1. CONCLUSION

In Chapter 1 the research problem was defined, Chapter 2 provided a literature background on the formation of clays and the importance of the role the elements (variables) play in the manufacturing process. Chapter 3 illustrated the variability of the elements in the top-face clay, the correlation between the elements and their full physical properties, and the effect the elements have on the final properties of the brick. Chapter 4 provided a background on the regional and mine-scale geology, while Chapter 5 focussed on a detailed geostatistical background. Chapter 6 detailed the geostatistical analysis of the top-face clay, Chapter 7 focussed on variography and Chapter 8 provided the ordinary kriging estimation grades for both the top-face upper and the lower clays.

The historical mining data for the combined top-face clay stockpiles revealed noticeable fluctuation of the variables. The variability of these elements in the top-face clay proved to illustrate the quality inconsistency of the top-face clay. Table 9.1 illustrates the top-face clay variable fluctuation between the stockpile (combined top-face upper and lower clays) and the individual upper and lower clays.

Table 9-1. Fluctuation of variables in the top-face clay stockpiles compared with the top-face upper and lower clays.

Top-face	SiO_2	Al_2O_3	Fe_2O_3	K_2O	L.o.I
Stockpiles	6 - 71 %	5 - 37 %	1 - 14 %	2 - 3 %	9 - 18 %
Upper clay	0 - 66 %	0 - 33 %	9 - 6 %	4 - 3 %	8 - 10 %
Lower clay	0 - 66 %	2 - 26 %	0 – 5 %	0 – 1 %	7 – 10 %

The top-face clay occurs as an upper and lower clay in the pit and therefore the two clays were treated as separate entities for the purposes of geostatistical evaluation and analysis. The geostatistical analysis indicated that the top-face upper and lower clays were indeed two different clay types. The geostatistical analysis indicated that two populations were likely present within the top-face lower clay. Unfortunately, the limited data available did not permit further investigation of the phenomenon.

Apart from the differences noted between the top-face upper and lower clays, it is evident from Table 9.1 that contamination with other clay types is a contributing factor to the variability of the top-face clay stockpiles. This is evident from the longer variability range of the stockpiles compared with the shorter variability ranges for the top-face upper and lower clays. This factor serves to illustrate further the complexity of the deposit and the difficulty of distinguishing between the clay types in the pit, urging further investigation and classification.

The top-face upper clay is lower in SiO_2 (and higher in Al_2O_3, Fe_2O_3 and K_2O) compared with the lower clay. The SiO_2/Al_2O_3 ratio in the top-face upper clay is 2.14 and that in the top-face lower clay is 2.57. The lower SiO_2/Al_2O_3 ratio in the top-face upper clay is indicative of higher clay content. Higher clay content will promote increased drying and firing shrinkage properties during the manufacturing process, with lower water absorption properties of the fired brick. In contrast with the higher clay content in the top-face upper clay, the lower clay content in the top-face lower clay will lessen drying and firing

shrinkage and increase water absorption of the fired brick (assuming all the other properties remain constant).

Another important finding was the difference in the K_2O and Fe_2O_3 content between the two clays. The higher K_2O (3.30 percent) and Fe_2O_3 (2.08 percent) content in the top-face upper clay would definitely have a more significant effect on the intensity of the colour development of the brick than would the lower K_2O (0.57 percent) and Fe_2O_3 (2.41 percent) content in the top-face lower clay.

Potassium oxide is a strong flux that promotes the liquid phase at high temperatures. The liquid phase is introduced by the illite and mica minerals. Upon heating, the following are introduced: (1) a liquid phase from 950 °C upwards, (2) excessive firing shrinkage between 1 030 °C and 1 100 °C, and (3) a melting point between 1 050 °C and 1 150 °C. Data analysis revealed a strong positive correlation between K_2O and mica, confirming that it originate from mica.

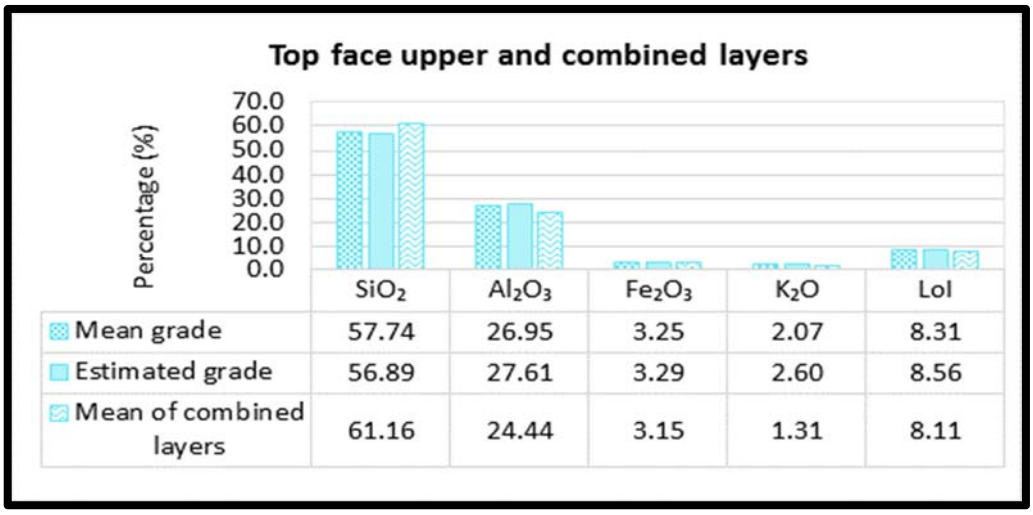
Iron oxide, on the other hand, is a strong colorant and is released from the illite structure at a temperature 900 °C and the montmorillonite structure at 800 °C. The Fe_2O_3 present in illite will cause an intense red colour of more than four percent. Iron oxide, introduced by haematite, is temperature dependent with regard to colour development. At low temperatures, an orange colour will develop and, as the temperature increases, a more intense red colour develops. A very strong positive correlation was found between Fe_2O_3 and the illite/smectite interstratification mineral.

In the presence of K_2O, Fe_2O_3 is likely to develop a dark colour at lower temperatures and in its absence a lighter colour (assuming all other properties remain constant). The low K_2O content in the top-face lower clay should contribute little to the development of the colour intensity in the brick if the Fe_2O_3 content was low (< 1 percent); however, the opposite was found for the top-face upper clay.

Geostatistical analysis indicated that the orientation of the top-face upper and lower clays was in an east–west direction rather than a north–south direction. The contour maps indicated that a higher degree of variable variations was present in the top-face upper clay than in the lower clay, rendering the top-face upper clay more variable with regard to consistency. The top-face upper and lower clay volume ratio was 3:1, indicating three times more top-face clay in the upper clay than in the lower clay.

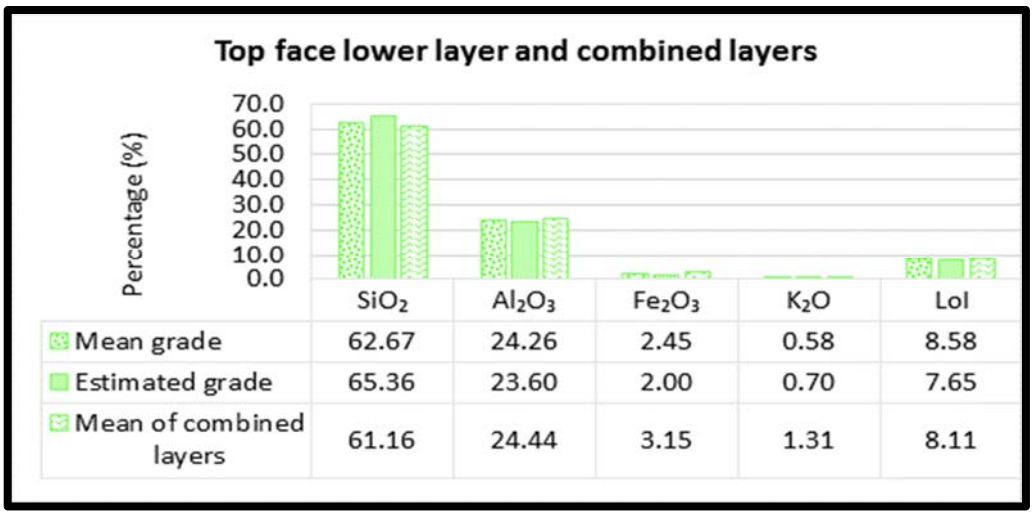
The construction of variogram models for both the five top-face upper and the lower clay variables proved to be successful. These variogram models served as a basis for ordinary kriging grade estimation. The kriging variance was the highest for the top-face upper clay variables, except for Fe_2O_3. The kriging efficiency was higher for the top-face Al_2O_3, Fe_2O_3 and K_2O upper clay variables, and lower for the SiO_2 and loss on ignition compared with the lower clay variables. The conditional bias for all the top-face upper clay variables was above 0.8, except for SiO_2 (0.64). The conditional bias for SiO_2 and loss on ignition were the only two variables above 0.7. The upper clay variables were better predicted than the lower clay variables, except for the top-face lower clay variables Al_2O_3 and Fe_2O_3. Generally, the variable grades were well predicted. The limited data available for the top-face lower clay hampered further investigation into the populations present. Such investigation could improve the estimated Al_2O_3 and Fe_2O_3 grades.

Comparing the estimated grades of the top-face upper and lower clays (Figs 9.1 and 9.2) with the mean of the top-face upper and lower clays combined indicated significant grade differences. The established practice of considering the top-face upper and lower clays as similar was found to be incorrect. The application of geostatistical techniques proved that these two clays were different, although they presented similar colour properties.



	SiO_2	Al_2O_3	Fe_2O_3	K_2O	LoI
Mean grade	57.74	26.95	3.25	2.07	8.31
Estimated grade	56.89	27.61	3.29	2.60	8.56
Mean of combined layers	61.16	24.44	3.15	1.31	8.11

Figure 9-1 Comparison between the mean of the combined top-face clays and the top-face upper clay mean and estimated grades.



	SiO_2	Al_2O_3	Fe_2O_3	K_2O	LoI
Mean grade	62.67	24.26	2.45	0.58	8.58
Estimated grade	65.36	23.60	2.00	0.70	7.65
Mean of combined layers	61.16	24.44	3.15	1.31	8.11

Figure 9-2 Comparison between the mean of the combined top-face clays and the top-face lower clay mean and estimated grades.

9.2. RECOMMENDATION

This study has shown that geostatistics could be applied in clay resource modelling and that the estimates obtained could provide valuable information for improved mine planning and product quality.

Therefore, it is recommended that stockpiles for the top-face upper and lower clays be constructed separately. That is, mining an upper clay top-face

stockpile separately from a lower clay top-face stockpile and not combining them, as is the practice. Separate stockpiling of these two clays would assist in controlling and improving the product colour and quality. Infill drilling is recommended for the top-face lower clay to obtain more data for further delineation of the occurrence with regard to its populations and to improve the Al_2O_3 and Fe_2O_3 grade estimation.

Inconsistency of the variables in the top-face upper clay could be countered by the top-face lower clay, i.e. the higher Fe_2O_3 (3.30 percent) and K_2O (2.08 percent) in the upper clay could be reduced in the product mix by blending in the clay from a separate top-face lower clay stockpile with a lower Fe_2O_3 (2.41 %) and K_2O (0.57 %) content. Additionally, the ratio of the top-face upper and lower clays is dissimilar and it is therefore anticipated that blending them, as is currently the practice, will cause depletion of the top-face lower clay prior to the completion of the top-face upper clay. Using the top-face lower clay as a diluting agent should improve the quality consistency of the raw material and would extend the longevity of the top-face lower clay domain. The practice of blending these two clays on one stockpile, because they seem similar, in reality exacerbates the quality inconsistency of the raw material. The reason for this is that the ratio of these two clays in the deposit is not consistent from mining season to mining season.

The orientation of the deposit in an east–west direction suggests grade continuity of the deposit in this direction. It is recommended that the current pit face be swung 90° to enable mining in an east–west direction along the direction of continuity. This would ensure minimal fluctuation of the grade. It is acknowledged that the initial costs for establishing a new pit face would be high because of the cost of removing the overburden to expose the clay. However, this cost could be regarded as ‘opportunity cost’. The option to swing the pit face will depend on the cost outlay for removing the overburden versus improving the product yields, which could sell at a higher margin.

The estimated grades for both the top-face upper and the lower clays could serve to predict the quality of the planned top-face stockpiles to be mined. Using the predicted grades as a guide, the volume of separate top-face upper and lower clay stockpiles could be predetermined. This, in turn, would allow manipulating of the quality of the top-face clay to the required specification by a feed ratio between the top-face upper and lower clay stockpiles during the blending process.

The predicted grade of the stockpiles prior to mining would also serve as an early warning system for the possible process adjustments needed (i.e. drying and firing process parameter changes). However, it needs to be emphasised that this option should be the last resort. Should the stockpile quality differ year on year, process adjustments could be made well in advance to counter the raw material quality changes in the process. It was, however, the aim of the study to ensure quality consistency of the raw material in an effort to prevent unnecessary process adjustments. The estimated grades established for the deposit are advantageous because this knowledge assists in preventing product quality and colour variations, provided that the process is under control.

It is strongly recommended that estimations for the sandy kaolin, chocolate, red kaolin, stained top-face, and smectite domains also be established. Sandy kaolin and chocolate clays intersect the top-face clays and estimates for these clays would allow better control of each raw material, which, in turn, could prevent the contamination of the stockpiles.

The accuracy of estimates is highly dependent on the quality of the data collected. It is strongly recommended that the chemical data from the core logging samples be utilised in block models to provide kriging estimates and grade distribution. This would provide more insight into the quality of the clay deposits, which, in turn, is required for mine planning and consistent quality clay extraction.

Another investigation that could follow from this study is the particle-size distribution within each clay. The physical nature and the deposition of the clay sediments could also contribute to the inconsistency of the raw material. Although this study was not focused on particle-size distribution and segregation, such a study could shed further light on the variability of the clay.

Additionally, it is recommended that the geostatistical methods and techniques applied in this study be extended to all ISO certified factories.

REFERENCES

Bohling, G., (2005), Kriging. Kansas Geological Survey. October 2005, viewed 10 September 2015, <http://people.ku.edu/~gbohling/cpe940/Kriging.pdf>

Brindley, G.W., (1974). Thermal reactions of clay minerals and clay mineral mixtures. Clay mineralogy and ceramic processes and products, 33-45, Bologna.

Brownell, W.E., (1976). Structural Clay Products. Applied Mineralogy. New York: Springer.

Coombes, J., (2008). The Art and Science of Resource Estimation, Perth: Coombes Capability.

Cooper D.R. & Schindler P.S., (2003). Business Research Methods. New York: Brent Gordon.

Corobrik. (2009). National product catalogue. Internal document.

Corobrik. (2010). Corobrik Lawley. Raw material manual. Internal document.

Deer, W.A., Howie, R.A., and Zussman, J., (1992). *An introduction to the rock forming minerals.* Harlow: Longman Group Limited.

Deutsch, C.V., Journel, A.G., (1992). Geostatistical Software library, New York: Oxford University Press.

Dohm, C.E., (2012). Introduction, printed notes distributed in the course Geostatistical Methods in Mineral Resource Evaluation (MINN 7006), May-2012, University of the Witwatersrand, Johannesburg.

Geologiese Opname. (1986). 1:250 000 Topo-Kadastrale reeks van Suid Afrika. Staatsdrukker. 2526 West Rand.

Goovaerts, P., (1997). Geostatistics for Natural Resources Evaluation. New York: Oxford University Press.

Grimshaw, R.W., (1971). *The chemistry and physics of clays and other ceramic materials.* 4th ed. London: Ernest Benn.

Horn, G.F.J., Strydom, J.H., (1998). The Mineral Resources of South Africa. Clay. Handbook 16. Council for Geoscience.

Isaaks, E.H. and Srivastava, R.M. (1989). An Introduction to Applied Geostatistics, New York: Oxford University Press.

Jones, D.H., (1984). Unstable ground conditions associated with Karoo outliers in the dolomitic environment of the far west rand. PhD Thesis. University of Pretoria.

Johnson, M.R., Anhaeusser C.R., Thomas, R.J. (2006). The Geology of South Africa. Sedimentary rocks of the Karoo Supergroup. Geological Society. South Africa, 461-499.

Johnson, M.R., Van Vuuren, C.J., Visser, J.N.J., Cole, D.I., Wickens, H. de V., Christie, A.D.M. and Roberts, D.L., (1997). The foreland Karoo Basin, South Africa. *In:* Selly, R.C. (Ed), *Sedimentary Basins of Africa.* Elsevier, Amsterdam, 269-317.

Kingery, W.D., Bowen, H.K. & Uhlmann, D.R., (1976). *Introduction to Ceramics.* 2nd edition. New York: John Wiley and Sons.

Lurie, J., (1984). *South African geology for mining, metallurgical, hydrological and civil engineering.* 4th ed. Johannesburg: McGraw-Hill.

McCarthy, T. and Rubidge, B., (2005). *The story of Earth and Live. A South African perspective on a 4.6 billion-year journey.* Cape Town. Struik Nature.

McCarthy, T., (2009). *How on earth? Answers to the puzzles of our planet.* Cape Town. Struik Nature.

McKillup, S and Dyar, M.D., (2010). *Geostatistics Explained.* Cambridge: Cambridge University Press.

Millot, G., (1970). *Geology of Clays*. Berlin, Heidelberg, New York (Springer), Paris (Masson *et Cie*), London (Chapman & Hall).

Sacmi. (2002). *Applied ceramic technology, volume 1.* Italy: Sacmi. Unpublished.

SABS. (1986). South African Bureau of Standards. Burnt-clay masonry units SANS 227:1986.

Stein, V., (1982). *Brick and Tile Making. Procedures and Operating Practice in the Heavy Clay Industries.* The raw materials for brick and tile making. Bauverlag GmbH, Berlin.

Van Vuuren, C.J., (1981). Depositional models for the Vryheid Formation in the northeastern part of the Karoo Basin – a review. Ann. Geol. Surv. S. Afr., 15, 1-11.

Velde, B., (2010). *Origin and Mineralogy of clays.* Berlin Heidelberg: Springer-Verlag.